Behaviour, properties and structure of complex fluids upon spreading

Christophe Kusina

PSL
UNIVERSITÉ PARIS

THÈSE DE DOCTORAT
DE L'UNIVERSITÉ PSL

Préparée à l'ESPCI Paris

Comportement, propriétés et structure des fluides complexes à l'étalement

Behaviour, properties and structure of complex fluids upon spreading

Soutenue par
Christophe KUSINA
Le 23 septembre 2019

Ecole doctorale n° 397
Physique et chimie des matériaux

Spécialité
Physico-chimie

Composition du jury :

Daniel, BONN Professeur, University of Amsterdam	*Président*
Catherine, BARENTIN Professeur, Institut Lumière Matière	*Rapporteuse*
Guillaume, OVARLEZ Directeur de recherche, Université de Bordeaux – CNRS	*Rapporteur*
José, BICO Maitre de conférences, ESPCI Paris	*Examinateur*
Annie, COLIN Professeur, ESPCI Paris	*Directrice de thèse*

ESPCI PARIS | PSL

Moi, si je devais résumer ma vie aujourd'hui avec vous, je dirais que c'est d'abord des rencontres. Des gens qui m'ont tendu la main, peut-être à un moment où je ne pouvais pas, où j'étais seul chez moi. Et c'est assez curieux de se dire que les hasards, les rencontres forgent une destinée…

Otis, a.k.a Edouard Baer

Remerciements

Tout d'abord, je voudrais remercier Annie Colin, pour m'avoir donné l'opportunité de travailler avec elle, via un stage puis tout au long de cette thèse au cours desquels j'ai certainement plus appris qu'au cours de toutes mes années d'études rassemblées. Malgré tes nombreuses responsabilités et occupations professionnelles, tu as toujours su te rendre disponible, me challenger et développer de nombreuses compétences qui me seront certainement utile tout au long de ma carrière.

Directement lié, je voudrais également remercier l'équipe de physico-chimie de L'Oréal qui m'a suivi tout au long de cette thèse et avec qui nous réalisions ces travaux. Odile Aubrun, Jean-Baptiste Boitte et Danielle Le Verge, vous avez été des piliers très important dans la structuration de cette thèse et avez apporté de nombreuses discussions scientifiques extrêmement riches et pragmatiques. Bien qu'on ne se voyait que rarement, j'ai particulièrement apprécié nos échanges constructifs qui résonnaient pour moi comme un souffle d'air nouveau dans cette thèse. Merci beaucoup d'avoir été là je suis très heureux de continuer l'aventure avec vous.

Je remercie également, Catherine Barentin et Guillaume Ovarlez pour avoir accepté de rapporter mon travail, ainsi que José Bico et Daniel Bonn pour avoir accepté d'être membre de mon jury de thèse. Ce fut un grand plaisir d'échanger scientifiquement avec vous.

Les personnes ayant le plus de culture auront certainement reconnu la citation ci-dessus qui, en plus d'être une punchline emblématique de la culture cinématographique française reflète effectivement un mode de pensée que je partage a posteriori. La vie est effectivement faite de rencontres et j'aimerais remercier toutes ces personnes que j'ai rencontré et sans qui je n'aurais jamais réussi à être où j'en suis aujourd'hui. Merci donc à Alexandra Nel, Gilbert Limarola, Jean-Laure Dormieux, Christophe Honorat, et les autres professeurs que j'ai eus en bac STL et BTS chimiste, pour m'avoir permis de sortir de l'échec scolaire et de décoller vers de nouveaux horizons équipé d'un sac rempli de confiance en soi et de connaissance. Merci également à Catherine Régniez pour m'avoir fait découvrir le monde professionnel des parfums qui me passionnait depuis longtemps et pour m'avoir également poussé à exploiter mon potentiel en allant en école d'ingénieur.

Nouvel environnement, nouvelles rencontres, merci à Arno Wahler, mon officiel parrain d'école d'ingénieur, pour m'avoir accompagné et soutenu au cours de cette aventure loin d'être simple, et pour m'avoir poussé à sortir de mes zones de confort – conseil que j'applique encore aujourd'hui avec beaucoup plus d'assurance et d'envie qu'il fut un temps. Ton expérience m'a vraiment permis de prendre du recul et de gagner en maturité sur de nombreux points. Je te dois vraiment beaucoup pour ça.

Enfin, dernière étape de mes études, et dernière rencontre clé, Wilbert Smit. Tu as vraiment été une source d'inspiration et d'énergie sans pareil, j'ai extrêmement aimé

travailler et synergiser avec toi au cours de cette thèse. Vraiment un grand merci d'avoir été à mes côtés tous les jours, de m'avoir apporté tes connaissances, ton expérience et ton enthousiasme. Surtout ne change pas, ta bonne humeur rayonne et c'est vraiment très agréable.

Bien sûr, il me reste de nombreuses personnes à citer dans ces remerciements. Parce qu'effectivement, faire une thèse c'est bien, mais ça se passe beaucoup mieux quand on est accompagné de ses amis. Vous êtes nombreux et si je devais faire une petite partie sur chacun d'entre vous, mes remerciements seraient certainement plus longs que la thèse elle-même. Ainsi permettez-moi de vous rassembler.

Astrid, Béné, Hervé, Jeanne, Mathieu, merci, d'avoir été présents depuis le lycée, et même jusqu'au jour de ma soutenance. Je sais que vous en douterez encore, parce que c'est dans votre nature de souligner toutes mes maladresses, mais j'espère avoir pu vous démontrer que j'avais une part d'intelligence à travers cet exercice.

Bertrand, Thibault, Maximilien et Pierre, merci d'avoir illuminé nos années d'écoles, et celles qui ont suivies, en les agrémentant de nombreux fous rires. D'autre part, ne m'en voulez pas d'être parti chez la concurrence pour la thèse, CP un jour, CP toujours.

Les ami(e)s de thèse à l'ESPCI, Guillaume, Louis, Claire, Mélanie, Sandrine, Wilbert, Julie, Ludo, Paul, Gaëtan, Ondine, Xavier, Anne-Cha, Ekoé, Cécile et tous ceux que j'ai oubliés, vous avez été incroyables. Merci et bravo à vous de m'avoir supporté dans les moments positifs avec mes blagues et jeux de mots nuls, et dans les moments moins positifs que l'on traverse tous à un moment donné. Pendant ces trois années vous avez été les rayons de soleil de ma vie et j'espère que vous accepterez de garder ce rôle par la suite. Rien de tout ça n'aurait été possible sans vous, vous avez été un soutien psychologique sans faille. Vous m'avez vraiment donné envie de me lever tous les matins et je souhaite à toute personne de rencontrer des personnes comme vous.

Tom, Louis, Krystal, Arthur, Alban, notre amitié n'est certainement pas banale pour le commun des mortels, mais vous savez tout autant que moi à quel point elle est puissante et franche. Je vous remercie très sincèrement pour votre soutien quotidien qui lui aussi est particulièrement exceptionnel. On n'a pas fini de *chevaliser* ensemble.

Last but not least, merci beaucoup à ma famille, et particulièrement à mes parents qui m'ont toujours accompagné et soutenu à travers mes différentes aventures professionnelles et personnelles, et pour les valeurs qu'ils m'ont respectivement transmises. Enfin, merci à mon frère pour cette complicité qu'on a tous les deux et qui représente également une source d'énergie débordante pour moi. C'est vraiment à toi que j'aimerais dédicacer cette thèse, parce qu'au final tu es le seul autre scientifique de la famille Kusina et que je sais que tu en feras bon usage.

Résumé de la thèse en français

Bien qu'anodin à l'échelle du consommateur, l'étalement des produits cosmétiques est une étape primordiale pour former un dépôt homogène sur la peau et permettre aux différents actifs (hydratants, solaires, anti-âge) d'être le plus disponible possible pour jouer leur rôle. Au cours de cette thèse réalisée dans le laboratoire CBI-MIE de l'ESPCI et en collaboration avec l'Oréal, nous avons étudié le comportement des fluides complexes au cours d'un étalement sous contrainte dans le but de mieux maitriser le dépôt formé sur la peau et d'optimiser les performances des produits cosmétiques.

L'étalement des fluides complexes fait appel à une science riche et polydisciplinaire, c'est pourquoi l'état de l'art qui débute ce manuscrit présente les différents axes scientifiques qu'il est nécessaire de maitriser pour aborder cette thèse, mais aussi de l'avancement des recherches dans ces domaines au moment où cette thèse est rédigée.

La première partie de cet état de l'art aborde les aspects fondamentaux de la rhéologie, son principe de fonctionnement, les outils utilisés pour réaliser ce genre de mesures, les résultats majeurs que nous pouvons en tirer, et fait état du comportement des différents types de fluides complexes et de leurs spécificités. L'accent a été particulièrement mis sur les propriétés des suspensions de particules solides et molles. Les suspensions de particules solides présentent un comportement rhéoépaississant à suffisamment haute fraction volumique. Ceci est lié à la gêne stérique des particules entre elles, qui, ne pouvant pas se déformer, ont un coefficient de friction non seulement élevé, mais qui varie et augmente avec la contrainte de cisaillement via la diminution du film de lubrification formé par le solvant entre chacune d'entre elles. A l'inverse, pour des systèmes contenant des particules molles, comme les gels ou les émulsions, la structure mésoscopique est capable de se déformer sous contrainte et on observe un phénomène de rhéofluidification.

Par la suite, l'état de l'art traite des propriétés de mouillage et des modes d'étalements de différents types de fluide. Des rappels sur les énergies de surface et les configurations thermodynamiquement stables lors d'expériences de mouillage sont faites en statique mais également en dynamique. Les expériences de Landau-Levich ont été précurseur dans la prédiction des épaisseurs de films obtenus par retrait de plaques depuis un bain de fluide newtonien. Ils ont particulièrement réussi à expliquer le phénomène comme étant une compétition entre les forces visqueuses que subit le fluide via le retrait de la plaque du bain, et les forces capillaires qu'exerce le ménisque qui tend à retenir le fluide dans le bain. Une loi de prédiction de l'épaisseur en ressort mettant en relation la vitesse de retrait de la plaque, la viscosité du fluide, la tension de surface et la longueur capillaire.

Une étude d'étalement de fluides newtonien par une lame souple, présentée par Seiwert, fait état d'une dépendance assez similaire, à l'exception que la tension de surface représentant la force du ménisque dans le cas de l'enduction par trempage est remplacée par la rigidité de la lame qui représente la force de la lame qui empêche l'entrainement visqueux du liquide.

La formation de films non newtoniens est plus complexe mais a été décrite dans le cas d'une enduction par trempage d'une plaque pour des fluides à seuil comme les gels de carbopol. On en retire que l'épaisseur du film croit avec la contrainte seuil du gel mais les modèles de prédictions restent globalement empiriques. De même, il n'existe pas de littérature prédisant l'épaisseur obtenue lors de l'étalement de fluide complexe par une lame souple. La lame et le doigt étant tout deux déformables, cela représente l'expérience la plus cohérent à mettre en place pour simuler l'étalement d'un produit cosmétique par un doigt.

La deuxième partie de cette thèse porte sur la rhéologie de systèmes cosmétiques modèles. Dans un souci de compréhension globale de la physique de l'étalement, nous avons formulé un produit cosmétique volontairement simple par rapport à la complexité que l'on peut retrouver dans la réalité. Dans notre cas, notre formule est composé d'une phase aqueuse volatile (de l'eau), contenant une espèce liquide non volatile (du glycérol) ainsi que de charges en suspension (de l'amidon) et un agent de texture (un gel de carbopol). Les gels de carbopol ont été caractérisés par mesures rhéologiques en oscillation et en écoulement et montrent un comportement de fluide à seuil rhéofluidifiant, la contrainte seuil augmentant avec la concentration en gel dans l'eau comme prédit dans la littérature.

L'amidon, souvent utilisé comme particule rigide microscopique modèle, a été étudié dans l'eau et a montré une certaine instabilité à température ambiante résultant en un gonflement suivi d'une déstructuration. Nous avons associé cette instabilité à la pénétration de l'eau dans les particules d'amidon et à la solubilisation progressive de l'amylose contenue dans l'amidon. La solubilisation de l'amylose a essentiellement lieu dans des conditions diluées (i.e. $< 20‰_{v}$), agitées et dans l'eau. Elle impacte fortement la rhéologie des suspensions pouvant passer d'un comportement de fluide newtonien à celui d'un fluide à seuil via le gonflement des particules et la dispersion des chaines d'amylose dans l'eau. L'instabilité des amidons ayant été démontrée, nous avons décidé de réaliser nos expériences dans la semaine qui suivait la préparation des échantillons.

Les profils rhéologiques des formulations modèles contenant à la fois de l'eau, du glycérol, de l'amidon et du carbopol, sont apparus comme étant relativement proche de celui des gels de carbopol. Bien que la pente soit affectée par la présence de glycérol et la valeur du seuil par la présence d'amidon, le mélange reste un fluide à seuil rhéofluidifiant.

La troisième partie est consacrée aux expériences d'enduction par trempage des fluides à seuil dans une géométrie axisymétrique. A la différence du cas où l'on trempe une plaque dans un bain de liquide, la géométrie axisymétrique induit un champ de contrainte équivalent tout autour de la tige lors de son retrait. Les équations de Stokes ont été résolues et ont permis de décrire le flux de matière à l'intérieur du bain. Lors du retrait de la tige, la quasi-totalité du bain reste dans son état solide car la contrainte que le fluide subit n'est pas suffisamment élevée pour le faire s'écouler. Seules les zones proches des parois de la tige et du réservoir subissent des contraintes de cisaillement suffisamment grandes et s'écoulent au cours de l'expérience. C'est cette couche fluidifiée qui forme quantitativement le film de matière extrait à partir du bain.

Nous avons vérifié cette modélisation théorique en réalisant des expériences d'enduction par trempage dans des bains de différentes tailles, avec des gels de différentes contraintes seuil et avons mesuré les épaisseurs des films formés en utilisant un profilomètre optique. De même les vitesses calculées dans le bain ont été vérifiées par du suivi de bulles d'air implémentées dans le gel. Pour des grands seuils d'écoulement, nous avons observé que l'épaisseur du film formé dépend de la taille du bain, de la vitesse de retrait et de la rhéologie du fluide. Cependant, la tension de surface n'a pas d'impact n'a pas d'impact sur ces fluides. Pour des contraintes seuil plus faibles (i.e. inférieur à 18 Pa), nous revenons à un comportement plus proche de celui d'un fluide newtonien. Dans ce cas, la taille du bain n'a pas d'effet et l'épaisseur du film formé n'est fixée que par la vitesse de retrait, la viscosité du fluide et la tension de surface comme présenté dans le cas des expériences de Landau-Levich.

Dans la quatrième partie, notre intérêt se porte sur les expériences d'enduction d'un substrat rigide avec un fluide à seuil via l'utilisation d'une lame souple. En utilisant de nouveau le profilomètre optique nous avons mesuré l'épaisseur des films formés sur des substrats de PMMA sablés. Nous avons observé que cette épaisseur n'est pas constante et devient de plus en plus fine au cours de l'étalement. Dans certains cas, le dépôt peut même présenter des hétérogénéités et comporter des trous. Ceci est dû au volume du réservoir de fluide que l'on étale qui est de taille finie. Au cours de l'étalement le réservoir se vide et la contrainte exercée par le fluide permettant de soulever la lame souple s'amenuise entrainant la retombée de la lame et la formation d'un film de plus en plus fin.

Dans cette géométrie, nous avons également mené une étude théorique complète en résolvant les équations de Stokes sous la lame nous permettant de décrire la totalité du flux de matière au cours d'un écoulement. De façon analogue au cas de l'enduction par trempage, le fluide à seuil n'est dans son état liquide qu'à proximité de la surface de la lame et de celle du substrat. Le reste du matériau, ne subissant par une contrainte suffisamment grande, reste dans son état solide. Trois régimes d'écoulement ont été prédits et observés sous la lame. L'un d'entre eux permet une recirculation du fluide sous

la lame et c'est dans le cas où ce régime n'existe pas que le film se forme de façon hétérogène. Notre étude théorique nous a mené à écrire une équation de prédiction de l'épaisseur du film de fluide complexe formé, proche de celle décrite par Seiwert pour un fluide newtonien. Ainsi l'épaisseur d'un fluide à seuil formé par l'enduction d'un substrat rigide et rugueux avec une lame souple dépend de la rhéologie du fluide à seuil, de la vitesse d'étalement, de la longueur de contact entre le fluide et la lame, et de la rigidité de la lame. Dans le cas où le substrat n'est pas rugueux des phénomènes de glissement et de démouillage ont lieu et complexifient grandement l'étude. Dans ces conditions, le film de liquide ne se forme qu'une fois que la vitesse d'étalement dépasse une vitesse critique. Nous avons essayé de prédire cette vitesse critique en la comparant à une vitesse de démouillage pour des fluides à seuil. Bien que la théorie semble cohérente avec l'expérience pour des seuils faibles (i.e. < 15 Pa), les vitesses obtenues par l'étalement de fluide ayant un seuil plus haut sont bien plus grandes que celles prédites par le calcul. Cette vitesse critique n'est donc pas liée à un phénomène de démouillage mais à un autre phénomène que nous n'avons pas pleinement réussi à attribuer pour le moment.

Dans le dernier chapitre de cette thèse, nous nous rapprochons de l'application et de la formulation réelle des produits cosmétiques. Dans le monde des cosmétiques, il existe des tests standardisés pour tester les performances des produits cosmétiques. Nous avons créé un montage expérimental permettant de simuler ce test et de le rendre répétable d'un point de vue des forces appliquées et des vitesses d'applications qui peuvent parfois être dépendantes de l'utilisateur dans le cadre des tests réels. En appliquant des formules simples sur des substrats simples, comme des gels de carbopol sur des plaques de PMMA rugueux, on s'aperçoit que le dépôt est d'ores et déjà complexe et que les mouvements d'aller-retours qui interviennent au cours de l'application entrainent la formation de stries dans le sens du déplacement de l'applicateur. En appliquant d'autres formules, comme des suspensions d'amidon concentrés (i.e. $\sim 40\%_{v}$) dans l'eau, des bourrelets apparaissent perpendiculairement au sens de déplacement de l'applicateur. La formation de ces dépôts hétérogènes montre la complexité qui réside dans la science de l'étalement et l'impact que peut avoir des entrainements de matières non désirés ou des effets inhérents au comportement des matériaux comme le rhéoépaississement.

Dans cette partie nous nous intéressons également à l'effet dose de la glycérine et de l'amidon sur la qualité du dépôt. Il se trouve que la fraction volumique en amidon dans le dépôt sec fixe grandement la qualité du dépôt. Par exemple, une fraction volumique sèche en amidon supérieure à la fraction volumique d'empilement compact de ces particules dans leur solvant entrainera un dépôt au toucher sec et sera sujet à former d'importants défauts d'étalement. A l'inverse, une faible fraction volumique en particule dans le dépôt donnera un dépôt fluide plus pratique à étaler de façon homogène.

Les défauts d'étalement et plus particulièrement la formation d'agrégats lors de l'étalement est une question important en cosmétique, car elle est responsable, à la fois de la performance du produit, mais aussi de la sensation lors de l'étalement. C'est pourquoi, nous avons également investiguer les conditions d'arrachement du dépôt déposé en fonction de différents types d'applicateurs (mous, durs, lisses ou rugueux) et de différents types de substrats d'étalement (également mous, durs, lisses ou rugueux). En utilisant un programme d'analyse d'images nous sommes parvenus à déterminer le pourcentage de matière qui avait été arraché en fonction des matériaux du substrat et de l'applicateur ainsi que de la force d'application. Il en résulte que le dépôt s'arrache facilement dans le cas où le contact est bon entre l'applicateur et le substrat. A l'inverse, pour un substrat très accrochant et un applicateur plutôt glissant, très peu de matière s'arrache. Cela peut nous montrer qu'en plus de maitriser la physico-chimie des matériaux, de nombreuses innovations technologiques sont possibles sur le mode d'application des produits cosmétiques.

Introduction générale

De par ses nombreuses applications dans la vie de tous les jours, la physico-chimie des fluides complexes est aujourd'hui un domaine scientifique largement étudié. Souvent rencontrés dans l'industrie alimentaire, la pétrochimie et les applications cosmétiques, les fluides complexes présentent des comportements surprenants qui peuvent parfois être même contre-intuitifs. En s'intéressant à l'application cosmétique on remarque que l'étalement de ces types de fluides (crèmes, fonds de teint, mascaras, shampoings...) n'est pas trivial et peut avoir un effet tant sur l'efficacité des produits cosmétiques que sur les sensations ressenties par le consommateur lors de l'étalement. Ainsi, la compréhension des paramètres qui régissent leur étalement sur la peau permettra d'optimiser les formulations afin de satisfaire au mieux les consommateurs.

D'un point de vue scientifique, la diffusion d'une crème, d'une lotion ou d'un fond de teint est une thématique pluridisciplinaire. En effet, de nombreux paramètres doivent être pris en compte pour imiter l'étalement *in vivo* des cosmétiques via des expériences *in vitro*. Par exemple, lors de l'étalement, le consommateur applique une certaine force sur sa peau qui a également une élasticité, une rugosité et une tension superficielle spécifiques. Même si elle semble être une étape insignifiante, la simple mise en contact du fluide sur la peau pose déjà plusieurs questions scientifiques sur la nature du substrat. Par ailleurs, l'étalement des cosmétiques met en évidence d'autres questions concernant la rhéologie des fluides sous contrainte, les mécanismes de séchage des suspensions, ou encore l'évolution de la rhéologie au cours du séchage. Tous ces paramètres induisent une perception sensorielle lors de l'application. Certains tests consommateurs ont révélé des sensations glissantes, crissantes, voire la formation d'agrégats lors de l'étalement. Pour l'instant, même si la stabilité des cosmétiques lors du stockage et la caractérisation des dépôts sur la peau sont bien étudiées, les mécanismes responsables de ces sensations glissantes ou crissantes et leurs liens avec les formulations et leurs comportements à l'échelle microscopique ne sont pas encore bien compris.

Dans cette thèse, nous étudions le comportement à l'étalement de fluides complexes afin de répondre à des problématiques industrielles. Tout d'abord, nous proposons d'établir un état de l'art de la rhéologie et de la science de l'étalement. Ensuite, nous discutons de deux systèmes d'enduction, l'enduction par trempage et le revêtement par une lame, qui correspondent respectivement aux étapes de prélèvement et d'étalement des produits cosmétiques. Nous étudions la quantité de liquide prélevée et l'épaisseur du liquide étalé sur la peau. Dans la dernière partie, nous essayons de comprendre l'impact des charges de cosmétiques sur la qualité du dépôt.

General introduction

By its numerous applications in daily life, the physical-chemistry of complex fluids is nowadays a widely investigated field of science. Indeed, often met in food industry, petrochemistry and in cosmetic applications, complex fluids present surprising behaviour which can even be counter-intuitive. In the world of cosmetic products, it is common to meet complex fluids. The spreading of such fluids (i.e. creams, foundations, mascaras, shampoos …) is not trivial and can have an effect both on the efficiency of cosmetics and on the consumer perception during spreading. Thus, understanding which parameters lead the spreading of cosmetics on skin will help to optimize the formulations in order to get a better satisfaction from customers.

From a scientific point of view, the spreading of a cream, of a lotion or a foundation is a real multidisciplinary thematic. Indeed, numerous parameters have to be taken into account to mimic the *vivo* spreading of cosmetics via *vitro* experiments. For example, upon spreading, the consumer applies a specific force on his skin which also has a specific elasticity, roughness and surface tension. Even though it seems to be a meaningless step of the use of cosmetics, the "putting in touch" step of the fluid on skin already presents several scientific questions about the nature of the substrate. Moreover, the spreading of cosmetics highlights other questions concerning the rheology of fluids under stress, the drying mechanisms of suspensions, or even the evolution of rheology during drying. All these parameters induce a sensory perceptions during application. Some consumer tests have revealed the sensation of slippery, catchy, or even the formation of aggregates during spreading. For now, even though the stability of cosmetics during storage and the characterization of deposits on skin are well studied, the mechanisms responsible for these slippery or catchy sensations and their links with the formulations and their behaviours at a microscopic scale are still not well understood.

In this thesis we investigate the spreading behaviour of complex fluids in order to answer to industrial issues. First, we propose to establish a state of the art about rheology science and spreading science. Then we discuss, two coating systems, dip coating and blade coating, which correspond respectively to the pick-up and the spreading steps of cosmetic products. We investigate the quantity of liquid withdrawn and the thickness of liquid spread on skin. In the last part, we try to understand the impact of cosmetics fillers on the quality of the deposit.

Contents

Chapter 1: State of the art

I. Rheology of complex fluids 2

1. Fundamentals of rheology 2

a. Flow properties: non-linear regime 2

b. Viscoelastic properties: linear regime 4

c. Experimental rheology 5

2. Rheology of complex fluids: presence of particles within a liquid phase 8

a. Definition of random close packing. 8

b. Suspension of non-Brownian particles 10

c. Suspension of Brownian solid particles 11

d. Suspension of solid particles interacting with each other 12

e. Suspension of fluid particles 13

f. Rheology in confined geometry 14

II. Coating surfaces with complex fluids 15

1. Bases of wetting properties 15

a. Wetting properties in the static regime 15

b. Wetting properties in the dynamic regime 17

2. Dip-coating: Landau-Levich's case of reference 15

a. Landau-Levich's transition for Newtonian fluids: Critical velocity 19

b. Landau-Levich's transition for Newtonian fluids: Film thickness 21

c. Dip-coating of complex fluids 22

3. Blade Coating 24

a. Creating a film using blade-coating methods 24

b. Blade coating of Newtonian fluids 26

c. Blade coating of purely viscous non-Newtonian fluids 26

d. Blade coating of viscoelastic fluids 27

III. Outline of this thesis 28

Chapter 2: Rheology of a model cosmetic system

I. Towards the definition of a model cosmetic system....33
II. Rheology of carbopol systems....33
1. Preparation of carbopol gel....33
2. Surface tension and contact angle....34
3. Rheological characterization....34
a. Rheological behaviour of carbopol gel in the linear regime....34
b. Rheological behaviour of carbopol gels in the non-linear regime....35
III. Rheology of Corn starch dispersions....36
1. Stability of starch in water over time....37
a. Evolution of the rheology and particle size....37
b. Chemical Quantification....41
IV. Rheology of a model cosmetic formulation....43

Chapter 3: Dip coating of complex fluids

I. Experimental section....47
1. Experimental set-up....47
2. Film thickness measurement using a profilometer....48
II. Dip-coating of complex fluids....49
1. Experimental results....49
2. Theoretical approach....51
3. Capillary effect and gravity in dip-coating experiments....54
4. Discussion....55

Chapter 4: Blade coating of complex fluids

I. Experimental section....60
1. Experimental setup....60
2. Study of the scrapping blade....61
II. Formation of the liquid film and prevision of its thickness....62
1. Experimental measurements....62

a. Procedure....62
b. Spreading of carbopol gels on a rough substrate....63
2. Theoretical approach: prediction of the film thickness....64
3. Formation of instabilities within the coated film....68
a. Plug flow: $0 < \lambda i <$ h and $0 < \lambda o <$ h....70
b. Flow with a plug attached to the blade: $0 < \lambda i < h$ and $\lambda o \geq h$....71
c. Shear flow throughout slot: $\lambda o \geq h$ and $\lambda i \geq h$....72
d. Instabilities....72
III. Spreading on a smooth and non-wetting situation....74
1. Conditions for a film to form....74
2. Theoretical approach....76

Chapter 5: Using fillers in cosmetic products

I. Spreading of complex systems containing fillers – Screening spreading defects..82
1. Aggregate-formation characterisation test to rank goodness of formulations...82
2. Mimic of the in-vivo procedure by an in-vitro procedure....83
3. The formation of streaks during back and forth applications....84
a. Macroscopic observation....84
b. How do streaks form?....88
4. Formulation impact on the deposit quality....89
a. Preparation of simplex formulations and spreading default risk test....89
b. Observation of the dry deposit....90
c. Rheological approach....92
5. Impact of the substrate and the applicator on the spreading quality....95
a. Experimental set-up and method....95
b. Screening the substrate/deposit and applicator/deposit interactions....97

Chapter 1

State of the art

Summary: This chapter is devoted to the bibliographic research on the fields of science surrounding the subject of my thesis. We get back to fundamental rheological description of Newtonian and non-Newtonian materials through the behaviour of gels or concentrated suspensions. Then we summarise the coating problem that has been widely investigated in the literature. We make the link between basic wetting theories and complex analysis of the flow during coating in order to understand how a film of liquid is formed in miscellaneous coating geometries. The combination of these two topics gives us a good overview of the scientific knowledge to keep in mind for the thesis.

I. Rheology of complex fluids

1. Fundamentals of rheology

Etymologically "the study of flows" in Greek, the word "rheology" was invented by Bingham in 1929. During this period, two approaches existed to give a mechanical description of matter: solids mechanic and fluids mechanic. However, none of those was sufficient to explain the behaviour of complex fluids. Experimentally, rheology allows to measure flowing and viscoplastic properties of materials. This is a powerful tool to control formulations. Coupled to other methods, rheology also permits to create a link between the formulation, microstructure of materials and properties of products[1]. For example, in some studies, researchers were able to follow the progressive crosslinking of gels in real time[2], or even to understand the impact of solid particles within molten polymers by coupling rheology with a static light scattering method[3].

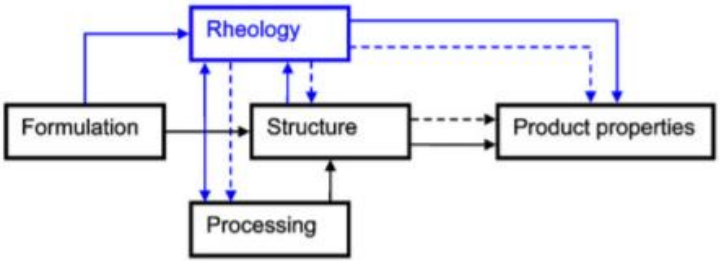

Figure 1: Representation of the omnipresence of rheology in the field of formulation sciences [from Averous 2011][1].

a. *Flow properties: non-linear regime*

The spreading of cosmetics on skin is characterized by a shearing motion described simply by a stretching experiment of a material between two parallel plates separated by a gap e. One of the plate is kept at rest while the second moves at a velocity V along the X axis. Using the non-slipping hypothesis, the material reacts to this solicitation and flows forming parallel layers of fluids that move at different velocities: from 0 for the layer in contact with the non-moving plate, to V for the layer in contact with the moving plate (Figure 2).

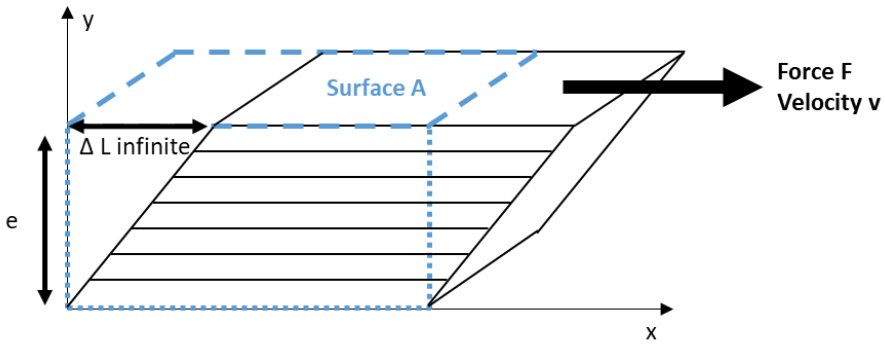

Figure 2: Simple infinite deformation along the X axis between two parallel plates.

Here are some technical definitions of the main rheology parameters. During the shearing motion, the frictional forces appear tangentially to the different layers. The shear stress results from these frictional forces reported to the layer surface and is expressed by $\tau = F/A$. The shear rate $\dot{\gamma}$ expressed in s^{-1} is the time derivative of the deformation ($\dot{\gamma} = \frac{dv}{de} = \frac{d\Delta l}{dt}$). The shearing viscosity η is defined as the rate between the shear stress and the shear rate $\eta = \frac{\sigma}{\dot{\gamma}}$.

The non-linear regime is associated to the sufficiently high deformations that induce a destructuration of the fluid and its flow. In this regime we focus on flowing properties of fluids. The typical experiment allowing to characterize the flowing behaviour of a fluid is the measure of the shear stress upon a shear sweeping (i.e. $\tau = f(\dot{\gamma})$). The literature reports the behaviour of all these complex fluids (Figure 3).

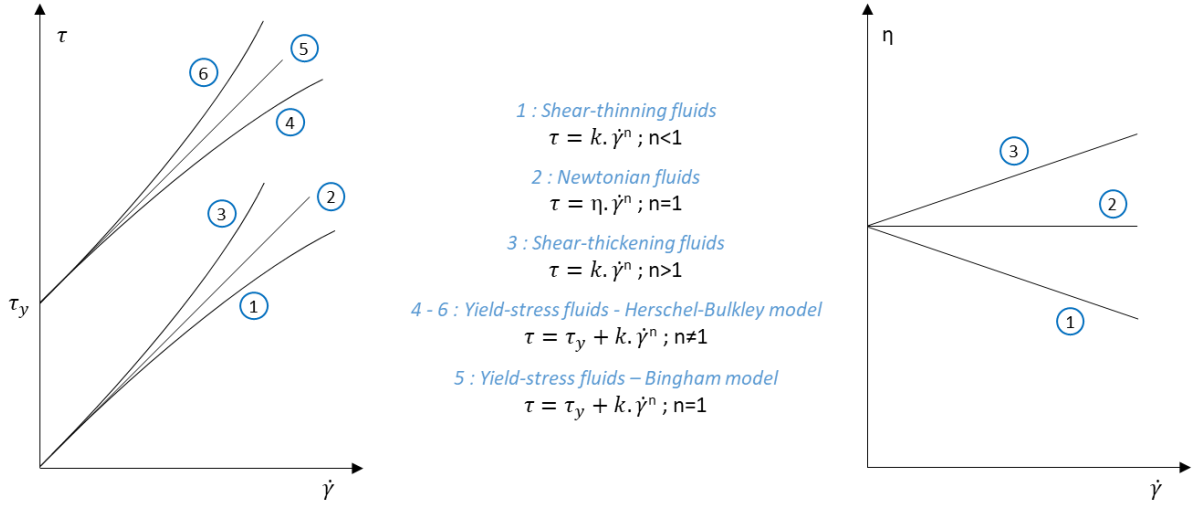

Figure 3: Schematic evolution of $\tau = f(\dot{\gamma})$ et $\eta = f(\dot{\gamma})$ for different complex fluids.

A fluid will be called Newtonian if its viscosity is independent from the shear rate it bears and, rigorously, if its extensional viscosity worth three time its shearing viscosity. A fluid will be called shear-thinning if its viscosity decreasing for an increasing shear rate, shear-thickening if its viscosity increases with the shear rate, and yield-stress fluid

if it flows only by reaching at least a critical stress. Some fluids show unstable viscosities upon a constant shear. After a resting time, these fluids can get back to their original state, or show hysteresis. These fluids are known as thixotropic fluids.

b. Viscoelastic properties: linear regime

Some materials present an organisation at a mesoscopic scale and can be characterized by elastic properties. These materials are called "viscoelastic materials". Their behaviour is intermediate to that of an elastic solid and a Newtonian viscous liquid. Because of their elastic properties, the structure of such materials continue to evolve at shear interruption because the material restores the harvested energy upon shearing. In order to characterize the viscoelastic properties of a fluid, we have to do the following experiment. Once again, we consider two parallel plates long enough to neglect edge effects, separated by a gap e. The material is place between both plates, one at rest and the second animated by an oscillatory motion along the x axis at a frequency f ($\omega = 2\pi f$) and an amplitude δL. This displacement correspond to an oscillating force along the x axis (Figure 4).

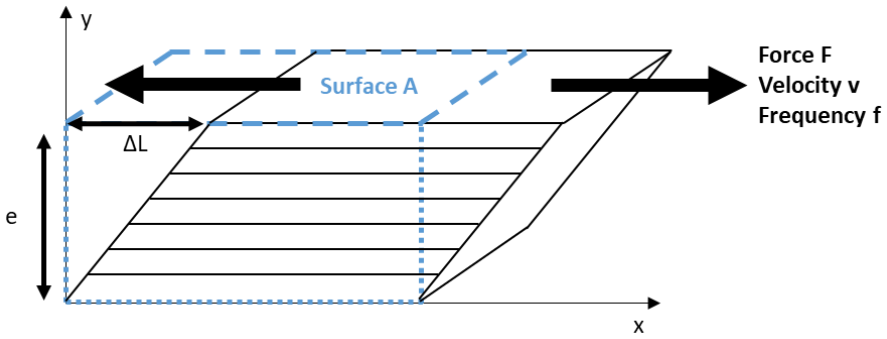

Figure 4: Simple oscillating deformation of a material between two parallel plates along X axis.

After a time t, the above plate has gone through a distance ΔL for its initial position. The shear deformation γ at time t is defined as the ratio between the distance travelled and thickness of the fluid element ($\gamma = \Delta L/e$). In this thought experiment, the deformation is a sinusoidal function of time, that is, under its complex form $\gamma(t) = \gamma_0 . \exp(i\omega t)$. Thus, the shear stress is also a sinusoidal function of time. However, it may be phase shifted from a value δ: $\tau(t) = \tau_0 . \exp(i\omega t + i\delta)$. The shear stress can be written as a function of the deformation as $\tau = G^* . \gamma$ with G^* the complex modulus expressed by two components: the elastic component G' called "elastic modulus" or "storage modulus" and the viscous component G'' called "loss modulus" or "viscous modulus", so that: $G^* = G' + iG''$. By separating both real and imaginary parts, we can express G' and G'' separately as: $G' = \frac{\sigma_0}{\gamma_0}\cos\delta$ and $G'' = \frac{\sigma_0}{\gamma_0}\sin\delta$. Also, working in the linear regime correspond to carry experiments under conditions where G' and G'' are constant and independent of τ_0 and γ_0 (Figure 5). In this regime, the structure of complex fluids are

not affected by the deformations applied to the material. It is only beyond the linear regime, i.e. beyond a critical deformation, that the material becomes unstructured.

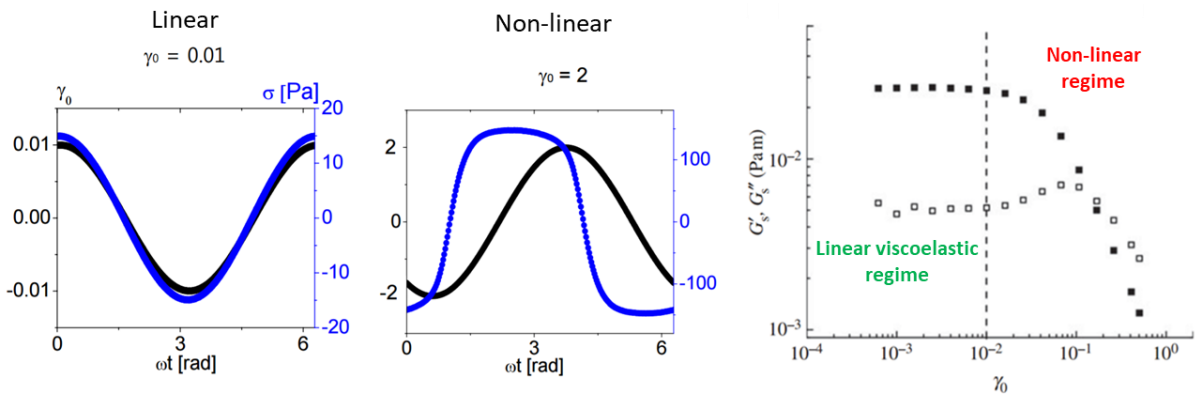

Figure 5: Characteristics of a non-linear experiment: for high deformations, the shear stress is not a sinusoidal function of time[4] [from Cloitre 2015] and G' and G'' depends on the deformation[5] [from McKinley 2012].

Materials always fit to one of the two following behaviours: either of a Newtonian liquid or an elastic solid behaviour. Simple Newtonian liquids have a zero elastic modulus and a loss modulus equal to the product of viscosity by pulsation ($\delta = 90°$). On the contrary, elastic solids have a zero loss modulus and a constant elastic modulus ($\delta = 0°$). Let's take the example of a purely viscous fluid for which the shear stress is proportional to the shear rate via the viscosity: $\tau = \eta\dot{\gamma}$. Since $\dot{\gamma} = \frac{d\gamma}{dt}$, by deriving we get $\tau = i\eta\gamma_0\omega\exp(i\omega t)$ hence $\tau = \eta\gamma_0\omega exp(i\omega t)\exp(^{i\pi}/_{2})$. A purely viscous fluid therefore has a phase shift $\delta = {}^{\pi}/_{2}$ and a stress $\tau_0 = \eta\gamma_0\omega$. By calculating G' and G'' we find $G' = 0$ and $G'' = \eta\omega$. By doing the same exercise with a purely elastic fluid, which means that according to the Hooke's law $\sigma = K\gamma$, we find $G' = K$ and $G'' = 0$. This is consistent with the definition of G' and G'' which correspond to the elastic and viscous terms of the fluid. Indeed, a purely elastic fluid does not have viscous component, whereas a purely viscous fluid has no elastic component.

c. *Experimental rheology*

Carrying the previous rheological measurements requires to set up experimental devices. The shear motions are generated by rotational rheometers equipped with different kind of geometries: Couette, parallel plates or cone and plate (Figure 6). In all cases, the sample is placed between the rotor (mobile part) and the stator (fixed part) of the rheometer. Even though these geometries are different from the theoretical ones we presented before, the rotational motion of the geometry is somehow similar to the infinite translation motion.

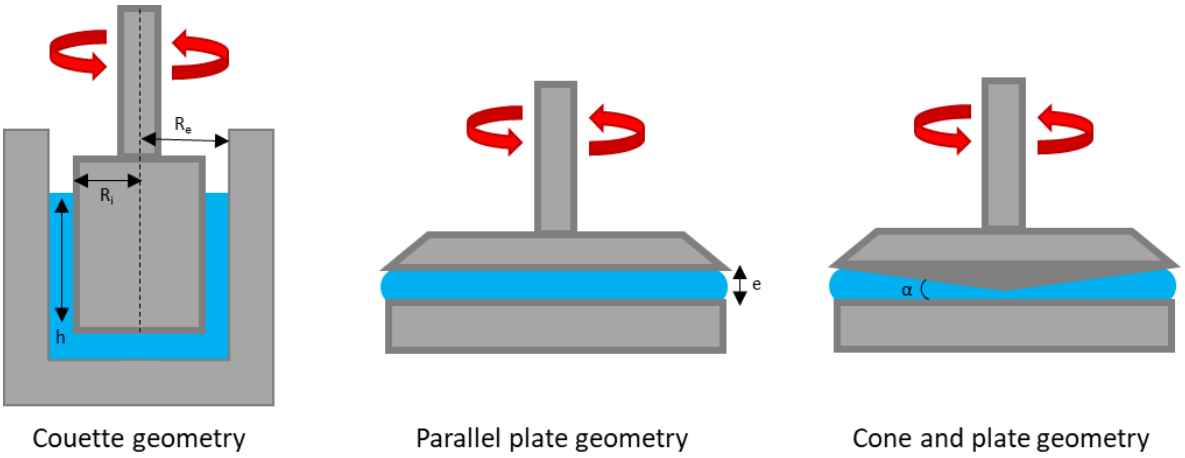

Figure 6: Schematic representation of Couette, parallel plate and Cone and plate geometries.

There are different kinds of rheometers, some are stress-imposed and others are deformation-imposed depending if the motor of the rheometer is in its head or in its core. Whichever is the rheometer, they both know the torque T delivered by the motor, the rotor angular rotation θ in the case of small deformations and the geometry rotational velocity Ω for large deformations. The formulas below should then be used to define a shear on a given surface and the stress exerted on that surface and relate them to the two measured parameters. By taking into account the symmetry of the flow, solving the equation of the conservation of the amount of motion makes it possible to obtain the stress field. It should be noted that this stress field is independent of the fluid under study. However, the stress may depend on the position in the geometry. To go further, it is necessary to be able to link the shear field to the torque and rotational speed parameters. This step is far from trivial and depends on the fluid being studied. Most rheometers at this stage make the following assumptions: the fluid is considered Newtonian, the fluid does not slip to the wall, and the flow is homogeneous and stationary. Under these assumptions, it is possible in each of the geometries to calculate an average stress and an average shear rate as a function of the two parameters C and Ω. The expressions of shear rates and apparent stresses are given in the Table 1 below[6].

	Couette	*Parallel plate*	*Cone and plate*
Shear rate $\dot{\gamma}$	$\dot{\gamma} = \frac{R_e \Omega}{R_e - R_i}$	$\dot{\gamma}_r = \frac{r\Omega}{e}$	$\dot{\gamma} = \frac{\Omega}{\alpha}$
Shear stress τ	$\tau = \frac{T}{2\pi {R_e}^2 h}$	$\tau_r = \frac{2T}{\pi R^3}$	$\tau = \frac{3T}{2\pi R^3}$

Table 1: Calculation methods used by the rheometer software to measure the shear rate and the shear stress for different geometries.

It should be noted that a more detailed analysis can be carried out either by taking into account the rheological law of the fluid (power law, yield stress fluid) or by applying Rabinowitsch's corrective formulas[7]. The choice of the different geometries depends on the viscosity of the fluid to be measured. In order to be in the torque range measurable or applicable by the rheometer, a parallel plate or cone and plate geometry with a small surface area for viscous fluids and a large surface Couette cell for low viscous fluids should be chosen. The cone and plate geometry is practical because the shear is constant throughout the entire cone gap. However, parallel plate geometry is often preferred over cone and plate geometry for the study of suspensions containing micrometric particles to avoid disturbances due to the low gap in the cone and plate geometry.

Figure 7: Photo of the rheometer in parallel plate geometry used in the laboratory. In order to make accurate measurements and avoid slippage, we use a hatched plane with a roughness of a few hundred microns.

In theory, rheometry is a particularly effective and accurate tool for measuring the response of soft material to stress. However, it is important to pay attention to different artefacts that are more or less independent of the measurement. For example, the presence of air bubbles in the sample and their evacuation during measurement may decrease the contact between the geometry and the sample. Similarly, at high shear rates - around 1000 s^{-1} - the sample can be ejected outside the geometry. These two phenomena can sometimes be observed with the naked eye, either by observing the condition of the sample before measurement or by observing the sample during measurement. Another artefact that is more difficult to spot is the slip. This is due to poor cohesion between the plane and the sample and can result in stagnation or even a decrease in the measured stress as the shear increases. In order to avoid this problem, and in order to have an accurate measurement, it is possible to use geometries with a rough surface [figure 8].

2. Rheology of complex fluids: presence of particles within a liquid phase

a. Definition of random close packing

The packing of particles is relevant to physicists, biologists, and engineers since packing fraction highly impacts the fluid properties. It is a key parameter to understand the flow of suspension. Let us discuss what happens when the concentration of particles is increased in a solvent.

- At low volume fraction (I), suspensions are diluted, the interactions between particles are low, and the rheological properties of the mixture are close to those of the continuous phase.
- At higher volume fraction (II), we enter a regime of a concentrated suspension in which particles begin to interact with each other.
- If we continue to increase the particle volume fraction, we obtain a stable packing where the viscosity starts to diverge at low shear rate giving birth to a low yield stress.

The minimal value of solid fraction allowing such a divergence of the viscosity is called the random loose packing[8]. Increasing the volume fraction of particles leads to the random close packing volume fraction. The random close packing (RCP) is an empirical parameter used to characterize the maximum volume fraction of solid objects φ_{RCP} obtained when they are packed randomly. At this volume fraction the particles are packed together in a configuration that does not optimize space to the maximum. Theoretically, the configuration that allows the better space optimization is the compact hexagonal packing which uses 74% of the space for perfectly spherical, hard and monodispersed spheres. However, experiments and computations shows that random close packing of such spheres is generally around 64% volume fraction[9,10].

The value of RCP is affected by the shape of the particles, and by the polydispersity of the sample. Using non-monodispersed and non-spherical solid particles, such as starch particles for example, gives a smaller random close packing volume fraction. Moreover, particles also interact with each other resulting in an interaction sphere larger than the particle size. The interaction shells around the particles are more or less large depending on the nature of the continuous phase, so the theoretical φ_{RCP} depends both on the nature of the particles and of the dispersant liquid.

Above the random close packing density, we obtain a regime in which there is not enough dispersant liquid to embed all particles. As in castles made of wet sand, the particles of such systems are linked by capillary bridges of liquid. This kind of mixture is generally inhomogeneous: it is hence called the “crumble state” (III). It is very difficult to carry rheological measurement on such materials because of the inhomogeneity within the system that lead to irrelevant measurements.

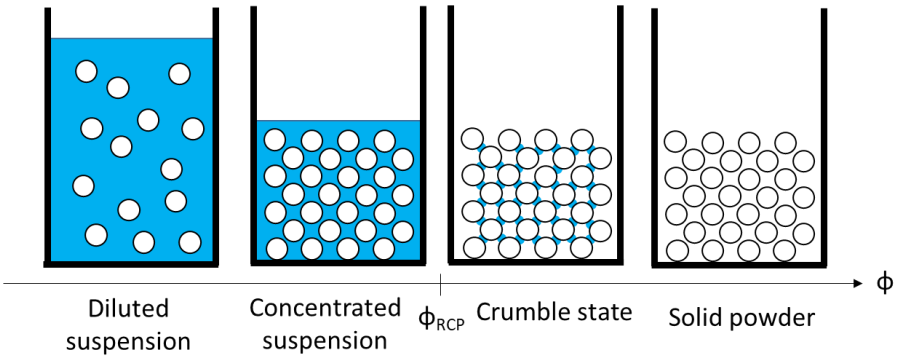

Figure 8: Schematic representation of steric obstruction within a suspension of solid particles in a solvent at different volume fractions

There are two main methods to measure the random close packing volume fraction of a system: the hand-made one, and the rheological one. The first method consists in progressively adding water to a known amount of starch powder stirred in a beaker. The goal of this experiment is to travel through the phase diagram in order to manually find the crumble state to concentrated suspension transition. The experiment is carried out in both ways (water in starch powder, or starch powder in water) in order to cross data and to get a precise measurement. By this method, we experimentally find the random close packing volume fraction of starch particles in water around 49%$_v$ and in glycerol around 54%$_v$. The second method consists in measuring the rheological properties of suspension at different volume fractions and in recording the minimum viscosity of the medium at the shear rate that gives rise to the shear-thickening behaviour. These viscosities can be plotted over the volume fraction using the Krieger-Dougherty model[11].

$$\eta = \eta_0 \left(1 - \frac{\varphi}{\varphi_{RCP}}\right)^{-[\eta]\varphi_{RCP}} \tag{1.1}$$

with η the viscosity of the medium, η_0 the viscosity of the continuous phase and $[\eta]$ the intrinsic viscosity.

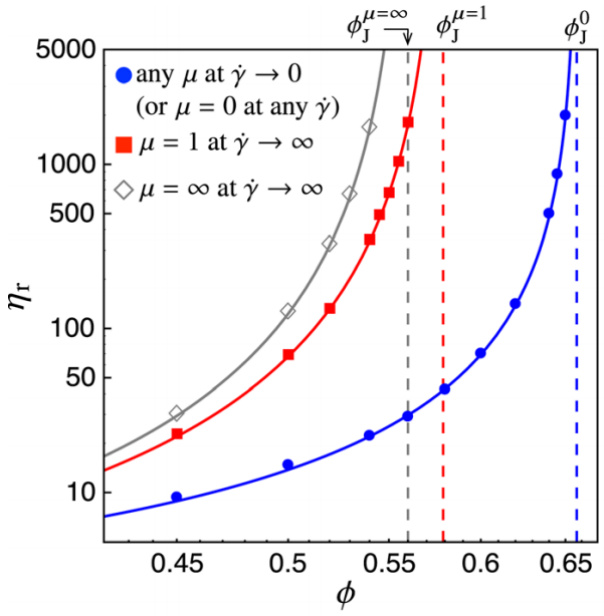

Figure 9: Relative viscosity ηr as a function of the volume fraction φ in the two limits $\dot{\gamma} \to 0$ and $\dot{\gamma} \to \infty$. The $\dot{\gamma} \to 0$ viscosity (circles) is independent of the friction coefficient μ as the friction is not activated at low stresses, which leads to a relatively lower viscosity diverging at a higher volume fraction φ_J^0 (which is the jamming point for frictionless systems). The $\dot{\gamma} \to \infty$ viscosity however directly depends on μ, as is seen from the difference between $\mu = 1$ (squares) and $\mu = \infty$ (diamonds) plots. In particular, the jamming volume fraction decreases with increasing μ. [From Mari et al. 2014][12]

Krieger-Dougherty's model finds a random close packing volume fraction at 50%v for the starch in water suspension, and 56%v for the starch in glycerol suspension. These results are really close to the results found by the hand-made method. It hence confirms that both methods are consistent and that the random close packing volume fractions are relevant for both continuous phase. One can note that the interacting shell around starch particles is thus larger in the case of water than in glycerol. From a formulation science point of view, it is clear now that if one desires to create a fluid complex formula, the volume fraction of particles should be kept as far as possible from the random close packing volume fraction.

b. Suspension of non-Brownian particles

Let us consider the complex fluids that we will have to study: dispersions, emulsions, gels and try to model their behaviour. Let's start by describing the suspensions of non-Brownian spherical particles. For these dispersions we will assume that particles only interact through solid contact forces (i.e. colloidal forces are neglected in this approach). This dispersion is characterized by 5 characteristic variables: the diameter of the particles, their density, the viscosity of the suspending fluid, the pressure and the shear rate. In this case we do not consider the forces of interaction between particles.

These quantities are expressed according to 3 types of dimensions i.e. mass, time, and force.

Thus, according to the Buckingham-Π theorem[13], all physical laws are expressed in terms of two dimensionless parameters. It is possible to choose a Iv number defined as the ratio of the characteristic time of a rearrangement η/P with η the viscosity of the suspending fluid and P the pressure, and the macroscopic characteristic time $1/\dot{\gamma}$ with $\dot{\gamma}$ the shear rate $Iv = \frac{\eta\dot{\gamma}}{P}$, and also the ratio between inertial forces and viscous forces: the Stokes number $St = \frac{\dot{\gamma}\rho a^2}{\eta}$. Within the limits of low Stokes numbers, the physical laws depend only on Iv. Thus we can write that $\tau = \mu(Iv)P, \phi = f(Iv)$ with τ the shear stress, P the pressure, ϕ the volume fraction of particles which is function of Iv. μ is a friction coefficient, taking into account the coefficient of solid friction between particles as well as a coefficient related to the stacking of the particles in relation to each other. Thus, we have $\tau = \mu(f^{-1}(\phi))\frac{\eta\dot{\gamma}}{f^{-1}(\phi)}$.

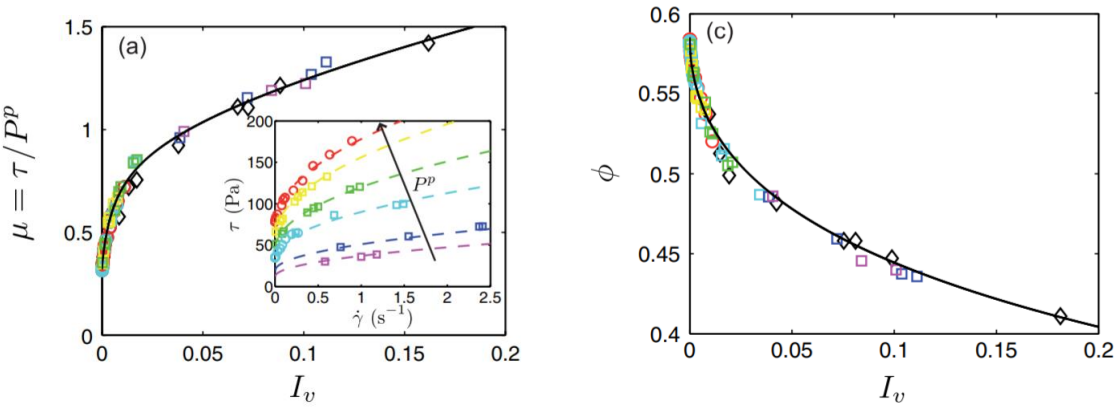

Figure 10: Friction coefficient μ and volume fraction ϕ as a function of the viscous number Iv. [From Pouliquen et al.[13]]

When the volume fraction distribution is homogeneous, a dispersion of non-Brownian particles with a low Stokes number is therefore Newtonian. Note that the system may appear non-Newtonian. Indeed, in the presence of even slight stress gradients, migration forces appear and induce variations in the particle fraction as a function of the shear rate. Non-Newtonian shear-thinning (i.e. suspension viscosity decreases when the shear rate is increased) or shear-thickening (i.e. suspension viscosity increases with the shear rate) behaviours are explained by the fact that these systems do not verify the initial assumptions of non-interaction between particles[13].

c. *Suspension of Brownian solid particles*

For particles sensitive to Brownian motion (i.e. micron-sized), since the motion of the particles is temperature dependent, the above analysis should take into account the Peclet number which is the ratio between the characteristic diffusion time and the flow time $Pe = \frac{6\pi\eta a^3\dot{\gamma}}{kbT}$. At low Peclet numbers, particles are subjected to Brownian motion

while they are non-Brownian at high shear rates. There is therefore a shear value beyond which the particles behave like non-Brownian particles. For lower shear rates, the particles are subjected to Brownian motion. Their spatial distribution is different, they take up more space, which results in a higher viscosity at low shear rates and therefore a shear-thinning behaviour. The viscosity of the suspension decreases as the shear rate increases.

d. Suspension of solid particles interacting with each other

In the presence of colloidal interactions between particles, it is also necessary to review the previous hypotheses. If these forces are repulsive, it is generally sufficient to replace the particle diameter with an effective diameter that takes into account the repulsive potential between particles. If these forces are attractive, the size to be taken into account in the analysis is not the particle size but the size of the aggregates.

The structure of the dispersion in the presence of colloidal forces may depend on the shear rate. For attractive particles, the shear stress can break the aggregates, resulting in shear-thinning behaviour. The attractive forces might be so high that an attractive gel is obtained exhibiting a yield stress. A greater stress than the yield stress must be applied for the system to flow. Applying this stress is like breaking these physical links between particles. Generally, the system does not recover its structure at rest, i.e. the rheological curve is different on the outward and return journey.

In other cases, in the presence of repulsive forces, the particles may become weaker than the particulate pressure forces[14]. The lubrication film between particles is broken at high shear rate. This results in a friction coefficient μ between particles that increases with the shear rate. The dispersion is therefore shear-thickening, as it is the case of starch particles or PVC marbles suspensions[15–17]. Depending on the volume fraction of particle, the shear-thickening effect can be either continuous or discontinuous[14]. For a low enough volume fraction, the viscosity increases smoothly with the shear rate, the shear-thickening is continuous. In such case, the effect is mainly due to the increasing friction in the lubrication film between particles. For higher volume fractions, increasing the shear rate make the shear stress to jump instead of increasing smoothly. This kind of jump is often attributed to the breakage of the lubrication film and to the formation of solid-solid frictional forces between particles[14].

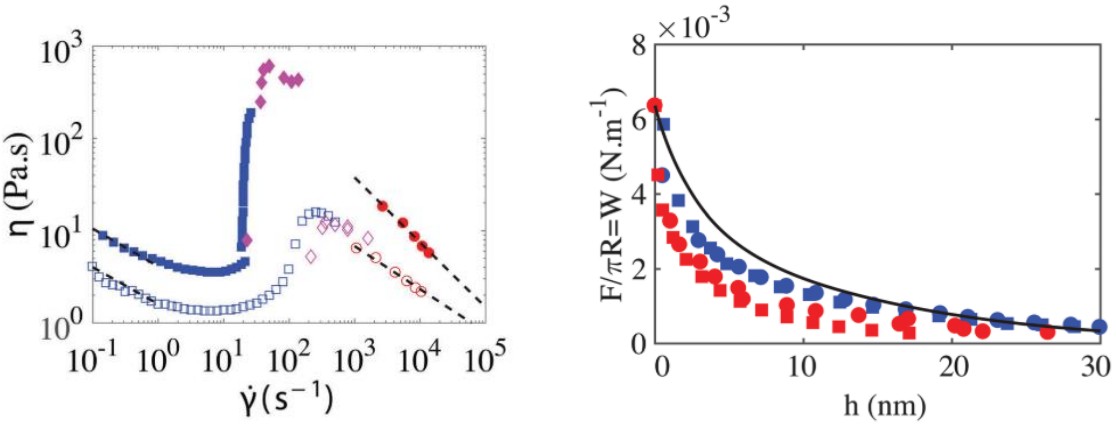

Figure 11: (left) Flow curves of 55‰ (open symbols) and 60‰ (closed symbols) PVC particles suspended in Dinch showing the different rhological behaviour of suspension as a function of the shear rate. (right) Impact of the distance between particles on their interaction potential. [From Chatté et al.[16]]

e. *Suspension of fluid particles*

Most of these behaviours will be found on fluid particles, i.e. diluted emulsion droplets. Only shear-thickening will not be observed[17,18] since the failure of a lubrication film corresponds to the coalescence of two droplets and therefore simply to the appearance of a larger drop. Thus the interactions between particles decrease and the G' decreases, resulting in the appearance of a shear-thinning phenomenon. Surface tension is an important parameter in this system, hence the use of a fourth dimensionless variable. This is the capillary number Ca which compares the viscous forces to the surface tension: $Ca = \frac{\dot{\gamma}\eta a}{\gamma}$ which allows to take into account the deformation of the droplets. At high droplets concentration, the droplets deform and a yield stress fluid is obtained. To flow, the droplets must deform to escape from the cage formed by the other droplets surrounding them. Unlike attractive gels, the droplet after rearrangement will fall back into another similar cage and thixotropic behaviour will not be observed, i.e. the rheological curve is identical for both directions.

Such phenomenon are also observed for carbopol gels. These are often considered as model yield-stress fluids since they present simple elastic responds to small applied stress and only start to flow once a critical stress is exceeded. They are often successfully described by the Herschel-Bulkley equation $\tau = \tau_y + k.\dot{\gamma}^n$. Nevertheless, a recent study showed that carbopol gels are not as model as many people believe they are. According to Bonn *et al.*, the preparation method of carbopol gels may create thixotropic materials[19]. The stirring time is reported as a major parameter in the creation of such materials as it is responsible of a slow breaking of the carbopol polymer chains over time. Small fragments of polymer exhibit Brownian motion and induce depletion interactions that lead to the formation of thixotropic gels. On the other hand, modified carbopol gels with attractive interactions also present such thixotropic behaviours.

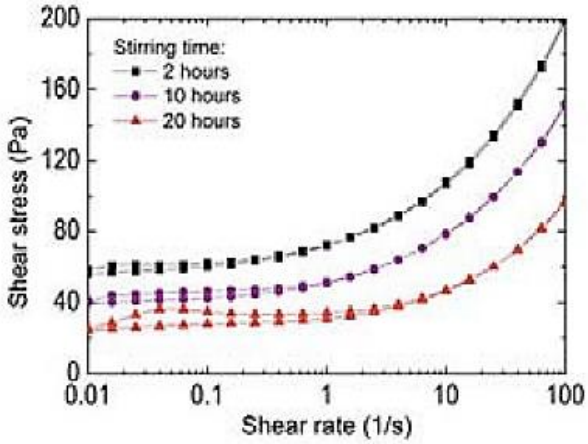

Figure 12: Flow curves of carbopol gels prepared with different times and showing an increasing thixotropic effect over time. [From Bonn et al.[19]]

f. Rheology in confined geometry

During the spreading experiment, complex fluids will be stressed into gaps whose typical size is in the order of magnitude of the particle size. First of all, we must note that in confined geometry the slip will have a very important impact. It will therefore be necessary to characterize this sliding speed in our approaches or at least check that it is weak due to the roughness of the set-up[20]. Moreover, as recently shown, confinement can reveal new behaviours. For example, it has been shown that the local viscosity of a concentrated emulsion depends on the size of the gap and the nature of the boundary conditions[21] (excluding slip problems). The fluidity model developed by Bocquet, Colin, Ajdari[22] accounts for this phenomenon. For an emulsion to flow, the drop must deform to get out of its cage. This requires a local microscopic constraint. When the rearrangement is done, this constraint is relaxed over the entire sample. Thus a rearrangement at a point J causes an increase in the local constraint at a point I. The rearranging probability of the drop in position I increases (Figure 13).

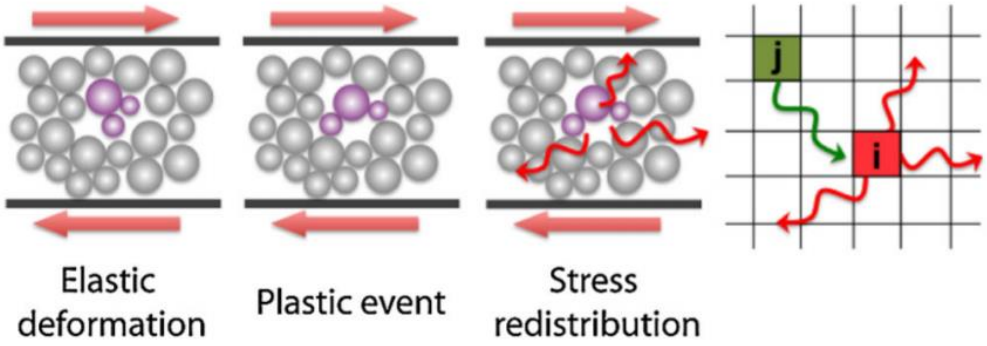

Figure 13: Redistribution of stresses following a ponctual plastic deformation [From Ajdari et al. 2009].

If the sample is subjected to a homogeneous overall stress and is infinite or large enough, this behaviour is not apparent. On the other hand, if the stress is not homogeneous, the active (high stress) zones will rearrange many times and will have an influence on the low stress zones which will have a higher rearrangement rate than if they were alone present and therefore a lower viscosity. These collaborative phenomena can be due to stress gradients but also induced by the walls. Rough walls can force rearrangements. Non-local behaviours are therefore particularly observable in confined geometry. It will therefore be important for our applications to analyse flow in geometries with low air gaps.

II. Coating surfaces with complex fluids

Coating surfaces with complex fluids is an everyday problem. Painting a wall, spreading butter on a slice of bread, spreading cement with a trowel or applying sun screen on skin are just a few examples. For all these application it is really important to understand how the coated film behaves during processing. In the following part we present a list of knowledge about coating experiments, and especially dip-coating and blade-coating.

1. Bases of wetting properties

a. Wetting properties in the static regime

By depositing a small amount of liquid on a solid surface, we observe that the liquid will spontaneously shape as a droplet more or less spherical. The behaviour of the deposited droplet depends on the wetting properties of the system. It represents the simplest thermodynamically spreading in a system where only gravity, surface tension and some eventual viscous forces apply. In our context, the wetting is the first scientific thematic that plays a role when it comes to put a cosmetic formulation in contact with skin. From a thermodynamical point of view, creating an interface costs energy. This energy is quantified by the surface tension symbolised by γ. It represents the energy required to create a specific length of interface, and is expressed in $N.m^{-1}$. By default, a liquid will shape as it costs the minimum amount of energy, so it will take the configuration in which the interface is the shortest. Since, the spherical shape is the one that allows the smallest surface/volume ratio, a levitating droplet will spontaneously take the shape of a perfect sphere to minimize its surface energy. The situation is a little bit more complicated in the case of a deposited droplet on a surface, since three different surface tensions has to be taken into account in this situation: the liquid/air, the liquid/solid and the solid/air interfaces and their surface tension, respectively γ_{LG}, γ_{SL} and γ_{SG}. Depending on these three surface tension the droplet will spread more or less on the substrate. A spreading coefficient, noted S, allows to predict the behaviour of the

droplet on the substrate by comparing if it is more favourable to create a solid/air interface than both a liquid/solid and a solid/gas interfaces simultaneously[23–25].

$$S = \gamma_{SG} - \gamma_{LG} - \gamma_{SL} \tag{1.2}$$

In strict logic, the surface tensions used in this equation take into account the thickness of the film which may differ from those measured with a macroscopic volume. If the spreading coefficient S is positive, whatever is the film thickness, the droplet will spread and form a molecular film. This is the situation total wetting. If S is negative, whatever the thickness of the film is, the droplet will never spread. At the beginning of the 19th century, Young has showed that the system will adopt an equilibrium angle θ_e (Figure 14) in order to equilibrate the forces applied on the droplet via the surface tension[26]. He has established the following equation linking surfaces tensions with the equilibrium contact angle.

$$\gamma_{SG} = \gamma_{SL} + \gamma_{LG} cos\theta_e \tag{1.3}$$

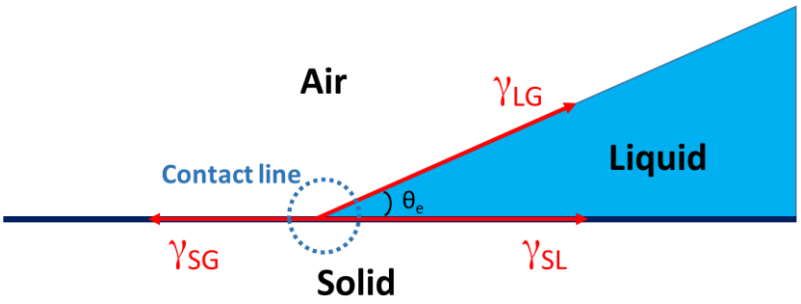

Figure 14: A contact line at the equilibrium and schematization of the surface tensions giving birth to a contact angle of equilibrium θ_e.

Based on the value of the contact angle θ_e, it is possible to quantify the wettability of a liquid on a surface. If the contact angle is zero, the liquid is totally wetting, on the contrary if the contact angle is 180°, the liquid is non-wetting. Then, if the contact angle is between 0° and 180° the wetting of the substrate by the liquid is partial. However if the sign of S depends on the film thickness, the wetting is called "pseudo-partial" (Figure 15). This situation is at the limit between partial wetting and total wetting, these liquids will create a nanometric liquid film on the whole surface of the substrate (if the total volume of the liquid allows it), but also a macroscopic droplet[27].

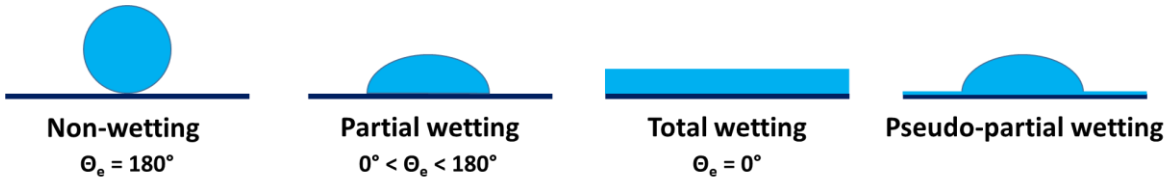

Figure 15: Different kinds of wetting depending on the contact angle θ_e.

For large volume, the shape of the droplet does not only depend on the surface tension. It also depends on the effect of gravity. Indeed, the surface tension effects have a finite range equivalent to the capillary length l_c. The capillary length is the distance from which the surface tensions effects are dominated by the gravity effects. From a macroscopic point of view, a curvature angle of the drop infinite, means that the capillary forces have no effect at this range. For most liquids, the capillary length is a few millimetres. The droplets that have a wider diameter than their capillary length present a constant thickness e, over the capillary effects, fixed by the value of the capillary length and the angle of contact (Figure 16).

$$l_c = \sqrt{\frac{\gamma}{\rho g}} \qquad e = 2l_c sin\left(\frac{\theta_e}{2}\right) \qquad (1.4)\ \&\ (1.5)$$

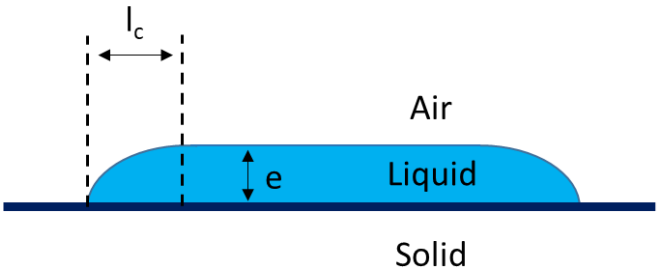

Figure 16: Highlighting of the capillary length on a wide droplet.

b. Wetting properties in the dynamic regime

Considering the wetting properties in their dynamic regime is equivalent to observe the contact angle formed by the liquid when it is moving on a surface. When a droplet flows along a sloping surface, the capillary forces caused by the surface tension – which was dominant at rest – become in competition against viscous forces induces by the motion of the fluid. From a microscopic point of view, we observe a contact angle that does not respect the Young's prediction. Depending if the motion applied to the droplet is positive or negative, we can observe two different angles:

the advancing and the receding angles, respectively θ_a and θ_r (Figure 17a). Once again, the wettability is crucial to understand the dynamic wetting phenomena.

For example, a perfectly non-wetting liquid deposited on a smooth sloping surface will adopt a spherical shape and flow freely downward the surface. On the contrary a perfectly wetting liquid will tend to spread on the smooth sloping surface hardly flowing downward since its receding contact line will stick to the surface. This is in the case of a partially wetting liquid that dynamic contact angles play specific roles. If the droplet moves at a velocity U, the advancing contact angle will also sustain a velocity U, however the receding contact angle will sustain an equal but opposite velocity $-U$. Some studies reported that the dynamic contact angles depend on the velocity U applied to the droplet: the higher the velocity, the more the dynamic contact angles diverge[28–30]. It is possible to determine a limit value for the advancing and receding contact angle at zero speed, however they are still separated by a hysteresis resulting by the equilibrium between gravitational and capillary forces if the surface is not plane (Figure 17b). For a plane surface, both advancing and receding contact angles will be equal to the equilibrium contact angle θ_e predicted by Young's law. A specific case has to be noted for rough surfaces. Indeed, we observe that the contact line of partially wetting liquids ($0° < \theta < 180°$) tends to remain stuck as a perfectly wetting liquid would have done on a smooth surface. Hence, we can consider that a partially wetting liquid on a rough surface will behave as a perfectly wetting liquid on a smooth surface.

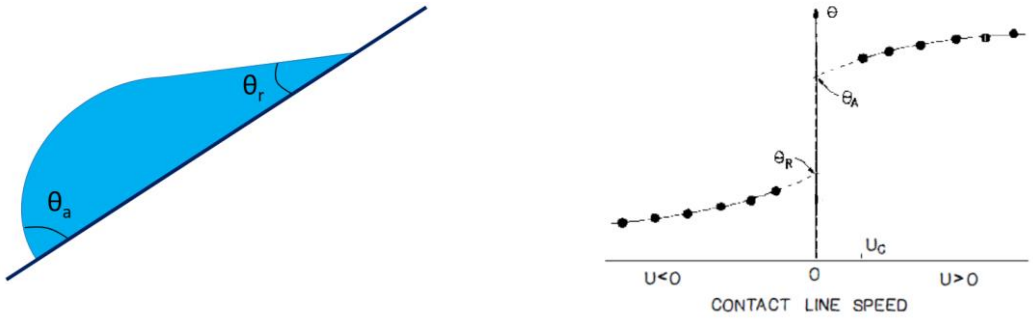

Figure 17: Representation of advancing and receding contact angles (on the left), the hysteresis separating them and their trending evolutions depending on the contact line velocity[31] *(on the right) [from Dussan 1979].*

Actually, the velocity parameter is not precise enough to describe correctly the hydrodynamic phenomena because it does not take into account the intrinsic characteristics of the considered fluid. A dimensionless number called the "capillary number" proportional to the velocity allows to consider the viscosity of the fluid η and its surface tension γ[32]:

$$Ca = \frac{U\eta}{\gamma} \tag{1.6}$$

The literature reports that the shape of a partially wetting droplet varies with its motion velocity, but more precisely, with its capillary number[28–30]. For low capillary number, a partially wetting droplet will keep its spherical shape because the surface tensions effect dominates those of the viscosity and counter the deformation of the liquid surface and the creation of a higher surface of contact. By increasing the capillary number, the shape of the droplet will start to deform because the viscous forces effect will become less negligible. The receding contact line may deform to adopt a sharper shape which will continue to deform with higher capillary number in the shape of an unstable rivulet giving birth to a droplet path via the Plateau-Rayleigh instability (Figure 18).

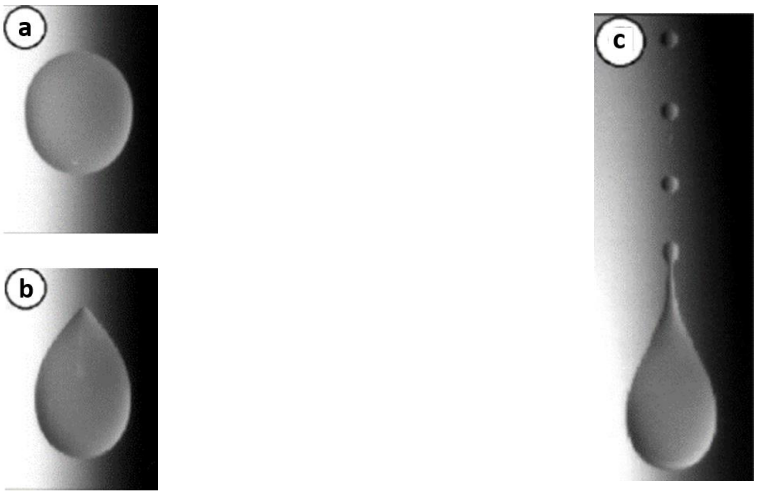

Figure 18: Different shapes of flowing droplets downward a sloping substrate for increasing capillary numbers. (a. Round droplet, b. Droplet deformed by the receding contact line in a sharp shape, c. droplet ending in an unstable rivulet forming a path of small droplets) [From Podgorski 2005].

2. Dip-coating: Landau-Levich's case of reference

a. *Landau-Levich's transition for Newtonian fluids: Critical velocity*

Similarly to a droplet of liquid that forms a contact angle on a substrate, a bath of the same liquid will also wet a dipped plate and form an equilibrium contact of the value θ_e. Accordingly, the surface of the bath is deformed by the presence of

the plate for a length corresponding to the capillary length, hence, a meniscus is created (Figure 19).

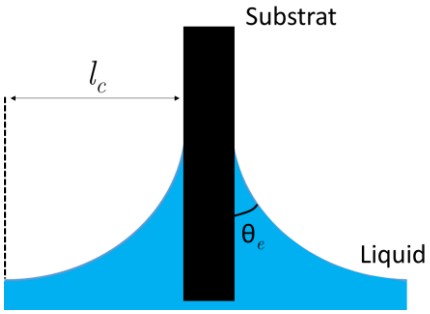

Figure 19: Deformation of the surface of a liquid bath by a plate dipped within the liquid.

As well as the experiment of the flowing droplet along a sloping plate, if the dipped plate is pulled out of the liquid bath, the system can adopt different behaviours depending on the withdrawing velocity, the viscosity of the fluid and the wettability of the substrate. A non-wetting liquid creates an inversed meniscus and will never stick to the surface. On the contrary, a perfectly or partially-wetting liquid on a rough plate will be dragged out of the liquid bath whatever the withdrawing velocity is. One more time, an intermediate case is adopted by the partially-wetting liquids on smooth substrates. During the withdrawing of the plate out of the bath, the meniscus endures a deformation, becomes higher and higher and the equilibrium contact angle θ_e will decrease and become a receding angle of contact under the effect of the withdrawing velocity. If the capillary number is sufficiently high, the viscous forces are stronger than the gravity and capillary forces which induce that the liquid is dragged out of the bath by the withdrawing plate. In this case, the meniscus does not equilibrate at an equilibrium height and a liquid film is formed on the plate. Consequently, a critical capillary number that splits the regime in which a stationary meniscus is observed to the regime that forms a film on the plate exists (Figure 20).

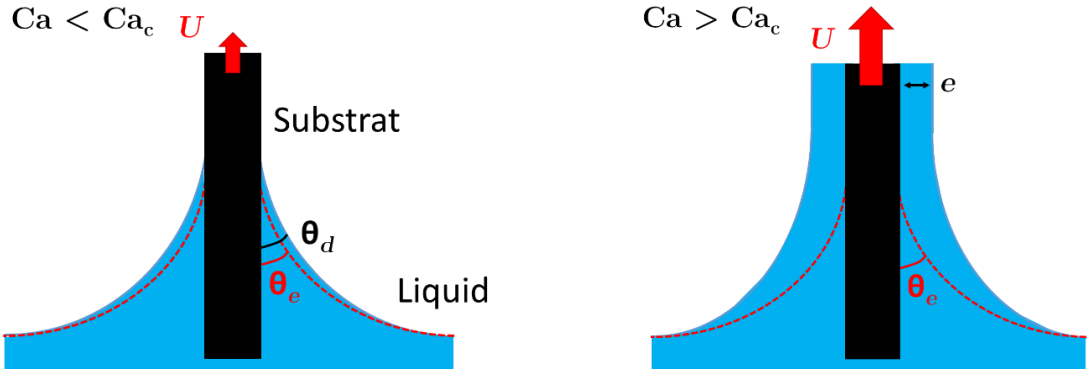

Figure 20: Highlighting of the Landau-Levich transition due to the rising of the substrate at a withdrawing velocity U. Case of a stationary meniscus (on the left) and of a dragged liquid film (on the right).

In 1922, Ward and Goucher[32] were the first to carry experiments onto this subject and observed a linked between the dragging velocity and the thickness of the dragged film. However, no clear theoretical model has been established between these two parameters in this study. It has been twenty years later, by Landau and Levich in 1942[33], and Derjaguin in 1943[34] that the first theoretical studies based on viscous and capillary forces have started to give a relation between the thickness of the film and the capillary number. Similarly to the flowing droplet, different shapes of the receding contact line are observed depending on the capillary number (Figure 21).

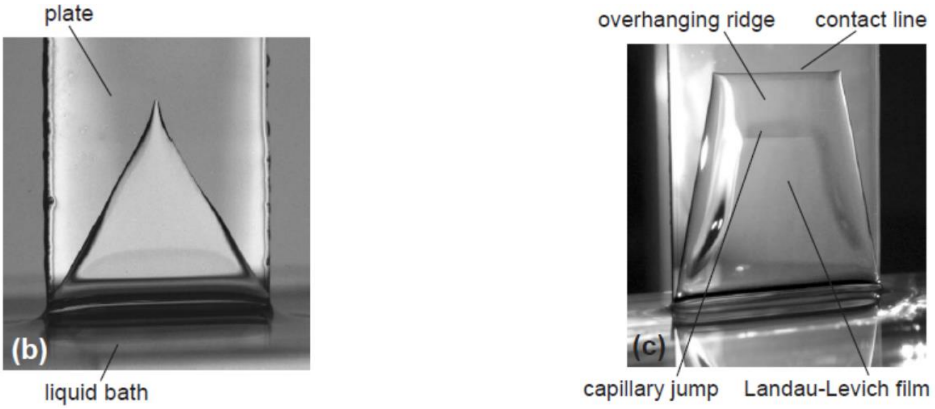

Figure 21: Different shapes observed upon dragging a plate out of a liquid bath at increasing velocities. b. static meniscus ($Ca<Ca_c$), c. dragging of a liquid film ($Ca>Ca_c$). The dragged film shows a buldge close to the contact line. [From Delon 2008].

Most bibliographic reports dealing with the dynamic Landau-Levich transition agree to claim that the receding contact angle, during dragging the plate, decreases for an increasing velocity[35–42]. The simple models wrote by de Gennes[43,44] and Cox-Voïnov[35,36] aren't able to predict the receding contact angle and its evolution close to the transition[45]. Indeed, they do not describe the whole hydrodynamic within the film and take into account an apparent contact angle which may locally vary. The more recent modelling of Andreotti[46] describes a consistent variation, i.e, a receding contact angle not equal to 0 at the transition and it varies with the capillary number close to transition. Experimentally, Andreotti has shown that for a liquid that wets a substrate with a contact angle of 35° the critical capillary number Ca_c is $9x10^{-3}$.

b. Landau-Levich's transition for Newtonian fluids: Film thickness

The description of the film is simpler. The Landau-Levich film, also called dynamic meniscus, formed for sufficiently high capillary numbers or for wetting fluids, has an unknown height l and a thickness e and is pretty well described. We can write the following equations:

$$F_{viscous} \sim F_{capillary} + F_{gravity} \rightarrow \frac{\eta U}{e^2} \sim \frac{\gamma k}{l} + \rho g \qquad (1.7)$$

The viscous forces per unit volume are expressed as $\eta . U/e^2$ with η and U are respectively the viscosity of the liquid and the velocity of the withdrawing plate. Following the Landau and Levich hypothesis claiming that the curvature of the dynamic meniscus is close to that of the static meniscus, it is possible to describe the curvature of the meniscus as κ, which represents the inverse of the capillary length l_c. We thus have an expression to describe capillary forces as $\gamma\kappa/l$. Finally, the gravity forces only depend on the density and the gravitational force, ρg. From these equations, it is possible to determine two fields of predominance. For capillary numbers higher than Ca_c but smaller than 1, one can consider the capillary number as negligible comparing to the capillary forces. In this visco-capillary field, the film thickness is described as:

$$e \sim l_c Ca^{2/3} \tag{1.8}$$

The quicker the plate is withdrawn, the higher the film thickness is. Thus, in the second predominance field in which the capillary number is higher than 1, the gravity effects cannot be neglected anymore. In that visco-gravitary field, ρg is at the same order of magnitude as $\gamma\kappa/l$. In 1964 Derjaguin expressed the thickness with the following law[47]:

$$e \sim l_c Ca^{1/2} \tag{1.9}$$

With an experimental set-up close of that of Landau and Levich, Ruschak and Blake[48] has shown in 1979 that it was impossible to increase infinitely the withdrawing velocity of the film. Similarly to the flowing droplet [Figure 18.c.], above a specific velocity the receding contact line destabilizes and forms a droplet path behind it. The maximum thickness that we can obtain by dip coating is then limited by this maximum velocity.

c. Dip-coating of complex fluids

Many studies have been carried out on the dip-coating of complex fluids, including a large part on yield-stress fluids in Coussot's laboratory. Previous studies performed by Coussot and co-workers deal with rough surfaces. This implies that the surfaces may be considered as wetting surfaces and therefore, a liquid film is dragged whatever the withdrawing velocity is. We previously mentioned that a yield-stress fluid behaves like a solid if the applied shear stress is low, and like a liquid once the applied shear stress exceed the yield stress. Unlike Landau and Levich's example, in which the experiment is performed on Newtonian liquids, most of the yield-stress fluid bath is in its solid state.

Coussot showed that the fluid recirculation in the bath due to the extraction of the plate from the yield-stress fluid bath was drastically reduced compared to that of a Newtonian liquid [Figure 22]. By observing the flows within the fluid, he was able to determine a frontier between the liquid zone and the solid zone of the yield-stress fluid and found that the thickness of this liquid layer does not depend on the drawing speed[49,50]. Unlike Newtonian fluids, the film formed by yield-stress fluids will return to its solid state once it has been removed from the bath. Indeed, in the bath the gel in contact with the substrate is fluidized because it bears a shear stress higher than the yield stress of the fluid. Once outside the bath, the shear became zero and the gel turns back to a solid. Thus, in the event that the fluid does not slide along the substrate, a static film is formed on the substrate.

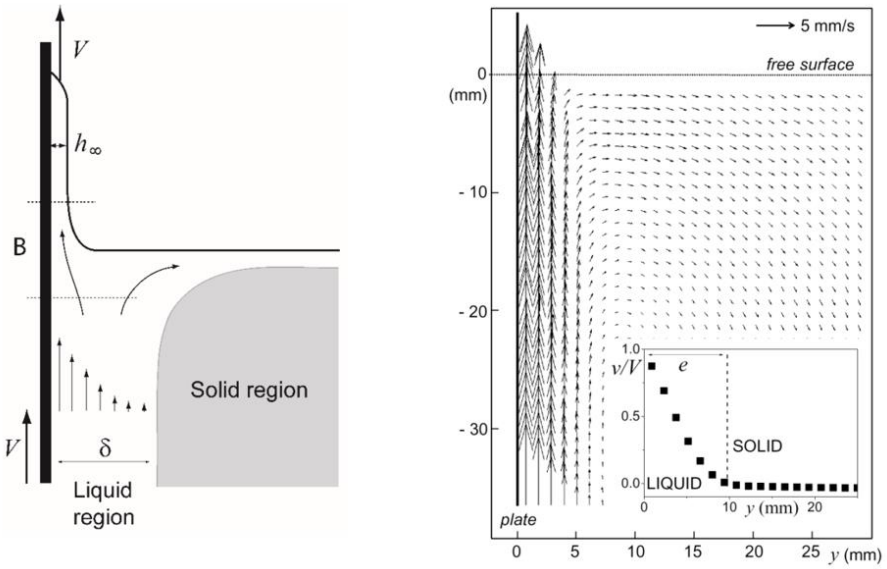

Figure 22: Schematic representation of liquid and solid thicknesses of a yield-stress fluid upon a dip-coating experiment (on the left). Rate of material flow within a carbopol gel (τ_y~34 Pa) upon a dip-coating experiment (on the right). The insert gives the normalized velocity depending on the distance to the plate [from Coussot 2014].

Coussot and collaborators used hydrophobic sandpaper to prevent slipping. Thus, with a rough substrate, he was able to show that the thickness coated during dip-coating of the carbopol gel is proportional to the gel yield stress and depends very little on the withdrawing velocity (Figure 23)[51]. The reported values are however striking. They increase with the yield stress but are much smaller than the thickness that may remain on the rod and may not drain in presence of gravity. The final thickness does not correspond to the maximum possible thickness associated with a simple free surface flow under gravity.

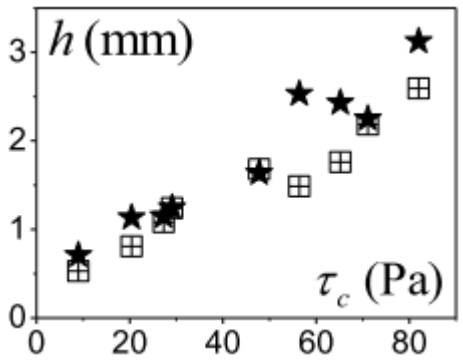

Figure 23: Relation between the yield stress of carbopol gels and the coated thickness by dip-coating of a rough substrate. (squares v = 1 mm/s, stars v = 10 mm/s) [from Coussot 2014].

3. Blade Coating

Blade-coating is a method commonly used to create thin films of controlled thickness on a surface. Interestingly, we will see that blade coating allows a greater flexibility to adjust the thickness of the desired film than dip coating.

a. Creating a film using blade-coating methods

The literature reports many different blade-coating set-ups, such as blade-over-a-roll coating[52–55], slot coating[56–58], roll coating[59–61] or blade coating[62–66] (Figure 24). All of these set-ups implement a static scraper spreading a liquid film over a moving substrate. Even though these set-ups are similar, they differ in the understanding of the material spreading and flow under the scraper, and also in the determination of the film thickness behind the scrapper. The slot-coating is a pre-metering system: the film thickness only depends on the mass flow under the blade but is independent of the scraping velocity or the viscosity of the liquid. Other set-ups are self-metering: the film thickness is fixed by both the viscosity and the scraping velocity, but also by the geometry of the system, and specifically, by the angle that the blade forms with the substrate. We will be furtherly interested in self-metering systems. However, as the soft-blade coating system is very specific, we will not consider it in the following generalities. In the event that we discuss these systems, we will make this clear.

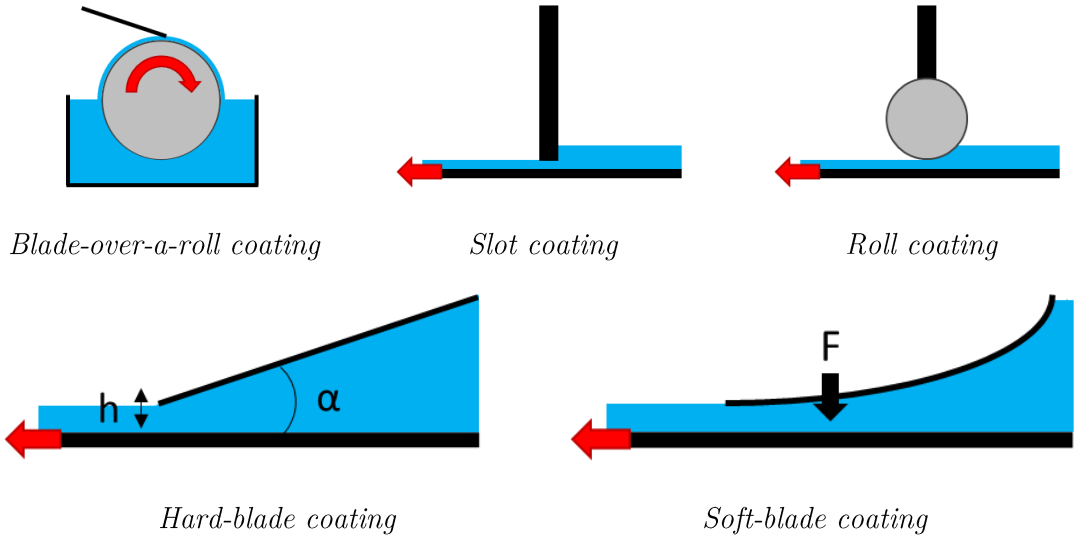

Figure 24: Schematic representation of blade-coating set-ups

First of all, researchers found that the behaviour of fluids during scraping is not that different of what we explained before for dip-coating experiments. Especially at low velocity for partially wetting fluids, they found that the liquid film is formed only if the scraping velocity is above a critical velocity. Based on a blade-coating system Deblais[67] et al. confirmed that it was necessary to exceed a critical capillary number to form the film, which is consistent with the previous results of Andreotti[46] for dip-coating systems. Deblais et al. also wrote an expression that allows to predict the critical capillary number depending of the fluid. The number does not depend on the rheology of the fluid, but only on its equilibrium contact angle on the surface θ_e, the capillary length l_c and the molecular length l'.

$$Ca_c = \frac{{\theta_e}^3}{9ln\frac{l_c}{l'}} \tag{1.10}$$

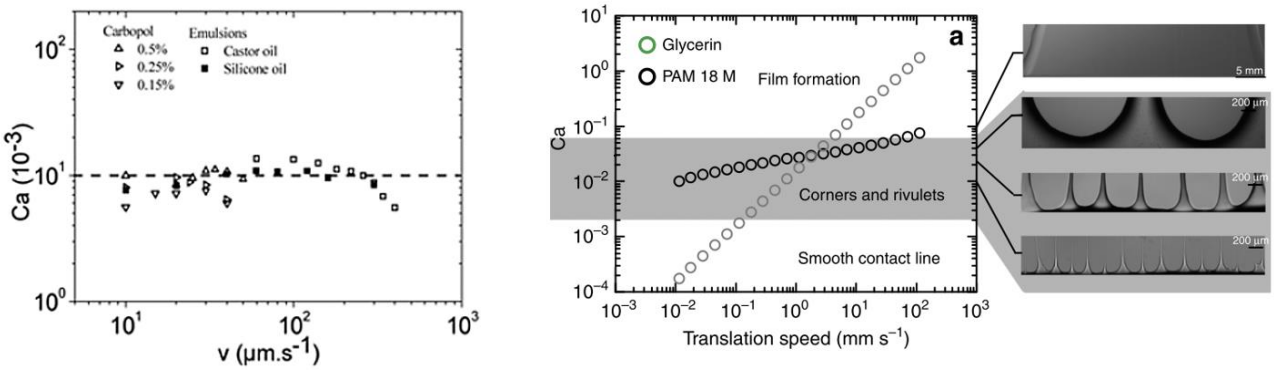

Figure 25: Critical capillary number required to form the liquid film as a function of the scraping velocity (on the left). Shape of the deposit obtained by blade-coating with a flexible blade as a function of the capillary number (right) [From Deblais et al. 2016].

However, in the case of an established film (i.e. $Ca > Ca_c$), the literature reports that the fluid rheology has a non-negligible impact on the thickness of the formed film. This is what we present in the following.

b. Blade coating of Newtonian fluids

After few millimetres behind the scrapper, the thickness of the film formed by the coating of a Newtonian fluid with a hard scrapper is constant along the surface. The film thickness is always smaller than the gap fixed between the scraper and the substrate but it is never lower than the half of its height. As we noted before, the film thickness is fixed by different parameters and especially by the characteristics of the rigid scraper[66]. For blade-over-roll systems, it has been confirmed by theoretical studies that the film thickness does not depend either on the scraping velocity[53,55], neither on the viscosity[52] of the fluid but the thickness increases with the width of the blade and with the diminution of its angle with the substrate.

For flexible blades, the behaviour is quite different. Indeed, for rigid blade, only the tilt of the blade and its height is tuneable. For flexible blade, the tip of the blade is always in contact with the substrate, so the gap cannot be fixed at another height than zero. In addition of that, the blade will apply an axial pressure on the substrate depending on the height of the hanging point, the tilt of the blade and its rigidity. Thus, with a flexible blade and a flexible substrate, Schmidt et al. showed that the thickness was smaller than expected[63]. On the other hand, by using flexible blade over a hard substrate Seiwert[64] recently proved that the film thickness increases with both the scraping velocity, the viscosity of the fluid, the length of the blade L and decreases with the blade rigidity B as:

$$h_{max} \sim L \left(\frac{\eta V L^2}{B} \right)^{3/4} \tag{1.11}$$

This result is very interesting because the thickness of the film under these conditions is fixed by an elastic capillary number. In this case, viscous forces tend to form the film while the elasticity of the blade tends to avoid it. This is really close to what was observed by Landau-Levich in the dip-coating configuration, except that the capillary forces of the meniscus are replaced by the elastic force of the blade. However, in both cases, the formation of the film is still controlled by the competition between viscous forces and capillary or elastic forces.

c. Blade coating of purely viscous non-Newtonian fluids

Coating purely viscous non-Newtonian fluids using a blade-over-roll coating set-up gives similar physical laws than what was described for Newtonian liquids. The film thickness has the same variation with the blade width and its angle with the substrate.

However experiments and theoretical approaches claim[52–54,59] that the film is thicker than in the case of non-Newtonian fluids since the film thickness increases for a smaller shear-thinning rheological parameter n. Another feature is that the film thickness decreases slightly for an increasing velocity.

d. Blade coating of viscoelastic fluids

Viscoelastic fluids aren't the simplest to understand since they show both viscous and elastic impacts that can give opposing contributions. More precisely high viscosity may hide elastic effects because of long relaxation times. By studying Boger fluids which are close to be purely elastic fluids (their viscosity is almost constant with a variating shear rate) Sullivan et al. explained that the elasticity of the fluid induces a diminution of the film thickness. This diminution can lead to thinner films than those observed in the Newtonian case if the viscosity is sufficiently low[52,53]. Mitsoulis' numerical works[55] confirms that the viscosity contribution of viscoelastic fluids leads to a higher film thickness while the diminution is actually due to the elastic contribution. Similarly to purely viscous non-Newtonian fluids the film thickness also decreases with an increasing scraping velocity. However, the behaviour of such liquids under a scraper is complex and there are still a lot of question about it. Davard and Dupuis[62] visualized the current lines under the blade and, even though there study are qualitative, they confirm the prediction established 25 years before by Sullivan about the role the viscosity and the elasticity play. Once again, the quantity of fluid found under and in front of the blade depends on the fluid rheology and the angle made by the blade with the substrate. Depending on the conditions, they were able to see dead areas where the liquid has a zero velocity, and even reverse flow in some cases (Figure 26). Thus, the visualization also reveals that the lubrication hypothesis is not valid since the flows has to be consider in both directions.

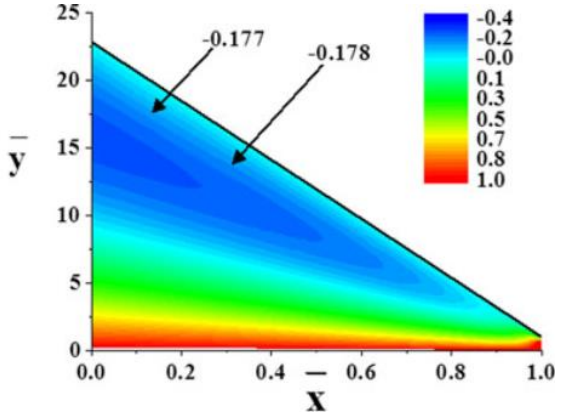

Figure 26: Flow velocity of a carbopol gel in a blade coating experiment (α=5°, h=0.6mm, v=0.167m/s, τ_y=570Pa) [From Yarin 2016][68]

The case of blade coating of yield-stress fluids is not the one that has been most studied. However, Sofou and Misouli's theoretical studies[61] extended to yield-stress fluids predict a behaviour relatively similar to that of purely shear-thinning fluids in relation

to the thickness of the film formed since the thickness increases when n decreases. Using a slot-coating system, Maillard[58] showed that unlike other liquids, yield-stress fluids such as carbopol gave a greater film thickness by a factor of 1.1 compared to the height of the gap between the scraper and the substrate, which highlights the elastic solid properties of the carbopol. In parallel, Deblais showed that the film did not form under all conditions and confirmed that a capillary number has to be exceeded for the blade coating of yield stress fluids[67]. On the other hand, he also showed the impact of the blade coating process with a rigid blade on an emulsion. If the spreading velocity and the gap are large enough the emulsion spreads, however if the gap is too small the emulsion can destabilize and reverse under the effect of shear stresses (Figure 27)[65].

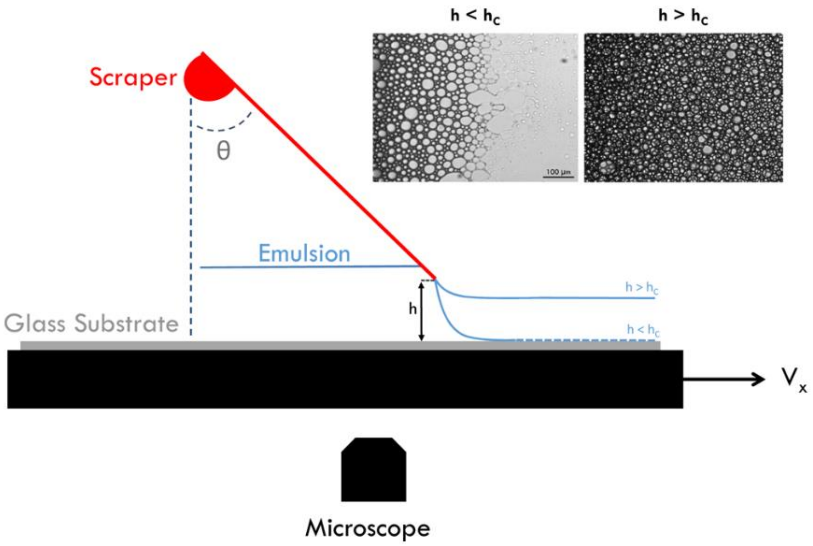

Figure 27: Blade-coating of emulsion with a rigid blade. Pictures show the structure of the emulsion that have reversed in the gap of low gap height.

III. Outline of this thesis

The previous bibliographic study shows that the spreading of Newtonian fluids has been studied in many wetting and non-wetting conditions. The spreading of complex fluids, however, remains a widely open academic problem. This question is central to my thesis.

For cosmetic applications, it is important to understand how a cosmetic product spreads. Cosmetic products must fulfil their roles which can be very varied. In most cases the quality of the deposit formed on the skin is a key parameter. For example, a suncare product is efficient only if the skin is uniformly covered by a film of constant thickness. The active matters inside the product play their role afterward. It is therefore fundamental to understand the mechanism of spreading to be able through the formulation to modify the parameters which govern the homogeneity and the thickness of the deposit, as well as the instabilities during spreading. The most relevant set-up

remains the blade coating with a soft blade since the blade is able to deform under the stress as the finger would do during realistic applications. Moreover, as far we know, no studies have been done to predict the film thickness of complex fluids using this geometry. Thus, there is a room for investigation in this field of sciences which is interesting for both academic and industrial interests.

Following this introduction, in a second part, we will focus on the preparation of simplex systems representative of cosmetic formulations. Therefore, we will describe:

- The rheology of simple systems

- The impact of the presence of particles on the rheology of a carbopol gel

- The behaviour of starch particles in solution over time.

From an industrial point of view, this second part will provide conclusions on the impact of certain formulation ingredients on the behaviour of the formulated mixture. It is an experimental part showing fundamental phenomenon that could be used as key parameters in formulation sciences.

In a third part, we will discuss the theme of dip coating of complex fluids, which has many academic and industrial interests. Therefore, we will investigate:

- How we can predict the thickness of the film formed during a dip coating experiment and what are the main parameters that determine it

- How the complex flow within the bath looks like

- The validity limits of the model we have established

- We will place our research in the framework of Coussot's studies[50].

For cosmetic applications, the main question is "How can we maximize the amount of material entrained when removing a brush from the inside of a tube filled with mascara?" Thanks to our model, we provide a phenomenological answer to this question.

In a fourth part, we will develop the case of blade coating of complex fluids with a soft blade. Academically, it is a configuration that is very little studied, so the field of investigation is free. We will therefore seek to:

- Understand the interaction between the elasticity of the blade and the viscous stress of the fluid during spreading

- Create a law that allows us to predict the thickness of the film formed based on key experimental parameters

- Describe the flow of fluid under the blade

- Predict areas of instability due to poor fluid recirculation under the blade

- We will place our research in the framework of Seiwert's studies[69].

Industrially, it is important to understand the parameters that govern the amount of material deposited during spreading. In this way, we can optimize the quantities of active ingredient to be used to improve formulation performance. Similarly, predicting instabilities prevents the formation of holes in the deposit that drastically reduce the activity surface of the applied product.

Finally, in a last part, we will study the formation of spreading defects during an application in the form of back and forth movements. We will try to explain:

- The formation of striations parallel and perpendicular to the movement during the spreading of simplex systems.

- The impact of shear thickening effects on the quality of the deposit.

- The impact of the formulation and quantity of particles on the nature of the deposit formed.

- The impact of the surface of the applicator and substrate and the normal force on the ability to release a pre-established dry film.

Each of these issues are directly related to the industry. As we pointed out, one of the major problems when spreading cosmetics is the formation of spreading defects, i.e. heterogeneities, holes, aggregates of matter. In this study, we try to understand which parameters to use to avoid the formation of these defects.

Take home message – Chapter 1

The coating systems have been widely investigated in the literature, both for Newtonian and non-Newtonian fluids. Understanding coating of fluids relates to wetting and rheological problems. In this first chapter we report:

a. Basic rheological features of Newtonian and non-Newtonian fluids and how they are measured. We get back to pre-required rheology knowledge and head to complex behaviours of highly concentrated suspensions in which particles interact with each other, based on the literature.

b. Different coating systems and how films of liquid are established. We investigated the literature surrounding both dip and blade coating systems and explored the known parameters that determine the thickness of the coated films depending on the geometry.

We observed that there were room for investigation in such scientific fields. For example, only empirical laws have been written on the prediction of the thickness of the films formed by dip coating of yield-stress fluids. On the other hand, no study was done on the blade coating of yield-stress fluids using a flexible blade. These thematic are of major interest for industrial applications, so we decided to further investigate the science around it.

Chapter 2

Rheology of a model cosmetic system

Summary: In this chapter, we focus on the preparation of a model cosmetic system. The material we prepare is made of a suspension of starch particles in a mixture of glycerol with a surfactant and an aqueous carbopol phase. We report the surface tension of such materials, the rheological behaviour of separated ingredients and the behaviour of the complex mixture. This way we have a clear understanding of the impact of each ingredient on the rheology of the complex material we formed.

I. Towards the definition of a model cosmetic system

Cosmetic products are, in most cases, very complex formulations. Some of them may contain more than a hundred different ingredients. From a practical point of view, increasing the number of ingredients in a formulation increases the complexity of the system both chemically and physically. The study of the stability of formulations during storage takes into account these complex effects. However, this thesis is not intended to study this type of phenomenon with a large number of constituents. We are looking more closely at the spreading behaviour of cosmetic products. To do this, and in order to remain as consistent as possible with industrial applications, we have created a simple model cosmetic formulation that allows us to investigate the impact of conventional cosmetic ingredients. This formulation consists of a mixture of aqueous carbopol gel, with glycerol which acts as a non-volatile hydrophilic phase, and starch as suspended solid particles. This system, although relatively simple from a formulation point of view, remains interesting from a rheology and physical-chemistry point of view. Let's proceed step by step, in order to understand the behaviour of this type of formulation during spreading.

II. Rheology of carbopol systems

1. Preparation of carbopol gel

Carbopol gels are all prepared by following the same preparation procedure. A stock gel is prepared by dissolving 3.5 g of pure carbopol 980 powder (Ashland) within 318.5 g of MilliQ Water. The mixture is stirred at 900 rpm (using a Hei-TORQUE Heidolph mixer) for one hour. Then 28 g of sodium hydroxide (1 mol/L) is added to the mixture – which jammed immediately – in order to adjust the pH between 6 and 7. The 1‰$_w$ carbopol gel is then stirred for two more hours to homogenate and let at rest overnight. Referring to Dinkgreve[19] and co-workers, using this procedure gives us non-thixotropic carbopol gels. A full set of such gels at different concentrations [0.05-1‰$_w$] is prepared by diluting the stock gel with MilliQ water. This preparation procedure may induce the formation of bubbles within the gels which are easily removable from the volume by centrifuging the gels at 2000 rpm (using a Beckman Coulter Allegra X-15R Centrifuge) for 1 to 3 minutes depending on the yield stress of the gel. We have also prepared a very similar set of gel by using a 1‰$_w$ PEG12 dimethicone (Dow Corning) solution instead of pure water. The prepared carboPEG gels have a much lower surface tension than the carbopol gels.

2. Surface tension and contact angle

The surface tension is generally determined by calculating the equilibrium point between surface forces and mass forces. However, since the yield stress has to be taken into account in this equilibrium, it is technically difficult to measure the surface tension of yield stress fluids such as carbopol gels. Some papers report that the surface tension of a yield stress fluid is around 10% lower than the surface tension of its continuous phase[70,71]. Thus we have measured the surface tension and the contact angle of the pure water and the 1 $\%_w$ PEG12 Dimethicone solution in water. We carried the measurement of the air/liquid surface tension by using the sessile droplet method, and the contact angle with a camera by putting a droplet of sample on a PMMA plate previously washed under ethanol then under water. These values are given in the following table.

Solution	Contact angle (°)	$\gamma_{L/G}$ (mN/m)	$\gamma_{L/S}$ (mN/m)
Pure water	72	70	19.3
PEG12-Dimethicone 1%	47	28	21.9

Table 2: Contact angle on smooth PMMA substrate and surface tensions of pure water and 1$\%_w$ PEG12-Dimethicone solution in water.

3. Rheological characterization

The rheology of carbopol gels is measured using 40 mm hatched parallel plate geometry made of PMMA on a TA Instrument DHR2 controlled-stress rheometer. The samples are placed at 25°C in a 1 mm gap and their rheological properties in both linear and non-linear regimes.

a. Rheological behaviour of carbopol gel in the linear regime

First, an oscillation stress is imposed to the materials using strains comprised between 0.1 and 100% at a constant 1 Hz frequency. Here, both storage and loss modulus are measured, but also the oscillatory stress. This experiment shows the behaviour of the material in the linear regime and the transition to the non-linear regime. At low strains, the deformation is not high enough to unstructured the material, it simply deforms as an elastic solid. However, high strains overcome the elasticity of the material and it will start to flow as a liquid. The oscillatory stress is linearly dependent of the oscillation strain in both regimes, but the slope of the straight lines is different and the transition is highlighted by the slope modification. Thus, the yield stress of carbopol gels can found by plotting both straight lines and finding the stress of the intersection point[72].

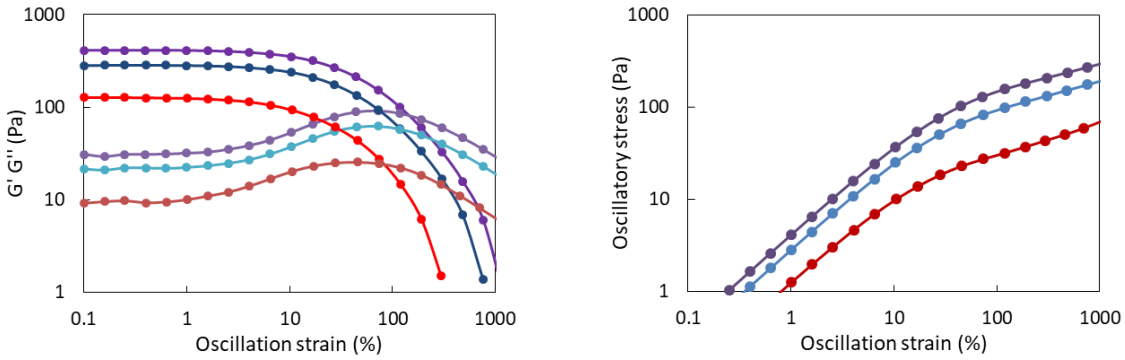

Figure 28: Evolution of the storage G', loss modulus G'' (on the left) and the oscillatory stress (on the right) of carbopol gels depending on the oscillation strain. Carbopol 0.15 (red), 0.5 (blue) and 1‰$_w$ (purple).

Second, an oscillation stress is imposed to the material using a constant 2.5% strain at frequencies comprised between 0.1 and 100 Hz. Under this strain, the carbopol gels are in the linear viscoelastic regime. Sweeping the frequency of deformation permits to screen the behaviour of the material in its solid elastic regime by measuring both storage and loss modulus.

b. Rheological behaviour of carbopol gels in the non-linear regime

Finally, different shear rates, from 0.1 s^{-1} to 100 s^{-1}, are imposed to the material until an equilibrium in the measure is reached and both the shear stress and the shear viscosity are measured. In this experiment the strain is infinite, so the material is always in the non-linear regime and flows at a specific shear rate. This experiment gives the flow curve of the material and shows its global flow behaviour (shear-thinning, shear-thickening, etc.). Carbopol gels are yield-stress fluids, their flow curves can be fitted by a Herschel-Bulkley model ($\tau = \tau_y + k.\dot{\gamma}^n$) with τ_y the yield stress, k the viscous parameter and n the shear-thinning index. The obtained values of τ_y and k are corrected using Rabinowitsch corrections in order to deal with the inhomogeneous shear rate in the parallel-plate geometry[73]. This model is convenient because it allows to determine the yield stress of the fluid, and also, it permits to calculate the shear stress for whichever shear rate the fluid bears and to understand what the stresses within the fluid are when it flows.

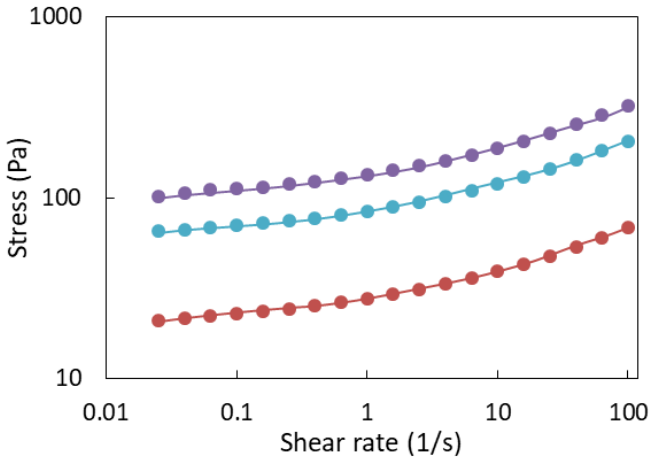

Figure 29: Flow behaviour of carbopol gels depending on the shear rate. Carbopol 0.15 (red), 0.5 (blue) and 1‰$_w$ (purple).

Carbopol gels we have made are therefore described by three characteristic variables as follow:

Carbopol Gel	τ_y (Pa)	k (Pa.s^n)	n
1	3.0	1.6	0.47
2	7.7	3.7	0.45
3	15.0	6.6	0.39
4	18.0	9.7	0.35
5	27.6	14.4	0.35
6	35.0	13.4	0.40
7	49.0	27.2	0.35
8	53.6	28.7	0.35
9	60.0	33.3	0.35
10	98.0	54.4	0.35

Table 3: Rheological characterisation of several carbopol gels based on Herschel-Bulkley fit.

In our case, we are more interested in flow curves than in oscillatory since in most cases dip coating and blade coating induce the liquid to flow.

III. Rheology of cornstarch dispersions

As we explained before, we are going to use cornstarch as a model filler. In order to characterize these systems, we have first study dispersions of cornstarch in water and glycerol. We observe that the rheological properties of cornstarch suspensions vary upon

time. We have therefore decided to follow this evolution along 2 months. We have analysed the role of the storage conditions on the evolution.

1. Stability of starch in water over time

In this part we are trying to understand how starch particles behave when they are dispersed in a hydrophilic continuous phase. First, we have discovered that starch suspensions in water undergo bacterial attacks and rotten forming mushrooms within one week. One can note that these bacterial attacks do not happen in glycerol-based media in which the conditions are not convenient to bacteria development. In order to solve this issue, we have prepared starch suspensions as previously described but we have added 0.5%$_w$ of a preservative (phenoxyethanol) in all aqueous phases.

a. Evolution of the rheology and particle size

Two sets of samples are prepared, one is continuously stirred and the other one is left at rest for the whole time of experiment. By following rheological properties of samples over time we observe that all samples present non-negligible modifications.

Non-stirred water-based samples show a modification in their shear-thickening behaviour. However the rheological evolution is consistent with a simple augmentation of the volume fraction (Figure 31a). In this case, the rheological modifications are likely due to a small amount of water that fill up the porous starch particles, resulting in a progressive modification of the effective volume fraction of the sample. We also observe this phenomenon by dispersing starch particles in a fluorescein solution. The suspension is centrifuged and the supernatant is replaced by pure water five time in a row. Particles are hence rinsed off with pure water and there is no trace of fluorescein in the dispersing water anymore. While particles are visible by their shiny shell in the fluorescein solution, they are completely shiny in pure water. It thus shows that they are filled up with fluorescein and confirms that starch particles are able to absorb water (Figure 30). However, since particles do not have the same level of brightness, we conclude that the absorption of water is not progressive, but need to overcome an energy barrier before starting in each particle.

In contrast, stirred samples show a different rheological behaviour. For instance, the initial 10%$_v$ starch volume fraction suspension shows first a Newtonian behaviour at high shear rate, then a continuous shear-thickening behaviour after one week of ageing and finally a yield-stress fluid behaviour after two weeks. The yield stress of the suspension increases and slowly stabilizes over several months (Figure 31c). One can note that a highly concentrated suspension (40%$_v$) do not evolve to a yield-stress fluid even though they are kept under stirring during the experiment time. (Figure 31b).

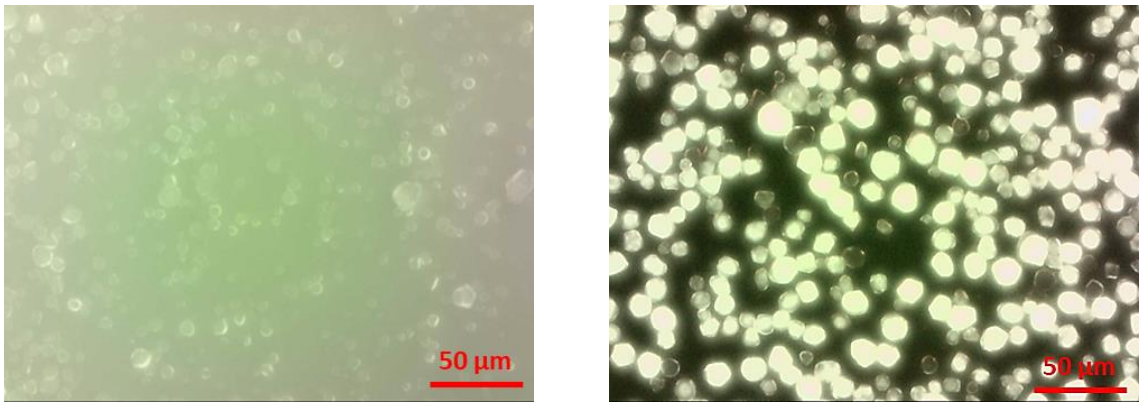

Figure 30: The picture on the left shows new starch particles in a fluoresceine solution by fluorescent microscopy. All the light emmision comes from the solution. On the right, particles have been let at rest in the fluoresceine solution for 3 days, then dispersed in pure water and observed by fluorescent microscopy. This picture shows that only the particles are fluorescent, proving that water has come through particles during the 3 days ageing.

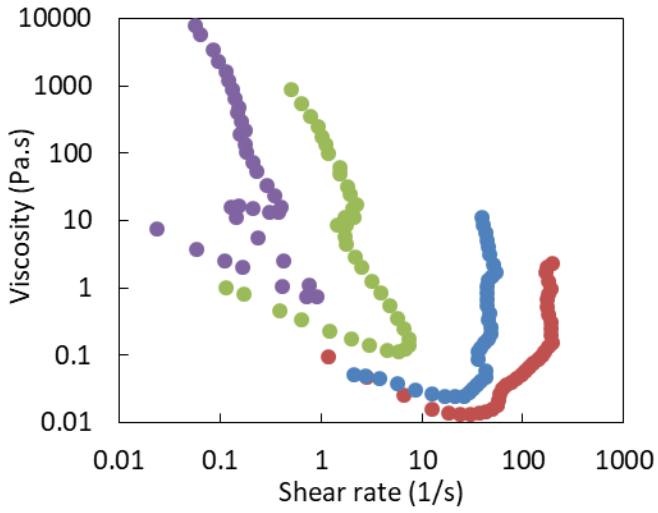

a

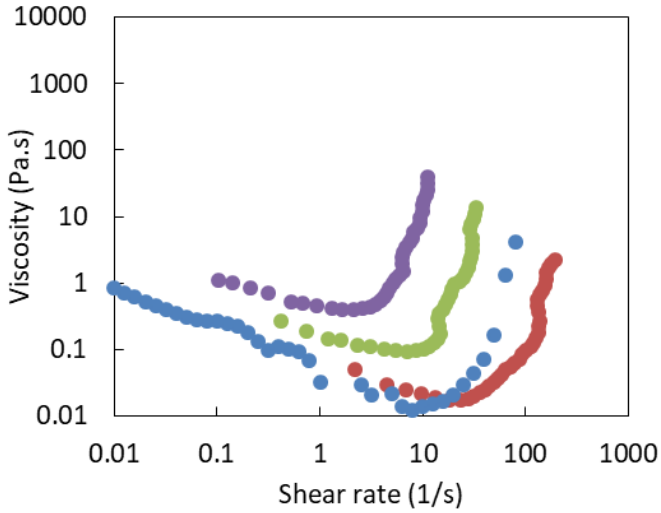

b

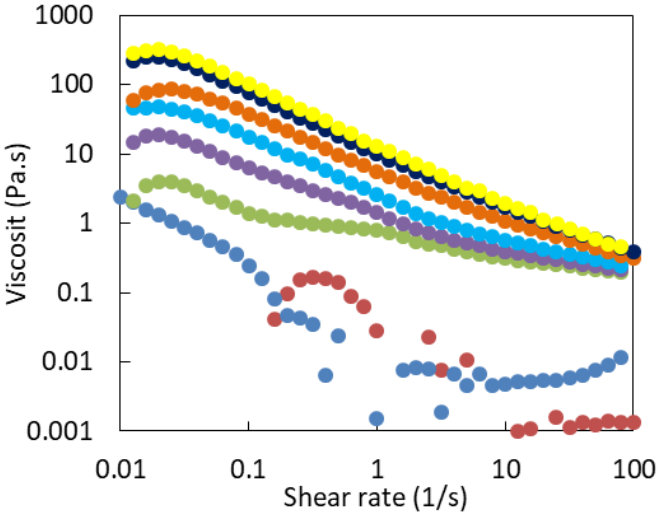

c

Figure 31: (a) Flow behaviour of cornstarch suspension in water depending on the volume fraction (40.0%$_v$ (red); 41.9%$_v$ (blue); 43.9%$_v$ (green); 45.9%$_v$ (purple)). (b) Evolution of the rheological properties of a stirred 40%$_v$ cornstarch suspension over time (t0 (red); t5d (blue); t21d (green); t28d (purple)). (c) Evolution of the rheological properties of a stirred 10%$_v$ cornstarch suspension over time (t0 (red); t7d (blue); t14d (green); t21d (purple); t28d (cyan); t56d (orange); t70d (black); t84d (yellow)). The flow curves are obtained by a stress-imposed method.

It is clear that the structure of starch evolves when it is stirred in water at low volume fraction (<20%$_v$). Both conditions have to be verified, since the rheological properties of a lowly concentrated non-stirred sample and a highly concentrated stirred sample do not evolve into a yield-stress fluid over time. Under such conditions, water interacts with starch particles swelling and softening them along the experiment time. In parallel we followed the granulometric size of particles, so we can interpret the evolution of rheological properties as follows: at T_0, the starch non-Brownian particles are not concentrated enough to come into contact, so the suspension shows a shear-thinning behaviour at low shear rate and a Newtonian behaviour at high shear rate[14,16]. After one week of stirring, the particles of diluted systems increase in diameter (Figure 32). The maximum reached size depends on the initial volume fraction of particle within the suspension (d_{max}(10%$_v$) = 19,7 µm, d_{max}(20%$_v$) = 17,7 µm). It is, by the way, also occurring in the case of glycerin solvent, although the effects are less pronounced (d_{max}(10%$_v$ in glycerin) = 16,4 µm).

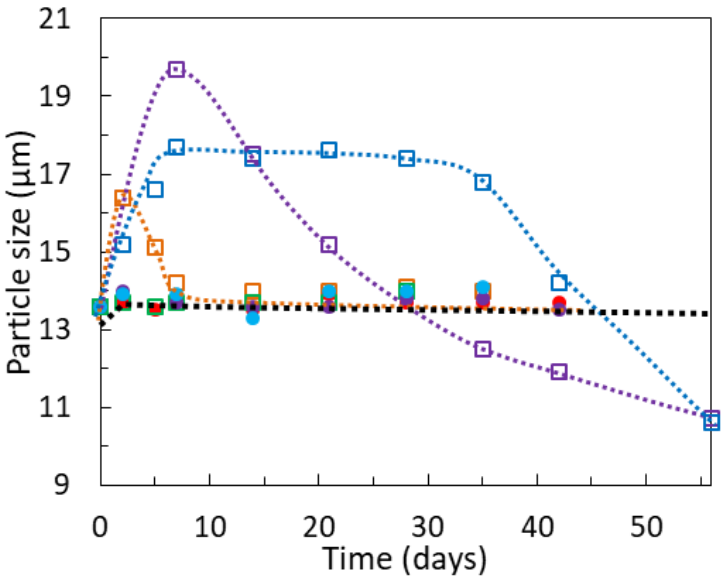

Figure 32: Evolution of the suspended particle size over time.
Stirred sample (empty squares): Orange: 10%$_v$ starch particles in glycerol, Blue: 20%$_v$ starch particles in water, Purple: 10%$_v$ starch particles in water, Green: 40%$_v$ starch particles in water.
Non-stirred samples (full circles): Red: 20%$_v$ starch particles in water, Purple: 40%$_v$ starch particles in water, Cyan: 20%$_v$ starch particles in glycerol. The black dashed line shows the general evolution of non stirred sample.

The increase in size causes the particles to get more into contact under shear. As a result, the swelling slightly increases the Newtonian viscosity of the suspension. However, at this stage, the starch particles remain mainly hard since the shear-thickening behaviour observed at high shear rates can only be created by frictional forces between hard particles[15]. After two weeks, the starch particles have softened and the rheology of the bulk gives the behaviour of a yield-stress fluid very close to what we could observe with a concentrated emulsion[74]. At this stage, it is impossible to make a correlation between the reference curves and the aged sample curves. The yield-stress behaviour proves at least that the particles within the samples are soft. However, the granulometric size measurement shows that in some case the particles size begins to decrease again. Referring to the size measurement, the particles seem like they unstructured during the deflation since the final size can reach smaller values than the initial diameter of particles. Microscopic observations also confirm that after 42 days of stirring, the shape of the particles have changed dramatically: they lose their initial structure and become less round and more irregular (Figure 33).

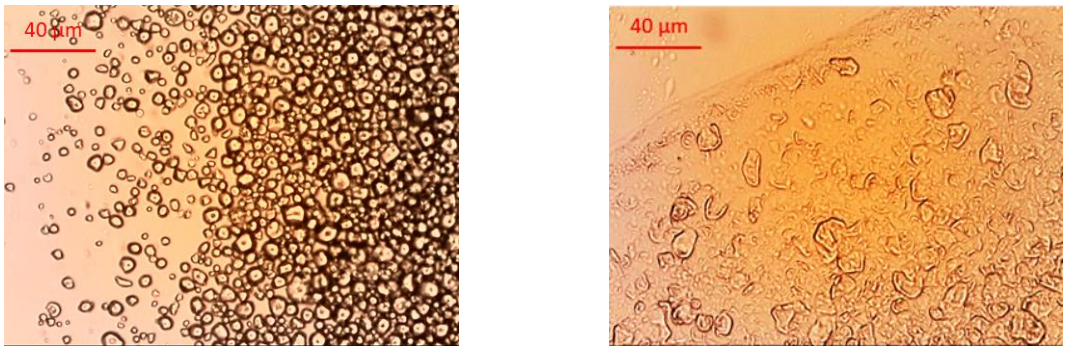

Figure 33: Pictures of a 10%$_v$ starch particles suspension in water before and after 42 days of stirring.

b. Chemical Quantification

In order to know how starch particles decompose in water we centrifuge the suspension and determine the composition of the supernatant liquid phase. We have studied two starch suspensions at 10% volume fractions. One is continuously stirred during 42 days while the other is stored at rest. After centrifugation, both supernatants look different since the stirred sample is turbid whereas the sample kept at rest is perfectly transparent (Figure 34a). This indicates that the stirred sample contains particles large enough to diffuse the light (i.e. > 200 nm). The aqueous phase contains insoluble particles that remain dispersed even after centrifuging the suspension. This indicates that these particles are not starch particles, but much smaller starch aliquot. We filter the previous supernatants with a 2 µm mesh and analyse using Dubois's characterization method which is a specific reaction to sugars using sulfuric acid and phenol[75]. The reaction forms orange molecules from sugar exhibiting a sharp peak at 485 nm by UV-visible spectroscopic analysis. The intensity of the peak is linked to the quantity of sugar molecules within the sample. Using such reagent, the sugars that compose starch particles (i.e. amylose, amylopectin, and glucose) react and form an orange dye (Figure 34b). The stirred sample is diluted 25 times in order to avoid any possible saturation in the spectroscopic measurement. The analysis shows a peak at 485 nm for both samples.

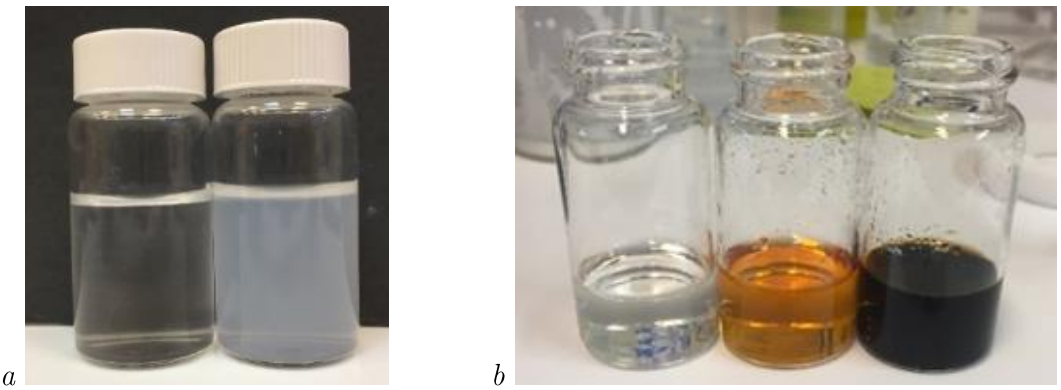

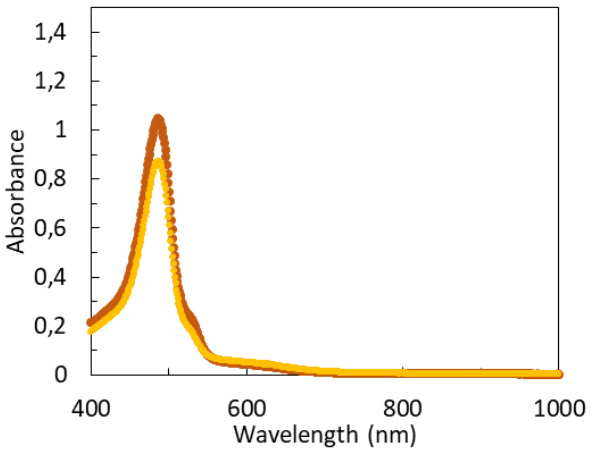

c

Figure 34: (a) Supernatant of centrifuged samples initially containing 10‰ of starch in water. Before centrifuging, the sample on the left was kept at rest during 1 month, while the sample of the right was kept under stiring during 1 month. (b) Reaction of supernatant with phenol and sulfuric acid (smaple from left to right correspond to the blank sample contaning only phenol water and sulfuric acid, the kept-at-rest sample, and the kept-under-stirring sample.(c) UV-visible spectrum of the reaction bulks. Yellow curve corresponds to non-stirred sample stored during 1 month, and the orange curve corresponds to the sample stored under stiring for 1 month. Note that the stirred sample as been diluted 25 times before doing the Dubois' reaction.

By comparing their intensities relatively to their concentrations, we can conclude that the stirred sample contains about 20 times more sugar than the sample kept at rest.

However, the formed molecules and their UV-visible spectroscopic signal depends on the initial sugar we transformed. Still, the UV-visible spectroscopy signatures are not sufficiently different to distinguish sugars from each other. Therefore, this experiment cannot be specific of amylose since we transform and detect all sugars. Starch particles are known to be a mixture of two main molecules: amylose and amylopectin which are both solid at room temperature. They differ by their solubility in water: amylose is soluble while amylopectin is not. Amylopectin is a reticulated polymeric frame for starch particles while amylose is mostly dispersible in water. During the time of the experiment and due to the constant stirring, the amylose is simply washed out from the starch particles, leaving behind an empty shell of amylopectin. The washing out of amylose explains how the particle size can decrease that low. Also, the particle size fixes at a final constant size around 10 µm, which should approximately correspond to the empty shell of amylopectin. At the end of the experimental time, most of the amylose is dissolved by water and is contained within the aqueous phase. As the supernatant of the stirred sample is turbid, we know that, more than amylose alone, the aqueous phase is also loaded with small particles which may come from the amylopectin shell. Even though the amylopectin is insoluble in water, the experiment shows that the stirring in water leads to amylopectin decomposition. However, this is happening at a slower velocity than

the solubilisation of amylose in water. Thus there is no doubt that the sugars detected by Dubois's characterisation method[75] mainly come from the dissolved amylose in water and that the quantity of amylopectin aliquot detected is comparatively low.

It is now clear that starch particles are not stable over a long period of time in water. Furthermore, the decomposition chemistry remains complex in spite of our investigations. In order to have good repeatability in the experiments, we decide to run our experiments in a short range of time after preparing the sample, before observing starch particles degradations. Therefore, all the following experiments are carried out within the week after their preparation.

IV. Rheology of a model cosmetic formulation

In this section we propose to investigate the rheology of starch suspension in carbopol and compare it with the rheology of a neat gel. We stirred energetically the particles inside a carbopol gel in order to have a homogeneous mixture and to break the cluster of particles. We observe that implementing particles, even at low volume fraction, significantly modify the rheology of the gel. Most notably, the yield stress decreases when the volume fraction of starch particles increases.

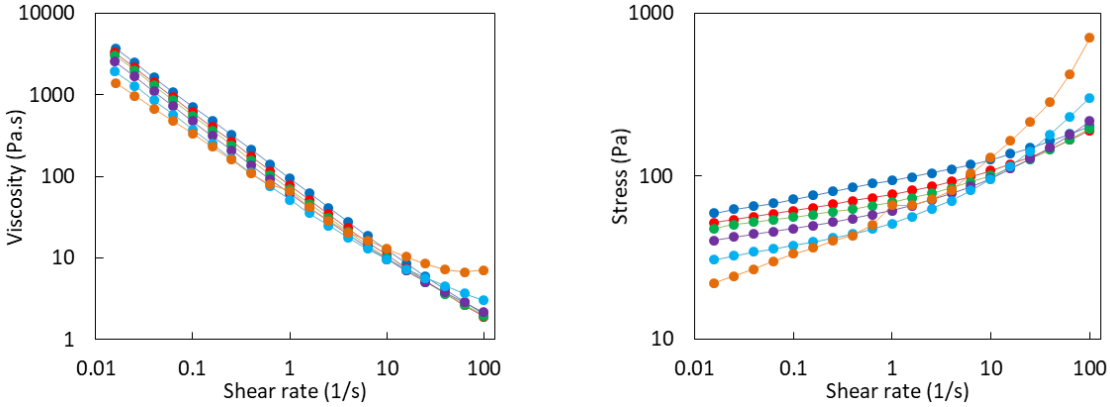

Figure 35: Evolution of the rheological flow behaviour of a 0.3%$_w$ carbopol gel depending on the volume fraction of starch particles. 0%$_v$ (blue); 11.8%$_v$ (red); 21.1%$_v$ (green); 28.6%$_v$ (purple); 34.8%$_v$ (cyan); 40%$_v$ (orange).

A 0.3%$_w$ carbopol gel which initially has a 71 Pa yield-stress, presents only a 36 Pa yield-stress if the gel is also composed of 40%$_v$ of starch. Surprisingly, at this volume fraction, we begin to observe a Newtonian-like behaviour at high yield stress for this volume fraction of starch. However, starch particles are hard to concentrate at high volume fraction and the mixture do not behaves as a fluid at this stage. Therefore, we were unable to carry our experiments at higher starch volume fraction. Thus we couldn't observe clear shear-thickening as we could have expected for higher volume fraction.

As a conclusion, at low volume fraction ($\varphi < 40\%_{\text{v}}$), the mixture of starch particles with carbopol gel remains a yield-stress fluid that behaves like a solid at rest, and flow under a sufficiently high shear stress. However, we will see later that drying such material is not trivial and induce complex physico-chemical effects.

Take home message – Chapter 2

In this chapter we created a model cosmetic system that we will use in the following chapters. This model system is made of a suspension of starch particles in a mixture of glycerol with a surfactant and an aqueous carbopol phase.

a. We studied the rheological behaviour of such materials by formulating it step by step, i.e. adding ingredients one after the other. We observed that the rheological properties of gel are modified by the presence of starch particles.

b. We observed that the stability of starch particles in water is not simple and involve complex dissolutions and chemical modifications. We explorer this phenomenon by determining the evolution of the quantity of sugar in the continuous phase of starch suspensions, but also by granulometric and rheological measurements.

Chapter 3

Dip coating of complex fluids

Summary: In this chapter we deal with the dip-coating experiments. Specifically, we study how a film forms in the axisymmetric case and what are the parameters that fix the thickness of the film. We propose a model and a full theoretical approach of the flow in the bath to predict the film thickness. Then we compare those results with those obtained by previous research and discuss the impact of capillary effects or drainage, that haven't been taken into account until then. For cosmetic applications we give important formulation tools to enhance the quantity of matter withdrawn from a tube as in mascara applications.

Dip coating is a coating technique in which an object is immersed into a fluid reservoir and then pulled out. During the withdrawal, a liquid film is entrained by viscous drag. The dip-coating process is low cost, waste free, and easy to scale up[76]. Applications are found in many sectors ranging from manufacturing industry to food industry and cosmetics, especially when it comes to pick up products from a tube as in mascara application. In such applications predicting the thickness of the entrained film is of major interest both for industrial and scientific perspectives.

I. Experimental section

1. Experimental set-up

We proceed to dip-coating experiments in an axisymmetric system. This way, we avoid edge effects and we get a homogeneous stress field within the bath. To do so, we fill cylindrical containers of various radii r_2 (13, 17, 21.5 and 33 mm) up to 14 cm height with carbopol gels as a model yield-stress fluid. A r_1 (2.5, 5 or 10 mm) radius acrylic rod is vertically immersed in the bath over a length of 10 cm. The internal stress of the gel in the container is preset by a first immersion and retraction of the rod. This way, we manage to increase the repeatability of experiments. At any time the immersion of the rod is performed at the same speed as the retraction. In order to avoid wall slip[77,78] and to ensure complete wetting of the carbopol gels on the acrylic rods, the rods are sandblasted, leading to a roughness of ~10 µm and subsequently treated by an oxygen/argon plasma[79] (Diener Pico). The coating thickness is directly measured using a profilometer (Keyence LJ-V7060K).

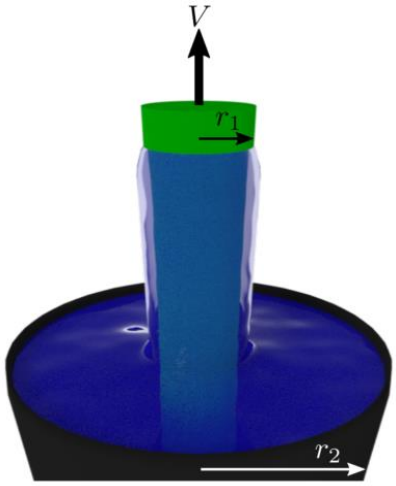

Figure 36: Illustration of the dip-coating experimental set up in the axissymetric case consisting in a rod in a cylindrical bath

2. Film thickness measurement using a profilometer

In our work, we study the thickness of the film formed by coating complex fluids, and more precisely, carbopol gels on PMMA substrates. In order to carry these measurements, we use a profilometer able to measure thicknesses based on optical reflexions of a laser on the surface. The process is simple, we first measure the position of the substrate with a scan used as a reference. Then, we fix all the coating parameters (velocity and distance), dip the rod into the sample, and run the scan during the withdrawing of the rod that is now coated with a gel layer. We finally calculate the difference between the two measurements to get the final thickness of the film.

However, the reflection of the surface might not be intense enough to get a usable signal. This is the case for carbopol gels. In most geometries, we are unable to get a strong reflected signal from the gel surface. Since the gel is transparent, we therefore measure the reflection from the substrate under the liquid film which is still strong enough to be measured. We can observe that the position of the substrate differs if there is a liquid layer of not. This is due to the refraction of the laser by the liquid layer. Therefore, we can calculate the thickness of the liquid layer by measuring the change of the substrate position through the liquid (Figure 37).

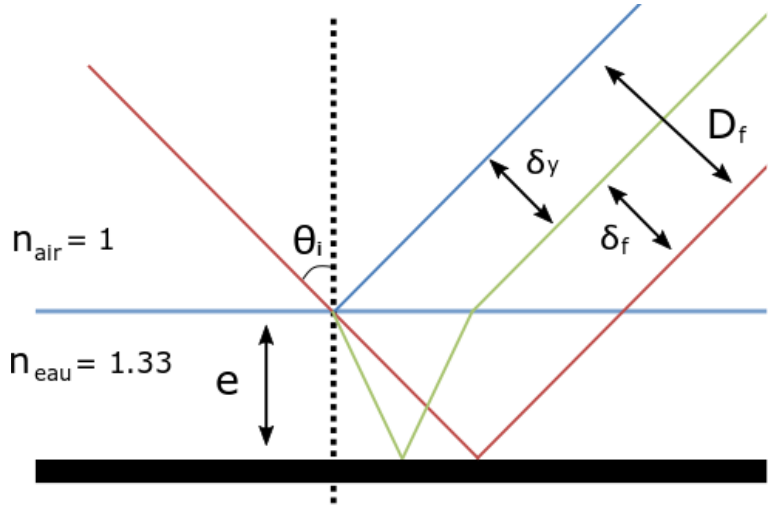

Figure 37: Illustration of the different ways the laser of the profilometer can reflect on the sample. Red line corresponds to the direct reflection on the clear surface. Blue line corresponds to the reflection of the laser beam onto the surface of the coated liquid. Green line corresponds to the reflexion of the laser beam onto the surface after being refracted by the liquid layer. During our experiment we compare the position of the red and green rays.

On the above schematic, the incident ray (in red) impacts the substrate (in black) with an angle $\theta_i = 17.5°$ in relation to the normal and is reflected with the same angle towards the detector. In the case of the ray would have been reflected on the liquid surface (blue ray), the angle of reflection would have been the same as the one reflected by the substrate. However the impact position on the detector would have been different. The number of pixels corresponding to the distance between these two impact points D_f

give the film thickness by a simple calculation. However, the only exploitable detection is the one refracted by the liquid, then reflected on the substrate (in green). The path difference δ_f observed on the substrate position depend on the film thickness and its refractive index. It is however possible to determine the film thickness thanks to δ_y and D_f. Since we are able to measure δ_f, we can obtain the film thickness by multiplying it by a factor $\alpha = D_f/\delta_y$. By resolving optical geometrical equations, we can write the following equation which shows that the α coefficient only depends on the refractive index of the liquid, which is the same whatever the film thickness is.

$$\alpha = \frac{\tan(sin^{-1}\left(\frac{\sin(\theta_i)}{n}\right))}{\tan(\theta_i)} \tag{3.1}$$

In the case of carbopol gels $n = 1{,}33$, yielding $\alpha = 3{,}7$. This coefficient has been verified experimentally with different materials of known thickness confirming that the equation is correct.

II. Dip-coating of complex fluids

1. Experimental results

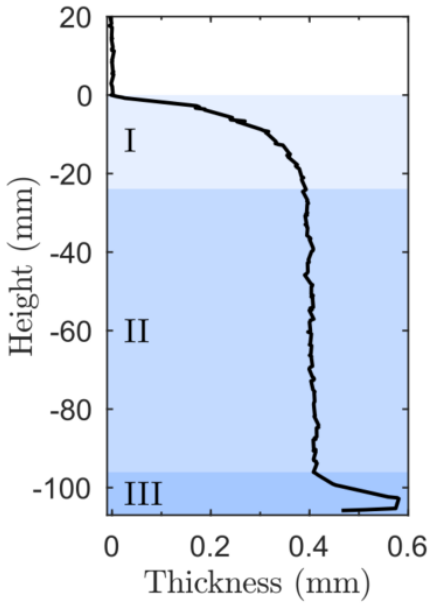

Figure 38: Typical thickness profile resulting from the dip coating. The coating profile can be divided into regions I, II, and III (see text).

A typical thickness profile from a dip-coating experiment is shown in Figure 38. The coating profile can be divided into three parts. In the wetting region (I), the coating thickness builds up until a finite value is reached. In the bottom region (III), the thickness increases as a result of the breakage of the meniscus when the rod leaves the liquid bath.

In the intermediate region (II), the coating thickness is uniform, which is associated with a steady flow. In our work, we focus on region II and denote the constant thickness by h. Its value is determined by averaging over 3-10 independent measurements.

In Figure 39 we show the experimental film thickness h for a 0.5%$_w$ carbopol solution in 1%$_w$ aqueous PEG-12 dimethicone in several configurations. The coating thickness increases with rod radius r_1 as well as the pull-out velocity V, see panel (a) and (b), respectively. Strikingly, the geometry also has a profound impact on the coating thickness. For instance, for a rod of radius $r_1 = 10$ mm, the thickness h increases from 0.35 ± 0.01 mm for $r_2 - r_1 = 7$ mm to 0.64 ± 0.03 mm for $r_2 - r_1 = 23$ mm. This result contrasts with the behaviour of Newtonian liquids, for which the coating thickness is independent of the bath size when the distance to the wall exceed two times the capillary length, i.e. for $r_2 - r_1 > 5$ mm[80]. The dependence with the bath size for a yield-stress fluid implies that the coating does not only induce a flow of a free surface under gravity, but that the coating process is governed by the flow inside the bath.

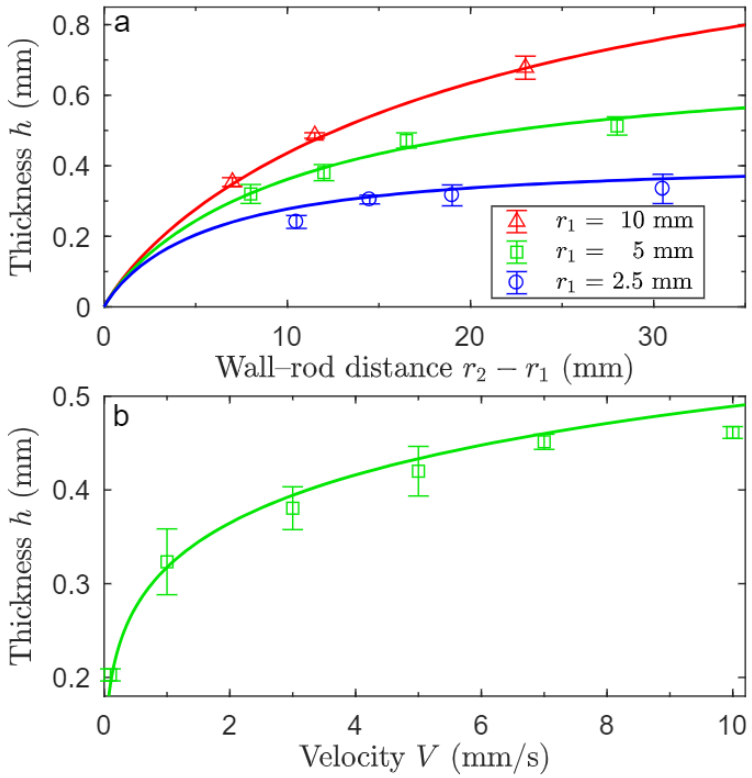

Figure 39: Comparison of the coated layer thickness between exprimental (data points) and the predicted values of equation (3.7) (solid lines) for a carbopol solution in aqueous PEG-12 dimethicone. The rheological properties are $\tau_y = 56$ Pa, $k = 26$ Pa.s^n, and $n = 0.35$. Error bars denote the standard deviation. (a) Coating thickness as a function of the distance between bath wall and rod for different geometrical configuration. The rod radii are 2.5 mm (circles), 5 mm (squares), and 10 mm (triangles). The withdrawal velocities is 3 mm/s. (b) Coating thickness as a function of withdrawal velocities. The rod and the bath are of radius $r_1 = 5$ mm and $r_2 = 17$ mm, respectively.

This result differs from the study by Coussot and co-workers in planar geometry, who reported no influence on the thickness of the deposit when the distance to the wall exceed 2 centimeters[81]. To solve the dip-coating problem for a yield-stress fluid, we must determine the fluid flow inside the bath.

2. Theoretical approach

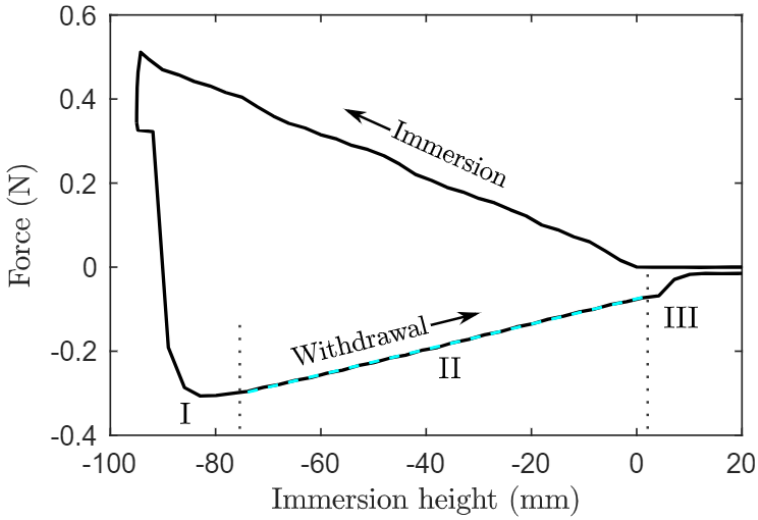

Figure 40: Force between rod and fluid reservoir during a dip-coating cycle as function of the immersion height as measured with a Discovery HR-2 (TA Instruments). The force curve corresponds to the coating profile shown in Figure 38. A rod of r_1 = 5 mm is immersed and withdrawn from a bath of r_2 = 33 mm with velocity V = 3 mm/s. The withdrawal phase is linked to the three regions of the coating profile (indicated by the roman numbers). In region II, the derivative of the force curve is constant (dashed line), indicating a steady flow. The rheological properties are τ_y = 56 Pa, k = 26 Pa.s^n, and n = 0.35.

For a laminar flow along the rod, the only non-vanishing stress component is the transverse stress τ_{rz}. For a yield-stress fluid, inertia forces are small compared to the viscous forces (typical Reynolds number < 0.1). Because of the low Reynolds number, the flow is governed by Stokes' equation:

$$-\rho g - \frac{\partial P}{\partial z} + \frac{1}{r}\frac{\partial r\tau_{rz}}{\partial r} = 0 \tag{3.2}$$

with fluid density ρ, gravitational acceleration g, pressure P, radial coordinate r, and vertical coordinate z. By integration of the Stokes' equation, a general solution for a flow through concentric annuli is obtained:

$$\frac{\tau_{rz}(r,t)}{\tau_y} = \frac{1}{\lambda_i(t) - \lambda_o(t)}\left(r - \frac{\lambda_i(t)\lambda_o(t)}{r}\right) \tag{3.3}$$

λ_i and λ_o, the locations of the inner and outer yield surface (Figure 41), respectively, are located according to the following conditions $\tau_{rz}(\lambda_i) = -\tau_y$ and $\tau_{rz}(\lambda_o) = \tau_y$, and have

to be determined. For elastoviscoplastic fluids, λ_i and λ_o depend on the deformation history and converge after a start-up time to their steady flow values[82]. In all our experiments, the rod length is long enough for a steady flow to be established, as evidenced from the constant region in the coating profiles (region II in Figure 38) and measurements of the force between road and reservoir (Figure 40).

In this situation, λ_i and λ_o do not depend upon time and can be determined by using no-slip conditions, i.e. $v_z(r_1) = V > 0$ and $v_z(r_2) = 0$, and mass conservation. The velocity boundary conditions impose

$$V + \int_{r_1}^{r_2} \dot{\gamma}\,(r)dr = 0 \tag{3.4}$$

with shear rate $\dot{\gamma} = \partial v_z/\partial r$. Mass conservation imposes that the retracted volume by the rod pull is balanced by a downward flow of the liquid in the bath:

$$2\pi \int_{r_1}^{r_2} r v_z\,(r)dr = -\pi r_1^2 V \tag{3.5}$$

To obtain the bath flow, one must specify a rheological model. Here we employ the Herschel-Bulkley model for which $\dot{\gamma} = 0$ for $\tau \leq \tau_y$ (solid regime) and $\tau = \tau_y + k\dot{\gamma}^n$ for $\tau > \tau_y$ (liquid regime). Using equation (3.3), the shear rate can be expressed as

$$\dot{\gamma} = \begin{cases} -\left(\frac{\tau_y}{k}\right)^{\frac{1}{n}} \left(\frac{\frac{\lambda_i\lambda_o}{r} - r + \lambda_i - \lambda_o}{\lambda_o - \lambda_i}\right)^{\frac{1}{n}} & \text{for } r_1 \leq r \leq \lambda_i \\ 0 & \text{for } \lambda_i \leq r \leq \lambda_0 \\ \left(\frac{\tau_y}{k}\right)^{\frac{1}{n}} \left(\frac{r - \frac{\lambda_i\lambda_o}{r} + \lambda_i - \lambda_o}{\lambda_o - \lambda_i}\right)^{\frac{1}{n}} & \text{for } \lambda_0 \leq r \leq r_2 \end{cases} \tag{3.6}$$

Using this expression of the shear rate, we perform a double iteration analogous to Fordham et al.[83] to fulfil equation (3.4) and (3.5). We obtain the two lengths λ_i and λ_o. The obtained flow is shown in Figure 41 and agrees quantitatively with experimental measurements of the velocity profile.

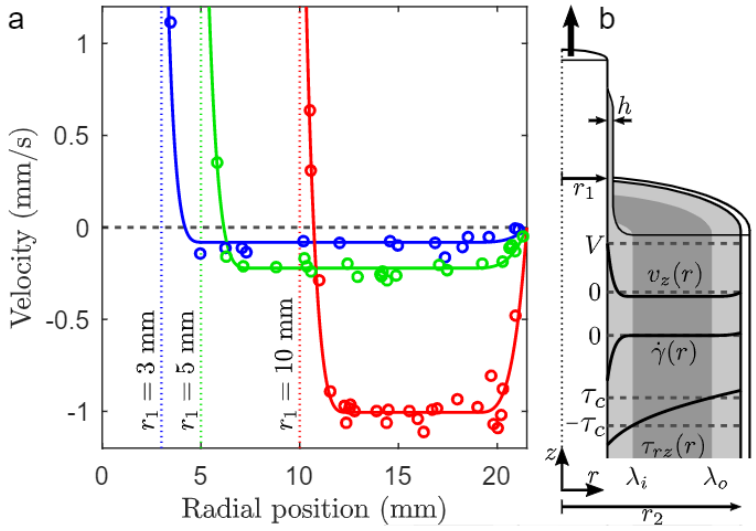

Figure 41: (a) Velocity profiles for rods of various radii r_1 withdrawn for a bath of r_2 = 21.5 mm with velocity V = 3 mm/s. The data points are obtained by tracking the flow of small air bubbles inserted perpendicular to the plane of observation. The solid lines result from the velocity and mass-conservation conditons (without fit parameter). The rheological properties of the carbopol gel are τ_y=14 Pa, k = 8 Pa.s^n, and n = 0.35. (b) Schematic of flow during the dip-coating experiment. Radial profile of the laminar flow inside the bath of the velocity v_z, shear rate $\dot{\gamma}$, and shear stress τ_{rz}.

The latter have been obtained by seeding a thin slit of the gel with some bubbles and by following their displacement. Two sheared zones close to the rod and to the wall of the reservoir are clearly evidenced. The displacement of the bubbles shows that there is no horizontal flow at the surface. Only toward the end of the rod, a horizontal flow brings matter from the sides to fill up the extracted volume below the rod ends. This flow occurs over a characteristic length of ~ 1-2 cm (typically over a distance comparable to r_2) and does not affect the previously calculated velocity profile.

When one assumes that the fluid in the liquid region between r_1 and λ_i is transferred onto the coating, mass conservation yields a layer of thickness

$$h = -r_1 + \sqrt{\frac{\int_{r_1}^{\lambda_i} r^2 \dot{\gamma}(r) dr}{\int_{r_1}^{\lambda_i} \dot{\gamma}(r) dr}} \tag{3.7}$$

In the meniscus region, the fluid turns progressively from a liquid to a solid behaviour.

The numerical values of the coating thickness h are plotted as solid lines in Figure 39 and are in excellent agreement with the experimental results. The influence of the geometrical dimensions as well as the velocity of the coating thickness is well-captured by the model. Note that the flow inside the bath depends on three independent length

scale (r_1, r_2, and the rheological length $V(k/\tau_y)^{1/n}$). Hence, at least two dimensionless parameters are required to describe the flow (e.g. r_2/r_1 and Bingham number $Bm = \frac{\tau_y}{k}\left(\frac{r_2-r_1}{V}\right)^n$). As a consequence, no single master curve for all rod sizes, bath sizes and velocities can be presented.

3. Capillary effect and gravity in dip-coating experiments

The quantitative agreement between model and experiment shows that the liquid moved upwards in the bath is completely transferred onto the coating. Our results indicate that both capillary effects and gravity play no role. Let us discuss these hypotheses.

Capillary effects play a role when the stress gradient in the deposit, τ_c/h, is less than the characteristic capillary pressure gradient in the meniscus close to the rod[84]. In our work the capillary length $l_c = \sqrt{\gamma/\rho g}$ is larger than the radii of the rods and the characteristic capillary pressure gradient is $\gamma/\sqrt{h{l_c}^3}$. This means that the capillary forces can be neglected for $\tau_y > (\rho g)^{3/4} h^{1/2} \gamma^{1/4}$. For the data in Figure 39 the criterion holds $\tau_y > 10$ Pa at most, which is well-fulfilled.

Drainage does not affect the coating thickness when the width of the liquid zone around the rod is smaller than the gravity-imposed drainage limit, i.e. $\lambda_i < r_1\sqrt{1 + 2\tau_y/\rho g r_1}$. This criterion is also fulfilled for the data in Figure 39.

To verify these analysis, we show in Figure 42 the outcomes of experiments with carbopol solutions with yields stress of 3, 8, 18 and 28 Pa in pure water, i.e. without PEG-12 dimethicone. Our model yields a good agreement with experiment when the yield stress is higher than 18 Pa. In this situation, capillary effects are small. Drainage can be neglected as soon as the yield stress is higher than 8 Pa for $r_1 = 2.5$ mm and higher than 18 Pa for $r_1 = 5$ and 10 mm. For yield-stress values of 3 and 8 Pa, the coating thickness is observed to vary little with bath size and our modelling does not describe the measured values. Capillary effects (at least in the case of 3 Pa for $r_1 = 5$ mm and $r_1 = 10$ mm in the case of 8 Pa) and drainage play a role.

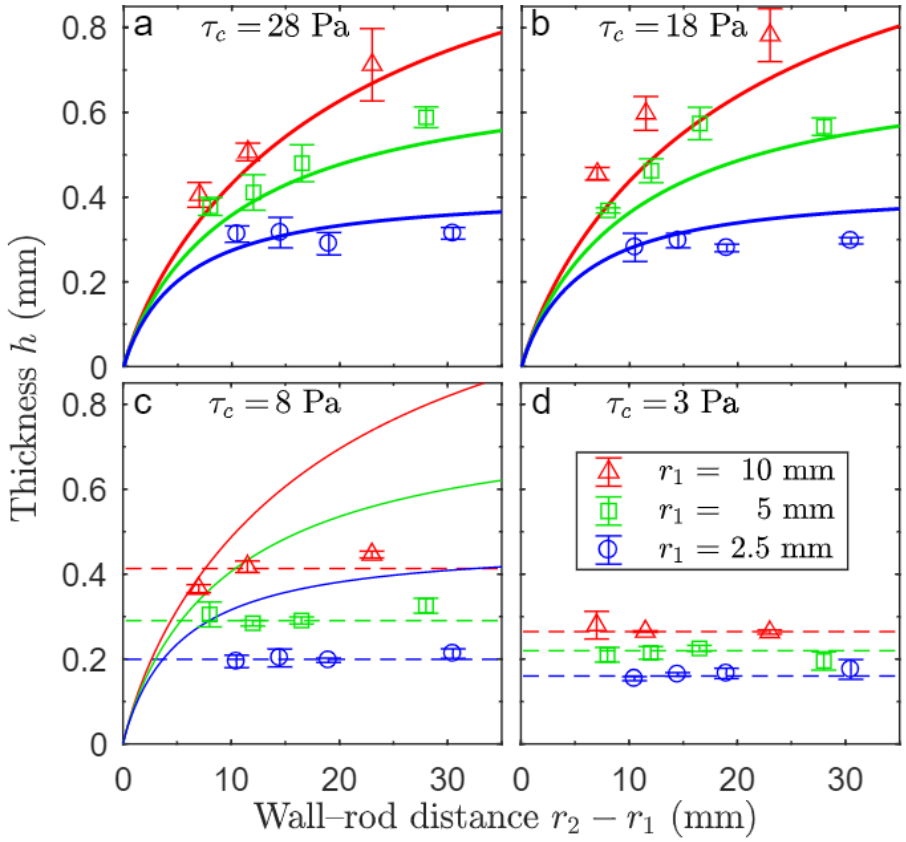

Figure 42: Transition from meniscus-shape regime to the bath-flow regime for dip coating from aqueous carbopol solution with increasing yield stress. The experimental data points are compared with the weighted averages per rod size (dashed lines) and/or the bath-flow model (solid lines). The withdrawal velocity is 3 mm/s. The rheological properties of the carbopol gels are: (a) τ_c = 28 Pa, k = 14 Pa.s^n, n = 0.35. (b) τ_c = 18 Pa, k = 10 Pa.s^n, n = 0.35. (c) τ_c = 8 Pa, k = 4 Pa.s^n, n = 0.42. (d) τ_c = 3 Pa, k = 1.6 Pa.s^n, n = 0.47.

4. Discussion

The good agreement found for large yield stress contrasts the observation by Maillard et al., who found a 40-60% thinner deposit than the total amount of fluid driven upwards[50,81]. Let us first comment that an implementation of our modelling in planar geometry predicts perfectly and quantitatively the size of the fluidized zone measured in the work of Maillard et al.[50] (see fig S1 in appendix II). This underlines that our modelling which originality is to take into account the boundary conditions and to write a zero-flux condition, captures quantitatively the flow in the bath in the steady low-Reynolds limit. The difference between our study and the work of Maillard et al. comes from the role of drainage. As suggested by the authors, gravity and drainage in the meniscus are responsible for the loss of matter.

One may wonder then, why the results of Maillard et al. differ from ours and why gravity does not interfere in the case of our rods. For a plate geometry, the thickness of the liquid region along the plate λ_i^{plate} is found to diverge as $\lambda_i^{plate} \propto L^{\frac{1}{1+n}}$, with L the

bath size (see appendix II). When the thickness of the liquid zone exceeds a critical value, drainage will occur in the meniscus region. For a plate, drainage likely occurs in the meniscus region, when the thickness of the liquid region along the plate λ_i^{plate} is larger than the drainage limit $\tau_c/\rho g$. In the experiment of Maillard et al. wide baths are employed and drainage interferes in the meniscus region as λ_i^{plate} exceeds $\tau_c/\rho g$, due to the scaling law of λ_i^{plate} as a function of the bath size.

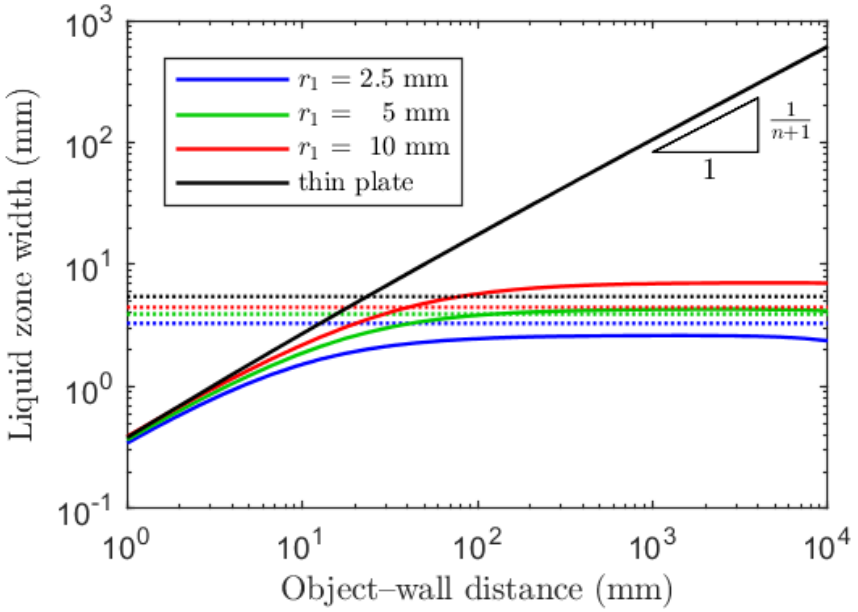

Figure 43: Thickness of the liquid zone around the withdrawn object as function of the bath size. The withdrawing velocity V is 3 mm/s. For a finite rod, the width of the liquid zone converges to the a constant value, whereas for a plate, the liquid zone thickness asymptotically increases as $L^{1/(n+1)}$ with L the bath size. The drainage limits for a yield stress of 56 Pa are indicated by the dashed lines with the colour matching the geometry.

In contrast for a cylindrical geometry, the location of the inner yield radius λ_i reaches a plateau value when $r_2$tends to infinity because the curvature of the withdrawn rod results in a faster dissipation of the stress field than in the case of a plate in which the stress field is linear (see equation (A.2) and (A.8) appendix II). Pulling out a finite rod thus entrains a smaller amount of liquid than pulling out a plate in a wide bath.

To conclude let us come back to the steady character of the flow. As pointed out by the measurement of the force on the rod and by the constant coating thickness, our rods are sufficiently long to establish a steady flow. An overestimate of the time required to reach steady flow can be made by assuming that steady occurs when the critical strain γ_c is reached at position λ_o, yielding the time $\frac{\gamma_c(r_2-\lambda_o)}{V_d}$ where V_d is the downward velocity of the fluid. Mass conservation gives $V_d = -V(r_1 + h)^2/(r_2^2 - r_1^2)$. The critical strain γ_c required to overcome the yield stress is smaller than 25% in the case of our gel (cf Figure 28 Chapter 2). It follows that the longest transient states in our experiments occurs for $r_1 = 2.5$ mm and $r_2 = 33$ mm and are smaller than the duration of experiment.

In summary, we have studied the axisymmetric dip-coating problem for yield-stress fluid. We observe that mass conservation and the flow inside the bath dictate the coating thickness for large enough values of the yield stress. As for Newtonian fluids, we show that geometry plays a critical role in the amount of liquid deposited on the pulled-out object. For Newtonian fluids, the shape of the meniscus differs for a plate and for a rod. For yield-stress fluids, the geometry determines the stress field and the amount of fluid in its liquid state and the quantity of matter that can be withdrawn.

These parameters are of major interest for cosmetic applications. For mascara application for example, we remind that the most important question was "how can we withdraw a maximum amount of matter from a cylindrical container with a brush?". With this study we propose clear physico-chemical parameters to enhance such withdrawal of matter. Until then, we focused on simple geometry, i.e. plate and cylindrical, that gave us a full understanding of the phenomena occurring during dip coating. It is clear that the quantity of matter withdrawn can be enhanced by modifying the nature of the coated piece. More complex surfaces with hairs as in the case of brushes could be an interesting perspective to study in the future.

Take home message – Chapter 3

In this chapter we study the parameters that fix the thickness of a film formed by dip coating experiments. We work in the axisymmetric case which consists in the withdrawing of a rod from a cylindrical bath. Under these conditions:

a. We managed to resolve Stokes' equations and to describe the whole flow inside the bath. As a result, we observe that a layer of the gel is flowing while the rest of the bath remains solid. This layer is quantitatively transferred into a coated layer and fix the thickness of the film on the rod.

b. For high yield stress, we observed that the thickness of the film depended on the size of the bath, the withdrawing velocity and the rheology of the fluid. In this case, the surface tension showed no impacts. However for low yield stress, we get back to behaviour closer to Newtonian liquids, for which the size of the bath has no influence, and the thickness of the film is only fixed by the withdrawing velocity, the viscosity of the fluid and the surface tension.

Chapter 4

Blade-Coating of complex fluids

Summary: In this chapter we focus on blade-coating experiments. Using a soft blade, we investigate the formation of films on rigid substrates and the parameters that fixe the thickness of the film. We observe that the film thickness is not constant over the whole spreading length, and that the deposit is not even homogeneous under some conditions. We made a full theoretical study of the flow under the blade in order to predict the behaviour of the spread fluid. This way we get a complete understanding of how carbopol gels spread and of the phenomenon occurring during spreading a complex fluid.

Blade coating is another method used to coat surfaces with miscellaneous liquids. In contrast with the dip coating method, blade coating consists in constraining the material with a blade making the fluid to spread on the surface and make a thin layer. Common examples are found in many applications such as, food science, building materials management or cosmetic applications. In this part, we propose to simulate a simple spreading motion in order to understand what the key parameters that control the quality of the deposit are.

I. Experimental section

1. Experimental setup

In order to carry blade-coating experiments, we imagined, designed and machined an innovative experimental set-up. It consists in a soft plastic blade hanged above a moving substrate. The liquid sample placed on the substrate is scrapped on the surface resulting in the formation of a few hundred of micrometre thick liquid film. The soft blade is hanged vertically by a fastening device which can be placed very precisely at a specific position thanks to a 3D-axis device driven by micrometrical position screws. Since the plastic blade is soft, it deforms by applying a contact pressure on the substrate which highly depends on the rigidity of the blade and the height of the hanging point above the substrate. The substrate is made of poly(methyl methacrylate) (PMMA) and can either be smooth or sandblasted in order to increase its roughness. It is placed in the base frame of a microscope stage which is able to move at different velocities (from 0.01 to 10 mm/s) towards x and y axis. It is important to keep in mind that only the substrate is moving during experiment, the soft blade is kept static. A microscope objective is set under the substrate in order to observe the microstructure of the formed film. Finally, a profilometer allowing to measure the thickness of the formed film is hanged above the blade-coating set-up.

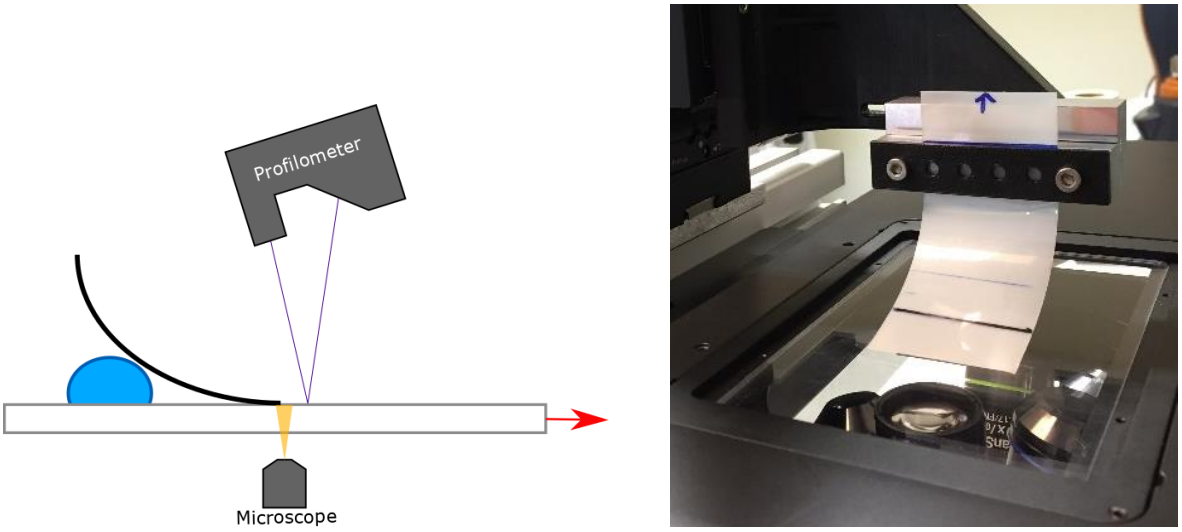

Figure 44: Schematic representation and picture of the blade-coating experimental set-up.

2. Study of the scrapping blade

We use 57 x 40 mm scraping blades composed of poly(ethylene terephthalate) (PET) of different thicknesses (125, 200, and 250 µm). First, we measure the force applied by the blade on the substrate. Not surprisingly, the force highly depends on the distance between the hanging point of the blade and the substrate (Figure 45). Since the blade is hung vertically, the contact with the substrate curves the blade. The more the blade gets deformed, the higher the force applied on the substrate is. We measure the evolution of this force depending on the height of the hanging point and the thickness of the blade. In the following graphic, the applied force is shown against y, which is the ratio between H and L, and the height of the hanging point and L the length of the blade, respectively.

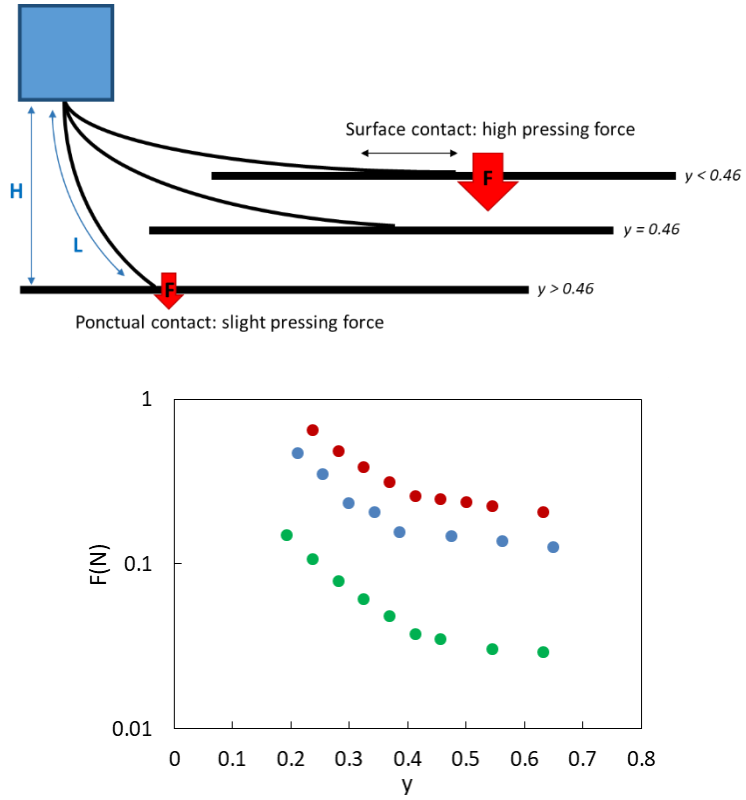

Figure 45: Representation of the shape of the blade depending on the height of the hanging point. The normal force applied by the blade varies as a function of height of the hanging point as displayed in the above graph. The color of the curves correspond to a blade with a thickness of 125 µm (green), 200 µm (blue) and 250 µm (red).

The force applied by the blade increases with the thickness of the blade but also with the proximity H between the hanging point and the substrate. The plot of the force against the proximity gives 2 straight lines corresponding to two geometrical regimes of the blade. For high y, only the tip of the blade is in contact with the substrate, since the distance between the hanging point and the substrate is not low enough to bend the blade sufficiently. The slope modification is characteristic of the configuration change of the blade. Indeed, for low y, because of the high deformation of the blade, the force is

applied on the substrate via a full surface area. At the slope changement point the blade is just tangent to the substrate. As Seiwert *et al.*[69] showed before, the blade is tangent to the substrate when y=0.46. According to the same authors, the thickness of the film depends on the configuration of the blade. In the tangent configuration, the film thickness is the largest. For the following experiment, we have decided to work in the tangent configuration.

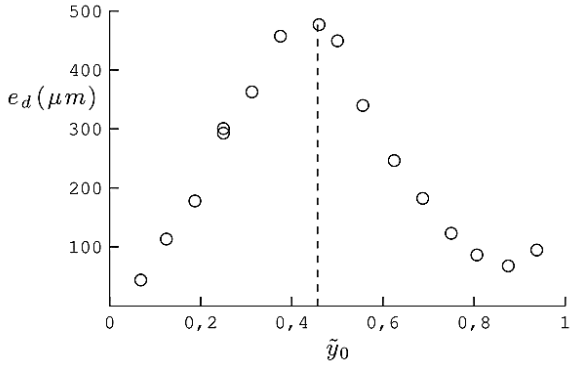

Figure 46: Impact of the ratio between H and L on the thickness of the formed film. The maximum thickness is obtained for y = 0.46. [From Seiwert 2013][69]

II. Formation of the liquid film and prevision of its thickness

1. Experimental measurements

a. Procedure

For the following experiments, the PMMA plate has been sandblasted and plasma treated in order to highly reduce wall slip and inhibit dewetting phenomena due to the PMMA surface tension. Also, we choose a rough 4 cm width scraping blade in order to avoid boundary effects in the measurement of the film thickness which is carried on 16mm width at the middle of the film surface. The 125 µm thick scraping blade is 5.6 cm long and is hanged at a height of 2.6 cm above the surface of the substrate resulting in a normal force of 35 mN. Both PMMA plate and scraping blade are cleaned using a soap solution first, rinsed with tap water, then with MilliQ water and then with ethanol before drying with compressed air between each experiments. The sample, 0.5 - 1 g of gel is heaped as a 40 mm long wormlike, 15 mm before the tip of the blade, and then scraped over 100 mm on the PMMA substrate at room temperature. The laser beam of the profilometer analyses the surface 5 - 7 mm after the tip of the blade in order to measure the film thickness where it is established and does not bear shear and capillary effects any more.

b. Spreading of carbopol gels on a rough substrate

In Figure 47 we show the 3D profile obtained by profilometric measurement of the film thickness.

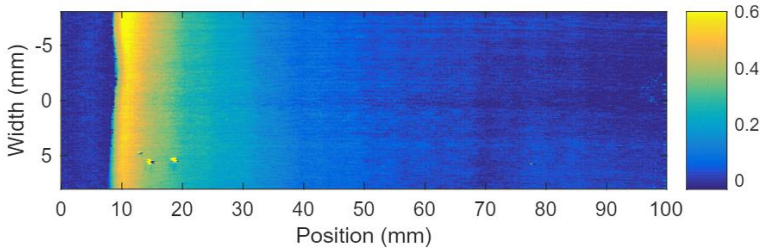

Figure 47: 3D profile of a carbopol coated film on a sandblasted PMMA substrate. The colormap indicated the thickness of the coated film from 0 to 0.6 mm.

Interestingly, spreading carbopol gels using a soft blade results in the formation of a film of variable thickness. The film thickness is first increased until it reaches a maximum thickness, then the film thickness decreases until it reaches 0. Unlike dip-coating, no constant thickness regime is reached during blade-coating by a flexible blade. We anticipate that this is mainly due to the fact that the opposite force to the liquid withdrawing is constant during dip-coating experiments. However, in the case of blade-coating, the opposite force is dependent of the size of the material reservoir behind the blade. During blade-coating spreading, regardless of the initial sample quantity and the yield stress of the gel, the reservoir empties significantly. Thus, the stress on the blade is not constant during spreading, it is constantly changing and no constant thickness regime, is observed.

In the following we analyse in more details the variation of the thickness of the layer as a function of the spreading velocity, the initial mass of sample and the yield stress. The data points in Figure 48 display the variation of the maximal height depending on the spreading velocity, the yield stress and the initial mass of sample. We report spreading velocities between 0.3 and 10 mm/s since we are experimentally limited by the motorized stage. In this range of spreading velocity, the thickness of the deposited layer increases with the velocity. Also, for a given velocity increasing the yield-stress of a gel leads to an increase in the maximum thickness of the coated film. And then, for a given yield stress and spreading velocity, increasing the mass of the initial sample gives a thicker film. The displayed dash lines correspond to the theoretical prediction of the film thickness as a function of multiple parameters that we discuss in the next part.

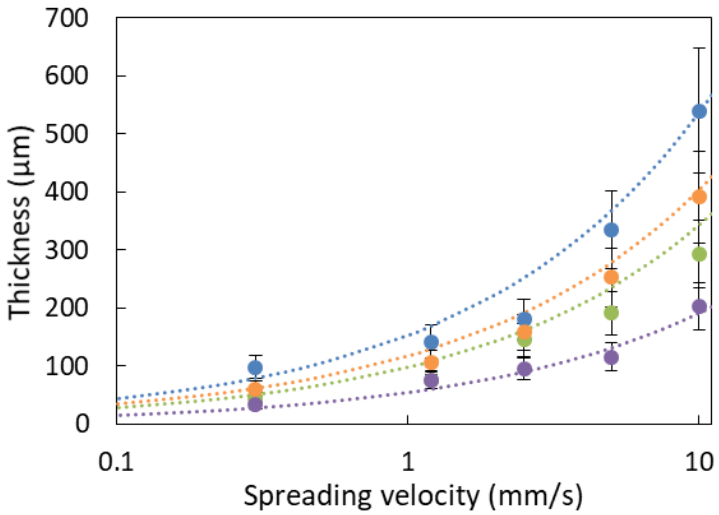

Figure 48: Evolution of the film thickness as a function of the spreading velocity for different carboPEG gels and mass of sample. Purple, green, orange and blue dots respectively correspond to a 0.5 g sample of a 20 Pa yield-stress carboPEG, a 0.5 g sample of 37 Pa yield-stress carboPEG, a 1 g sample of a 20 Pa yield-stress carboPEG and a 0.5 g sample of a 46 Pa yield-stress carboPEG. The dashed lines represented the fit obtained by the model we are describing just after (Equation 4.11).

2. Theoretical approach: prediction of the film thickness

Let us first consider what happens at the level of the blade. The blade and the plate are rough. We thus assume that the fluid perfectly wets the plate. To model the thickness of the deposit, we first recall the analysis of Seiwert et al. As noted by these authors, there is an important analogy between the classic Landau–Levich experiment where the fluid spread is limited by the capillary meniscus and our experiment where the fluid spread is limited by the elastic meniscus of the blade. It is possible to expect similar phenomena. However, this analogy has an important limit. It does not exist at the level of the elastic blade partial wetting situation. At rest, within the framework of the capillary meniscus there is a possibility of anchoring of the contact line.

When the system is non-wetting, it is necessary to apply a force greater than $\cos(\theta)\,\gamma_{LG} + \gamma_{SL} - \gamma_{SG}$ to make the meniscus advance. In the context of the elastic meniscus, this possibility does not exist. The force that applies at rest on the contact point is the reaction force of the blade support. The latter is vertical in the absence of friction or adhesion (case assumed in our experiments). There is no frictional or restoring force on the blade to be exceeded to evacuate the liquid. The blade will level up until the force induced by the flow F_f balances the force exerted by the blade F_b. In the Navier-Stokes equations the viscous term is expressed as $\frac{\eta V}{{h_0}^2}$ in scale law, with η the viscosity of the fluid, V the velocity of the moving plate and h_0 the thickness of the fluid under the tip of the blade. This viscous volumic force is therefore balanced by a pressure gradient.

If we assume that the balance is carried out on a size l from the end of the scraper, we can write:

$$\frac{\eta V}{{h_0}^2} \sim \frac{\Delta P}{l} \tag{4.1}$$

Here l is the length of the blade that is deformed by the fluid and ΔP represents the pressure exerted by the blade onto the fluid. However, Seiwert *et al.* expressed the force exerted by the blade as:

$$F_b \sim \frac{Bb}{{R_c}^2} \tag{4.2}$$

Hence

$$\Delta P \sim \frac{F_b}{lb} \sim \frac{B}{{R_c}^2 l} \tag{4.3}$$

with b the width of the blade, B the rigidity of the blade and R_c the radius of curvature of the blade. The rigidity B of the blade is a parameter calculated from the Young modulus E and the Poisson coefficient ν of the material as $B = \frac{E{h_0}^3}{12(1-\nu^2)}$.

The equilibrium can be written as follow:

$$\frac{\eta V}{{h_0}^2} = \frac{B}{{R_c}^2 l^2} \tag{4.4}$$

The difficulty lies in the determination of l. Indeed, the size region on which the forces are in equilibrium is such that the liquid thickness is of order h_0, but the shape of the scraper when it is deformed by the liquid remains unknown. Nevertheless, as in Landau–Levich–Derjaguin theory, we can assume that the static form of the scraper is undisturbed. The length l would then be the distance (counted from the end of the scraper) for which the blade reaches a height h_0.

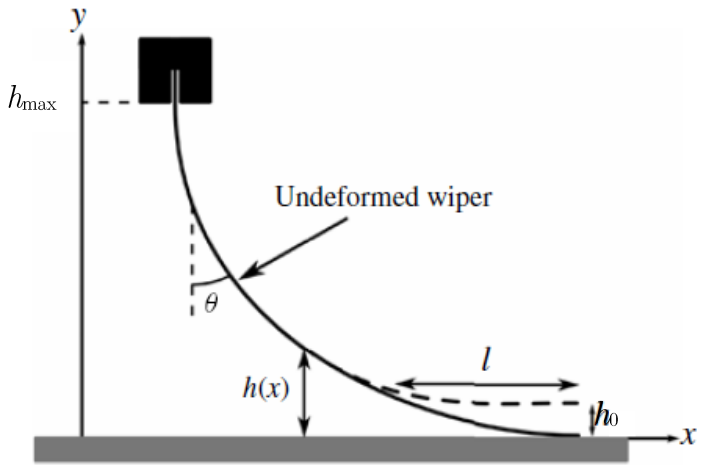

Figure 49: Shape of the blade during coating as described by Seiwert et al.[64]

In his work, Seiwert presented the details of the mechanic of the blade[69]. He showed that a zero contact angle and a zero curvature leads to:

$$l \propto (h_0 {R_c}^2)^{1/3} \tag{4.5}$$

Therefore, the equilibrium yields at:

$$h_0 \propto {R_c}^{5/3} \left(\frac{\eta V}{B}\right)^{3/4} \tag{4.6}$$

Seiwert worked on Newtonian fluids, but these equations are still valid in the case of non-Newtonian fluids. In our experiments, we study a yield stress fluid. Thus, the rheological properties of the fluid will modify the value of the deposited layer. Moreover, the use of a yield stress fluid introduces a new condition on the shape of the blade. To deposit a layer, it is required to level up the blade. In non-slip conditions, this can be done only if the fluid close to the blade is flowing. This implies that the shear stress below the blade has to be higher than the yield stress. Therefore, rheological law allows us to write:

$$\tau(0) = -\tau_y - k\dot{\gamma}^n \tag{4.7}$$

In this expression $\dot{\gamma} = \frac{\partial V}{\partial z} > 0$.

Since the film is thin and its thickness evolves slowly in the x direction, we will assume that the fluid flows only in the x direction. This way, the lubrication approximation is valid and we can write the shear stress at the blade as:

$$\tau(h) = \frac{\partial P}{\partial x} h_0 + \tau(0) \tag{4.8}$$

with $\frac{\partial P}{\partial x}$ is the pressure gradient and $\tau(0)$ is the shear stress at the level of the substrate. Following Seiwert study, we can express the pressure gradient as follow:

$$\frac{\partial P}{\partial x} \sim \frac{\Delta P}{l} \sim \frac{B}{{R_c}^2 l^2} \tag{4.9}$$

Since the fluid under the blade is flowing, we can assume that the limit conditions correspond to the case where the stress at the level of the blade is equal to the yield stress $\tau(h) \sim -\ \tau_y$.

Therefore, inserting equations (4.5), (4.7) and (4.9) in equation (4.8) gives the prediction of the film thickness for non-Newtonian fluids as:

$$h_0 \sim \left(\frac{kV^n {R_c}^{10/3}}{B}\right)^{\frac{1}{n+1/3}} \tag{4.10}$$

Note that we recover the Newtonian case gave by Seiwert from equation (4.10) when the yield stress is zero and for $n = 1$.

The major divergent item comparing to Seiwert study refers to the parameters R_c that we use. Seiwert shows that, for Newtonian liquids R_c corresponds to the length of the blade. However, the orders of magnitude predicted using the length of the blade are not consistent with our experimental data. Therefore, using L_c, the length of contact between the blade and the liquid, allow to get much better fits with the experimental data.

The parameter R_c relates to the curvature of the blade. Even though the curvature as to be taken from the hanging point of the blade for Newtonian fluids, in the case of yield stress fluid the curvature is focus onto the length of contact between the fluid and the blade L_c.

From an experimental point of view, using L_c makes more sense and allows us to explain to impact of the size of the sample onto the film thickness. Indeed, as we showed in Figure 48 using a larger amount of matter leads to thicker coated film. Furthermore, we observed that the film thickness wasn't constant during spreading experiment. As the volume of the fluid under the blade is decreasing upon spreading, L_c is also decreasing along the experiment time leading to thinner films over time.

In Figure 50 we present the film thickness measurement by two means. The first one, in red, is measured using the classic profilometer. The second one corresponds to the thickness predicted by the model following the evolution of L_c during the experiment. We find that both measurements are really close to each other. This way, using the

length of contact between the blade and the liquid is more consistent than using the total length of the blade since it gives us the dependence of the film thickness with the volume of the sample.

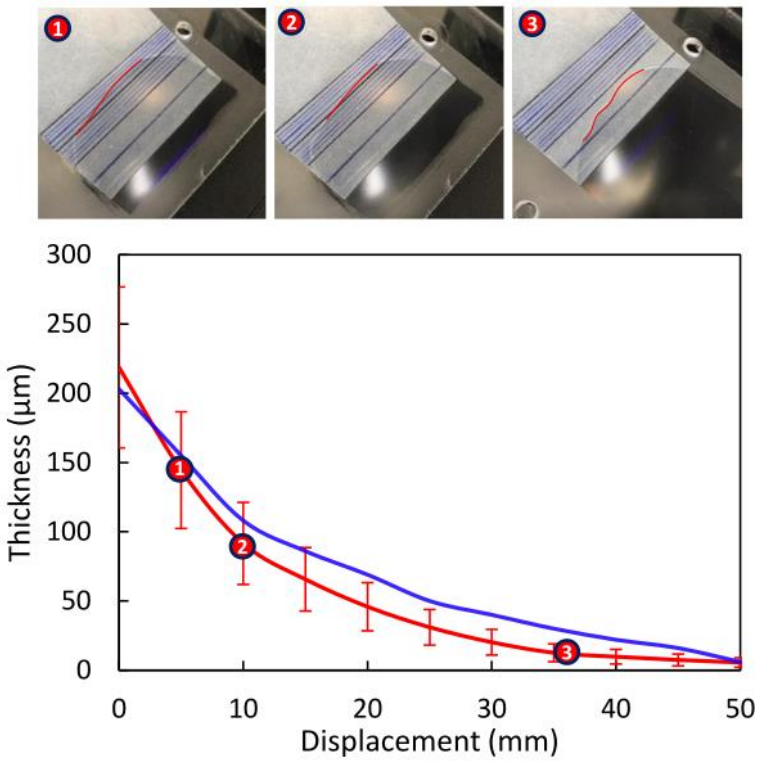

Figure 50: Highlighting of the length of contact L_c between the liquid and the blade at different moments. The above graphic displays the good agreement between the thickness of the film as a function of the position given by the profilometer and calculated by our model using the measure of L_c over time (Equation 4.11).

As a conclusion, we use Equation (4.11) to fit our experimental data in Figure 48 and find a very good agreement between the experimental thickness measurements e and the model with a proportionality constant equal to 1.

$$e \sim \left(\frac{kV^n {L_c}^{10/3}}{B} \right)^{\frac{1}{n+1/3}} \tag{4.11}$$

3. Formation of instabilities within the coated film

In the case of high yield stress fluids and high spreading velocity, we observed that the experimental data do not match the predictions. Such spreading conditions usually generate instabilities such as holes within the coated film resulting from flow issues under the blade.

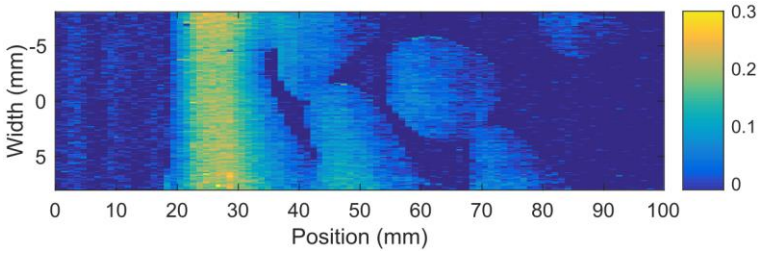

Figure 51: 3D profile of a carbopol coated film on a sandblasted PMMA substrate. The colormap indicated the thickness of the coated film from 0 to 0.3 mm.

Scale laws were enough to predict how high the blade would be raise up by the flow stress. However, to predict the formation of such instabilities we need to focus on the flow under the blade. For blade coating with a yield-stress fluid, the flow underneath the blade has similar characteristics as the flow inside the bath during dip-coating, as described in Chapter 3. Neglecting gravity and assuming a laminar flow, the Stokes' equation in Cartesian coordinates is given by

$$-\frac{\partial P}{\partial x}+\frac{\partial \tau_{zx}}{\partial z}=0 \tag{4.12}$$

Integrating this equation gives the general solution for the laminar flow of a yield-stress liquid through a slot as

$$\tau_{zx}(z)=\frac{2\tau_y}{\Delta}(z-\lambda) \tag{4.13}$$

with $\Delta = 2\tau_y/(\partial P/\partial x)$. We replace the integration constants Δ and λ by λ_i and λ_o which correspond to the position where $\tau_{zx}(\lambda_i) = -\tau_y$ and $\tau_{zx}(\lambda_o) = \tau_y$ such that

$$\Delta = \lambda_o - \lambda_i \tag{4.14}$$

and

$$\lambda = \frac{\lambda_o + \lambda_i}{2} \tag{4.15}$$

Hence, the stress field can be described by

$$\tau_{zx}(z)=\frac{2\tau_y}{\lambda_o-\lambda_i}\left(z-\frac{\lambda_o+\lambda_i}{2}\right) \tag{4.16}$$

The integration constant λ_i and λ_o are obtained from the continuity of velocity ($v_x(0) = V$ and $v_x(h) = 0$) and the conservation of the mass, which give the conditions

$$V = -\int_0^h \dot{\gamma}\,(z) \tag{4.17}$$

$$eV = \int_0^h v_x\,(z)dz = \Big[\, z v_x(z) \Big]_0^h - \int_0^h z\,\dot{\gamma}(z)dz \tag{4.18}$$

with the shear rate $\dot{\gamma} = \frac{\partial v_x}{\partial z}$ and e the coating thickness. In the previous equation we performed an integration by parts and used that $\Big[\, z v_x(z) \Big]_0^h = 0$.

We will now solve these equations for λ_i and λ_o. The relative value of λ_i and λ_o with respect to the local gap height yield three flow regimes (see Figure 52). We will discuss them in order of decreasing gap height.

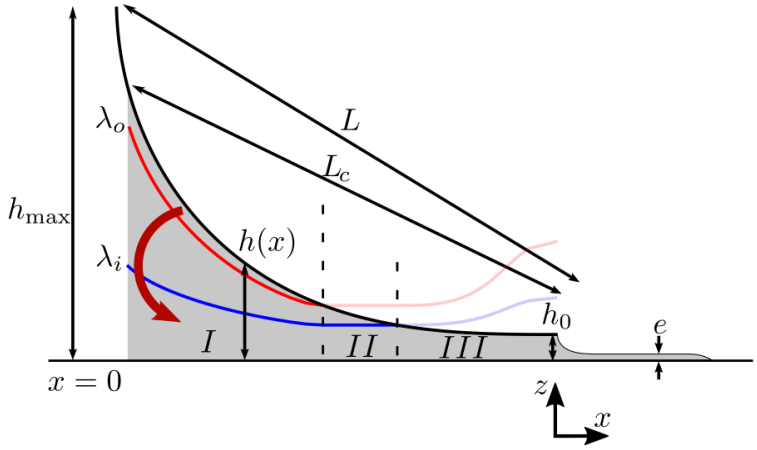

Figure 52: Schematic representation of the blade and the flow regime underneath.

a. *Plug flow: $0 < \lambda_i < h$ and $0 < \lambda_o < h$*

For a plug flow, we obtain the following shear rate from the Herschel-Bulkley model:

$$\dot{\gamma} = \begin{cases} -\left(\frac{2\tau_y}{k}\right)^{\frac{1}{n}} \left(\frac{\lambda_i - z}{\lambda_o - \lambda_i}\right)^{\frac{1}{n}} < 0 & \text{for } 0 \le z \le \lambda_i \\ 0 & \text{for } \lambda_i \le z \le \lambda_0 \\ \left(\frac{2\tau_y}{k}\right)^{\frac{1}{n}} \left(\frac{z - \lambda_o}{\lambda_o - \lambda_i}\right)^{\frac{1}{n}} > 0 & \text{for } \lambda_0 \le z \le h \end{cases} \tag{4.19}$$

Here h is the height of the blade, which is a function of x. Note that λ_i and λ_o consequently depend on the position x as well.

We resolve equations (4.17) and (4.18) by inserting equation (4.19). The integration (4.19) is carried out in the three regimes: $0 \le z \le \lambda_i$, $\lambda_i \le z \le \lambda_0$ and $\lambda_0 \le z \le h$. We thus obtain equations (4.20) and (4.21).

$$\frac{1+n}{n}\left[\frac{k(\lambda_o - \lambda_i)}{2\tau_y}\right]^{\frac{1}{n}} V = {\lambda_i}^{1+\frac{1}{n}} - (h - \lambda_o)^{1+\frac{1}{n}} \tag{4.20}$$

$$\frac{(1+n)(1+2n)}{n}\left[\frac{k(\lambda_o - \lambda_i)}{2\tau_y}\right]^{\frac{1}{n}} eV = n{\lambda_i}^{2+\frac{1}{n}} - (h + nh + n\lambda_o)(h - \lambda_o)^{1+\frac{1}{n}} \tag{4.21}$$

Therefore, we have two equations with the two unknown parameters λ_i and λ_o. We use numerical method to resolve the non-linear equations (4.20) and (4.21) and obtain λ_i and λ_o as a function of h which depends geometrically on x. In our conditions, the length of the scraping blade L is 5.6 cm and the contact angle formed by the blade with the substrate is zero. The shape of the blade leads to the hanging point $h_{max} = 0.46L$. Knowing these parameters, we can estimate the static shape of the blade $h(x)$ from The Elastica equation as described by Timoshenko and Gere in 1985[85] (see Figure 52).

b. Flow with a plug attached to the blade: $0 < \lambda_i < h$ and $\lambda_o \ge h$

Another case is a flow with a plug attached to the blade. In this case $\tau_{zx}(\lambda_i) = -\tau_y$ and $\tau_{zx}(h) \le \tau_y$.

$$\dot{\gamma} = \begin{cases} -\left(\frac{2\tau_y}{k}\right)^{\frac{1}{n}} \left(\frac{\lambda_i - z}{\lambda_o - \lambda_i}\right)^{\frac{1}{n}} < 0 & \text{for } 0 \le z \le \lambda_i \\ 0 & \text{for } \lambda_i \le z \le h \end{cases} \tag{4.22}$$

with $\lambda_i \le h$ and $\lambda_o > h$. The velocity and mass conservation conditions (4.17) and (4.18) give respectively

$$\frac{1+n}{n}\left[\frac{k(\lambda_o - \lambda_i)}{2\tau_y}\right]^{\frac{1}{n}} V = {\lambda_i}^{1+\frac{1}{n}} \tag{4.23}$$

$$\frac{(1+n)(1+2n)}{n}\left[\frac{k(\lambda_o-\lambda_i)}{2\tau_y}\right]^{\frac{1}{n}} eV = n{\lambda_i}^{2+\frac{1}{n}} \tag{4.24}$$

This solution yields

$$\lambda_i = \frac{1+2n}{n}e \tag{4.25}$$

$$\lambda_o = \frac{1+2n}{n}e + \frac{1}{n}(1+n)^{-n}(1+2n)^{1+n}\frac{2\tau_y}{k}e^{1+n}V^{-n} \tag{4.26}$$

c. Shear flow throughout slot: $\lambda_o \geq h$ and $\lambda_i \geq h$

When the flow is sufficient, the complete height of the fluid under the blade is in the fluid state, i.e. $\tau_{zx}(z) < -\tau_y$ for $0 \leq z \leq h$. The Herschel-Bulkley model gives a shear rate

$$\dot{\gamma} = -\left(\frac{2\tau_y}{k}\right)^{\frac{1}{n}}\left(\frac{\lambda_i - z}{\lambda_o - \lambda_i}\right)^{\frac{1}{n}} \tag{4.27}$$

with $\lambda_i \geq h$ and $\lambda_o > h$.

The velocity and mass conservation conditions (4.17) and (4.18) give respectively

$$\frac{1+n}{n}\left[\frac{k(\lambda_o-\lambda_i)}{2\tau_y}\right]^{\frac{1}{n}} V = {\lambda_i}^{1+\frac{1}{n}} - (\lambda_i - h)^{1+\frac{1}{n}} \tag{4.28}$$

$$\frac{(1+n)(1+2n)}{n}\left[\frac{k(\lambda_o-\lambda_i)}{2\tau_y}\right]^{\frac{1}{n}} eV = n{\lambda_i}^{2+\frac{1}{n}} - (h+nh+n\lambda_o)(h-\lambda_i)^{1+\frac{1}{n}} \tag{4.29}$$

As for regime *I*, these equations are solved using numerical methods and The Elastica equation and give the position of λ_i and λ_o.

d. Instabilities

In Figure 52 we show an approximation of the positon of λ_i and λ_o along the blade. It is important to remember that the flows occurring under the blade for $z < \lambda_i$ have a positive velocity. Conversely beyond the $z = \lambda_0$ limit, the material flow is the opposite. As a result, during spreading, a recirculation motion occurs within regime *I* from negative to positive speed zones. In concrete terms, the quantity of material spread on the substrate corresponds to the liquid zone under the limit λ_i. The area delimited by

λ_i is therefore constantly emptied and replenished by the area beyond λ_o until it is completely emptied, since regime *II* does not allow the fluid to recirculate. We postulate that the deposited film is unstable and forms holes if the fluid under the blade is only in regime *III* and *II*, i.e. when regime *I* is empty. In practice, the system is no longer able to form stable films once regime I has been emptied. However, before observing the formation of holes in the deposit, it is necessary to empty the entire volume below λ_i. Thus, although recirculation is no longer assured, it is possible to form a homogeneous film over a more or less long distance depending on the volume of fluid below λ_i and the thickness of the film formed.

Emptying regime *I* corresponds to reach the case of $\lambda_0 = h(x)$. Therefore, we have to calculate the limiting height of the blade that is equal to the expression for λ_0 from equation (4.26). Equating this λ_0 to a cut-off height w, and using the expression $e(k, V)$ from equation (4.11) we obtain

$$\frac{1+2n}{n} e(k,V) + \frac{1}{n}(1+n)^{-n}(1+2n)^{1+n}\frac{2\tau_y}{k} e(k,V)^{1+n} V^{-n} = w \qquad (4.30)$$

Solving this equation using $\tau_y \approx 2k$ (limit case of mass conservation) yields a stability relation between τ_y and V. The cut-off height w corresponds to the minimum height of liquid under the blade that allows the formation of a stable film. We choose to take $w =$ 6 mm since it corresponds to the same order of magnitude as the effective height our sample takes under the blade. The stability diagram for a cut-off height $w = 6$ mm is shown in Figure 53 and is in good agreement with the experimental results.

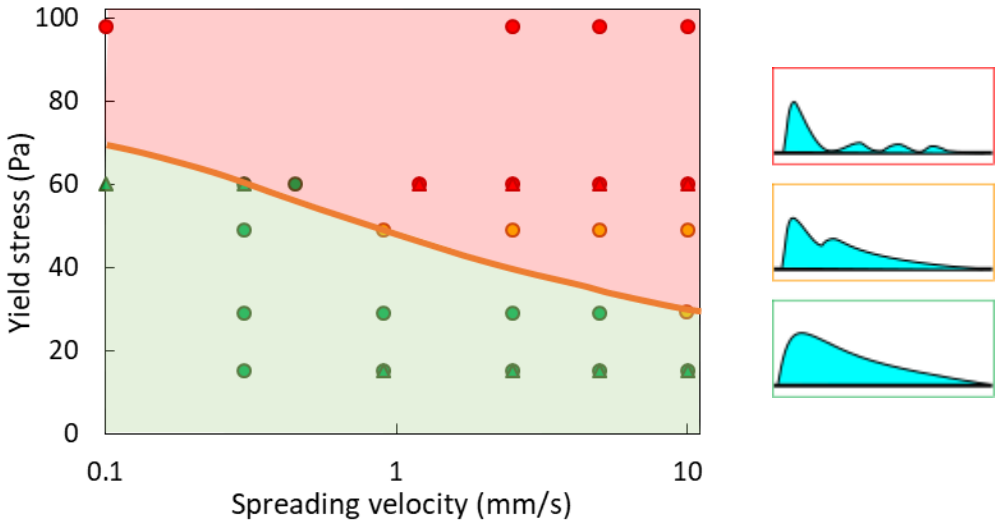

Figure 53: Phase diagram showing the field of stability of a coated film depending on the spreading velocity and the yield stress of the fluid

These data correspond to the spreading of 0.5 g of gel. For low yield stress and low spreading velocity, we evidence homogeneous films without holes over the entire 10 cm long deposit. These films correspond to green symbols in Figure 53. The profile of these

films are classic and show a sharp increase in the thickness at the beginning of the formation of the film, goes through a maximum, and then decreases. For high yield stress and high spreading velocity, we observe holes and bumps in the film. During the process, the part of the gel close to the surface of the substrate is spread. Then, aliquots of gel remain stuck to the blade without touching the substrate. When the blade levels down, these aliquot finally get in contact with the substrate. The new incoming quantity of fluid levels the blade up occasionally and form bumps within the film. Orange points correspond to the intermediate case where the film shows no holes but presents a heterogeneous decrease in the film thickness.

III. Spreading on a smooth and non-wetting situation

Until now we have worked on rough and plasma-treated PMMA substrate to avoid any slippage and dewetting effects during our experiments to favour the formation of homogeneous films. Under other circumstances, the film may either not form at all because the viscous forces that drive the film are lower than the capillary forces, or it may form and dewet afterwards because of the surface energies that are not thermodynamically favourable to the film stability. Thereafter, we will focus mainly on the establishment of the film, rather than its post-creation stability.

1. Conditions for a film to form

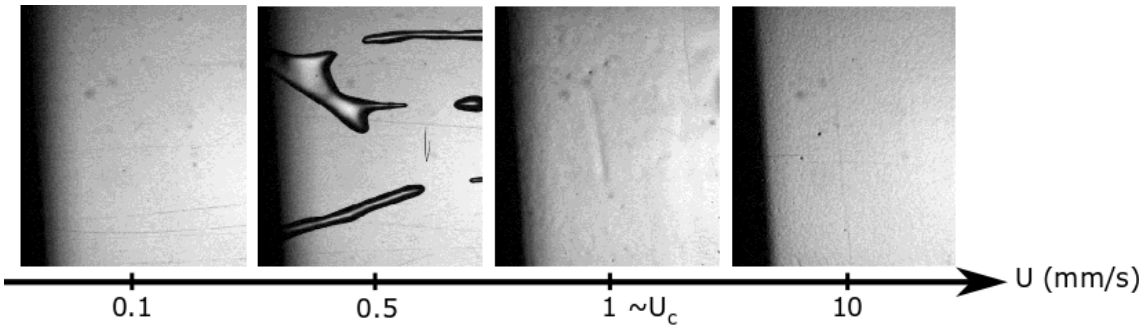

Figure 54: Picture of the deposit formed on a smooth PMMA substrate by the blade coating of a carbopol gel at different velocities. Rheological parameters are τ_y *= 15 Pa, k = 6.6 Pa.s*^{n} *and n = 0.39. The black shadow on the left of each picture correspond to the scrapping blade. The first picture shows a clean substrate, no film is formed. The second picture shows rivulets of carbopol gels that started to spread but do not form an homogeneous film. The third picture shows the first clear homogeneous established film and therefore is considered as the critical velocity. Then the last picture shows an established film, proving that for velocity higher than the critical velocity, a homogeneous film is always formed.*

As shown by numerous studies, both in dip coating[33] and blade coating[67] geometry, the condition to be verified to create a film on a surface is that the capillary number during coating must be greater than a critical capillary number. We therefore decided to undertake a series of blade coating experiments with different carbopol gels in order to

probe the value of the critical velocity formation of the film U_c according to the rheology of the gel. We used two types of gel, the first prepared in pure water, while the second contains 1%$_w$ PEG-12 dimethicone. The surface tension of the gel containing PEG-12 dimethicone is therefore lower than that of pure gels as we showed in Section 2. In Figure 54 we present the state of the deposit spread on the smooth PMMA substrate as a function of the spreading velocity for a given carbopol gel.

As expected, below a critical speed, no film forms and the gel gets stuck under the blade. Under these conditions, capillary forces predominate over the viscous forces that drag the film and prevent the gel from spreading over the substrate. As we approach critical velocity, we observe the formation of carbopol rivulets on the substrate, meaning that the capillary forces have been surpassed punctually by the viscous forces, but not enough to drag the entire film. Once the critical speed is reached, the contact line detaches from the blade and the film is formed. Thus, the viscous forces are greater than the capillary forces, the spreading velocity becomes greater than the dewetting velocity and the film is stable for all velocity above U_c. Analogously, in the case of a rough plate we considered a perfect wetting. Thus there was no critical speed since the dewetting velocity was zero.

In Figure 55 we show the evolution of the critical velocity of the film formation as a function of the yield stress of the gels used. Two blades differing only in thickness are used. This change in thickness (125 µm and 200 µm respectively) induces a change in pressing force, respectively 35 mN and 157 mN. Both pure carbopol gels and carbopol gels containing 1%$_w$ of PEG-12 dimethicone are used.

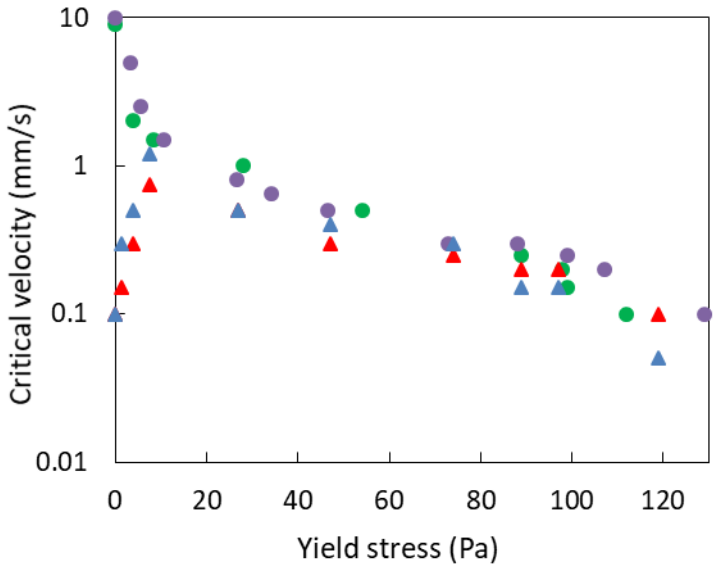

Figure 55: Evolution of the critical velocity of the film formation as a function of the yield stress of the spread gels. Green and red data correspond to a pressing force of 157 mN while purple and blue correspond to a pressing force of 35 mN. Pure carbopol gels are displayed by circles while carbopol gel containing 1%$_w$ of PEG-12 dimethicone are displayed by triangles.

For yield stress higher than 15 Pa, we observe that all data collapse around a master curve which presents a diminution of the critical velocity when the yield stress increases, whatever the pressing forces and the surface tensions are. In this situation, capillary effects are negligible comparing to the yield stress. For yield stress lower than 15 Pa, we observe a significant difference between the critical velocity of pure gels and gels containing 1‰$_w$ of PEG-12 dimethicone. Lower surface tension leads to lower critical spreading velocity, which is consistent with the fact that capillary forces are lower in this case, and less opposed to spreading. However, contrary to the overall trend, we observe an increase in the critical velocity with the yield stress in the case of gels containing 1‰$_w$ PEG-12 dimethicone for low yield stress. In order to get a better understanding of such phenomenon, we will study this system by a more theoretical approach.

2. Theoretical approach

Overall, there are three reasons that can justify the absence of film formation in our system:

- Either the blade blocks the fluid outlet because it does not rise.
- Either the film dewets from the surface on which it is being applied.
- Either the fluid slides and does not spread.

The first hypothesis is quickly ruled out because there is no adhesive force under the blade that prevents it from lifting off the substrate.

Therefore, let us consider the case of a dewetting front. The front is assumed to be of height e. From Stokes' equation, we find that the stress field is linear.

$$\tau_{zx}(z) = \frac{2\tau_y}{\lambda_o - \lambda_i}\left(z - \frac{\lambda_o + \lambda_i}{2}\right) \tag{4.16}$$

We know that the stress at the free surface is zero, i.e. $\tau_{zx}(e) = 0$. In case of no slip, $\tau_{zx}(0) < -\tau_c$, and we have a flow similar to regime *II* ($0 < \lambda_i < e$ and $\lambda_o > e$). The shear rate is given by

$$\dot{\gamma} = \begin{cases} -\left(\frac{2\tau_y}{k}\right)^{\frac{1}{n}}\left(\frac{\lambda_i - z}{\lambda_o - \lambda_i}\right)^{\frac{1}{n}} < 0 & \text{for } 0 \le z \le \lambda_i \\ 0 & \text{for } \lambda_i \le z \le h \end{cases} \tag{4.22}$$

The no-slip condition on the substrate gives $v_x(z) = V$, which gives the following velocity profile:

$$v_x(z) = \begin{cases} V - \frac{n}{1+n}\left(\frac{2\tau_y}{k(\lambda_o - \lambda_i)}\right)^{\frac{1}{n}}\left({\lambda_i}^{1+\frac{1}{n}} - (\lambda_i - z)^{1+\frac{1}{n}}\right) & \text{for } 0 \le z \le \lambda_i \\ V - \frac{n}{1+n}\left(\frac{2\tau_y}{k(\lambda_o - \lambda_i)}\right)^{\frac{1}{n}} {\lambda_i}^{1+\frac{1}{n}} & \text{for } \lambda_i \le z \le e \end{cases} \tag{4.31}$$

The unknowns λ_i and λ_o are determined by the following two conditions:

1. $\tau_{zx}(e) = 0$. This yields $\lambda_o + \lambda_i = 2e$.
2. In the case of a receding front, the flux is zero this gives the mass conservation condition

$$\int_0^e v_x\,(z)dz = 0 \tag{4.32}$$

Inserting the velocity profile yields

$$\frac{1+n}{n}\left(\frac{k(\lambda_o - \lambda_i)}{2\tau_y}\right)^{\frac{1}{n}} eV - e{\lambda_i}^{1+\frac{1}{n}} + \frac{n}{1+2n}{\lambda_i}^{2+\frac{1}{n}} = 0 \tag{4.33}$$

Replacing $\lambda_o = 2e - \lambda_i$ we obtain the following equation for λ_i:

$$\frac{1+n}{n}\left(\frac{k(e - \lambda_i)}{\tau_y}\right)^{\frac{1}{n}} eV - e{\lambda_i}^{1+\frac{1}{n}} + \frac{n}{1+2n}{\lambda_i}^{2+\frac{1}{n}} = 0 \tag{4.34}$$

The viscous stress of the yield-stress fluid on the substrate is given by

$$\tau_{zx}(0) = -\tau_y\left(\frac{e}{e - \lambda_i}\right) \tag{4.35}$$

The capillary force is given by

$$F_{cap} = \gamma(\theta_e - \theta_d) \tag{4.36}$$

with γ the liquid-air surface tension, θ_e the equilibrium contact angle, and θ_d the dynamical contact angle.

The viscous force is calculated by the following integral

$$F_{visc} = -\tau_y \int_a^{l_c} \frac{x\sin(\theta_d)}{x\sin(\theta_d) - \lambda_i}\,dx \tag{4.37}$$

with $a = 10^{-8}$ m the typical molecular size, l_c the capillary length, and λ_i the yield position, which depends on the local height $x \sin(\theta_d)$.

The critical velocity is calculated as the smallest velocity for which $F_{cap} = F_{visc}$ does not have a solution for θ_d. This corresponds to a Cox-Voinov approach for a yield-stress fluid.

In the following graph we show the result of the critical velocity as a function of the yield stress.

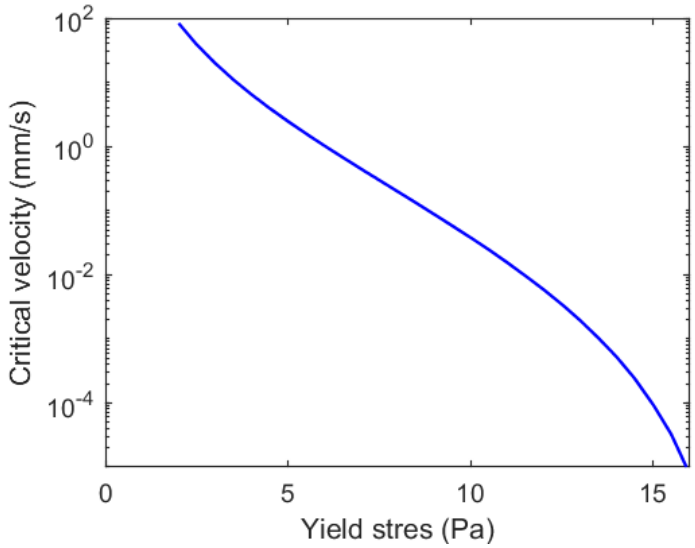

Figure 56: Prediction of the critical velocity to exceed to create a film of carbopol on a smooth PMMA substrate as a function of the yield stress. The cruve is obtained using $k = \tau_y/2$ *and* $n = 0.35$.

The above predictions of the critical velocity as a competition between capillary and viscous forces shows that the critical velocity decreases for an increasing yield stress. Even though the order of magnitude is in good agreement with our experimental results for very low yield stress, i.e. $\tau_y < 10\ Pa$, the prediction gives much lower critical velocity for higher yield stress. The disagreement between the model and the experimental results lead us to confirm that, the capillary effects are not the main cause of the existence of a critical velocity for yield-stress fluids.

Therefore we investigate the slippage of the fluid on the substrate. Paiola *et al.*[86] studied the slippage of carbopol gel in porous media and reported the evolution of the critical velocity as a function of the stress at the wall versus the yield stress ratio τ_w/τ_y. In our case we estimate this ratio to be around 1 – 2. Even though Paiola *et al.* showed that the critical velocity depends on the yield stress of the carbopol gel, they showed that for a $\tau_w/\tau_y = 1 - 2$, the critical velocity is around 0.1 mm.s^{-1} which is in the same order of magnitude than our experimental data. Further studies have to be carried out to get a better understanding of the spreading phenomenon on a smooth surface. However, it is consistent to think that in our case the critical velocity is mainly due to

slipping effects rather than capillary effects. Moreover, in the case of rough surfaces, the slipping velocity falls to very low values, allowing us to create films whatever the spreading velocity is.

Take home message – Chapter 4

In this chapter we study the formation of film by blade coating experiments. To do so, we spread carbopol gels on PMMA substrates using a soft blade made of mylar.

a. We managed to resolve Stokes' equations and to describe the whole flux under the blade. Resulting from the flow under the blade, we observe that, as for the dip-coating experiments, layers of gel are in their liquid state while another layer remains in its solid state.

b. We observed that three flow regimes exist under the blade. One of these regimes allows a recirculation of the fluid under the blade. If this regime does not exist, the formation of the film in heterogeneous.

c. We wrote similar equations than Seiwert to predict the thickness of the formed film. Our model permits to predict the thickness of yield-stress fluid films.

d. We also studied the case where slippage and dewetting were non-negligible, and manage to find the critical velocity was mainly due to slippage effect on smooth surface.

Chapter 5

Using fillers in cosmetic product

Summary: In this chapter we get closer to the real applications of cosmetic products on skin. We develop a back and forth spreading experiment to mimic the real motion of the hand during spreading. We use different kinds of material for the substrate and for the applicator, going from smooth and hard materials to rough and soft, closer to skin. Instabilities and spreading defects have been observed during spreading, we mainly investigate their formation. Rheological and drying effects are taken into account and lead to interesting tools for the formulation of cosmetic products.

I. Spreading of complex systems containing fillers – Screening spreading defects

As we mentioned earlier, cosmetics are made up of a large number of ingredients that can be miscible liquids, immiscible liquids or solids. In formulation, immiscible or solid species that are mechanically dispersed in a matrix are called "fillers". These fillers have various roles in a formulation. For instance, they can act as optical agents (pigments, titan oxide particles), provide better covering power, make the formula more adherent, or simply modify the density of the mixture. However, a too high solid rate can lead to the formation of heterogeneities in the deposit, such as aggregates or holes. These types of spreading defects are critical for the performance of cosmetic products, and need to be better understood.

1. Aggregate-formation characterisation test to rank goodness of formulations

In the industrial world, cosmetic products attributes can be evaluated by experts panels, beauticiens or consumers panels depending on its development stage. Even though this methods allow to compare the products according to spreading sensations and perceived performances, they are somewhat expensive, time-consuming, and may give different answers according to many parameters such as the application gesture or the skin type. Even though, the panel is generally chosen to correspond to a targeted type of person and the gesture can be taught to the panellists, humans remain unable to fix specific parameters that are interesting to scientifically study, such as the spreading velocity and the pressing force during spreading. Hence, it is difficult to quantify the quality of a cosmetic products. Thus, a more quantitative method has been developed, using a tuneable artificial skin and a pressing force captor. Moreover, a specific gesture procedure has been updated as followed.

- A mass of sample is deposited on a known surface corresponding to total amount of 2 mg/cm^2.
- The sample is spread on the surface by doing 15 rotations in 15 seconds.
- The deposit is let at rest for 45 seconds.
- The deposit is spread again by doing 15 rotations in 15 seconds.
- The deposit is let at rest for 2 minutes and 15 seconds.
- The final deposit is then spread by doing 5 fast rotations using a much higher pressing force

Following this test, we can estimate the quality of the formulation based on the aspect of the deposit. Basically, a good-quality formulation leaves a thin homogeneous film on the substrate. However, some other formulations may form spreading defects such as solid deposits, aggregates of particles or heterogeneities within the deposit. With this

test, the risk of formulation to form spreading defects is ranked between 1 for a low risk and 5 for a high risk. This test represents a good evaluation tool as for fully developed products, as for simplex formulations as we are interested in our project. However, since we are particularly interested in physico-chemical parameters that play a role in the formation of spreading defects, an in vitro set-up has been developed from our initial blade-coating set-up to mimic this test and perfectly control multiple parameters that we are still unable to fix by human hand.

2. Mimic of the in-vivo procedure by an in-vitro procedure

Until then we used a blade-coating set-up to spread formulations, however it is limited to simple motions such as one way straight lines. Making realistic and symmetric back and forth movements with the flexible blade is therefore impossible. In order to mimic hand-spreading we developed an experimental set-up of rod-coating. Since the rod is cylindrical, spreading in one direction is equivalent to spreading in the opposite direction. Two sticks are hanged to the stick at an extremity and cross a hanging devise composed of two ball-bearings that allow the cylinder to move up or down freely and with minimal frictional stress along z-axis. The cylinder initially made of smooth PMMA is 40 mm long and has a diameter of 15 mm. The surface of the cylinder can be easily change by sticking other materials such as leather sheet or artificial skin allowing us to study the impact of the roughness or the softness of the applicator.

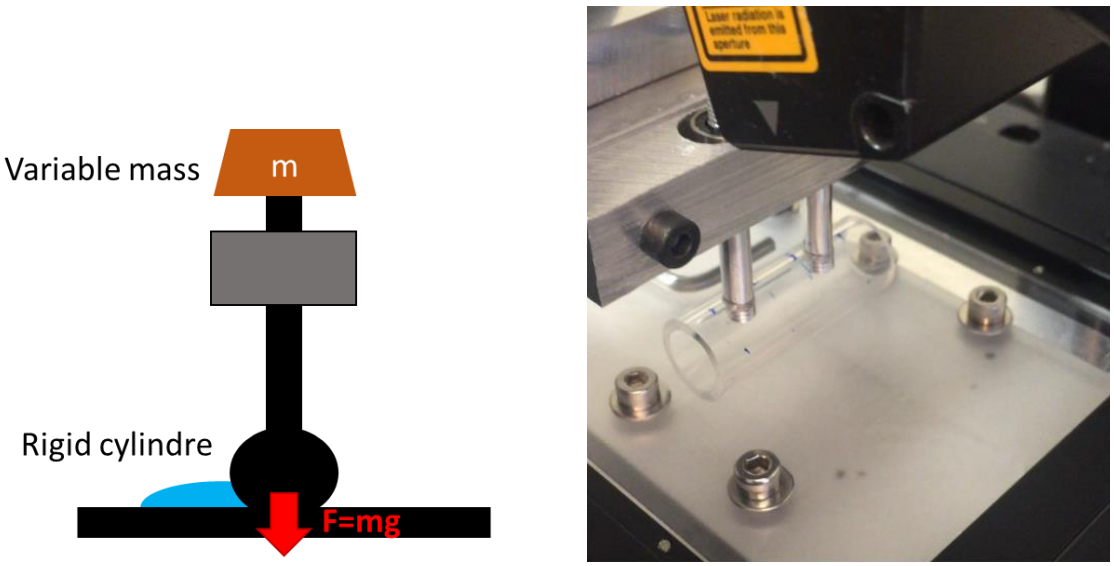

Figure 57: Schematic illustration (on the left) and (on the right) picture of the rod-coating set-up.

On the other hand, we can also modify the surface of the substrate by sandblasting the smooth PMMA, of sticking leather or artificial skin to it. Hence, we are able to study the impact of modifying the roughness or the softness of both applicator and substrate in order to see whether the quality of the deposited film changes.

The procedure we use to test formulations is very similar to the industrial procedure. The main difference lies on the mass of sample we use to perform our experiments. Since we want to measure film thickness with the profilometer we need to obtain film thicker than several dozens of micrometres. Thus, we decided to keep an initial mass sample around 0.5 g for a spreading surface of 40 cm^2 resulting in a general 12.5 mg/cm^2 of formulation. This important quantity of matter induces a much slower drying velocity, so we decided to extend the drying time between spreading sequences. We thus proceed as followed:

- The initial 0.5 g of sample is deposit as a coil behind the rod-coater
- The sample is spread on the surface by doing 15 back and forth movements at 10 mm/s.
- The deposit is let at rest for 5 minutes.
- The deposit is spread again by doing 15 back and forth movements at 10 mm/s.
- The deposit is let at rest for 5 minutes.
- The final deposit is then spread by doing 15 back and forth movements at 10 mm/s using a much higher pressing force.

With this experimental set-up, we also designed variable masses that can be put on top the stick that are hanged to the rod. In this way, we control the pressing and know how much it is worth. The range of force we use is from 59 mN – for the rod and the sticks without additional mass – to 17 N depending of the mass we added.

3. The formation of streaks during back and forth applications

In this part, we focus on a simple repeating back and forth spreading on rough PMMA substrate, without drying session. We observe instabilities, such as striations that form naturally during spreading and we try to investigate the nature of their presence.

a. Macroscopic observation

We first decide to spread simple Newtonian fluid such as a 30%$_w$ glycerol solution in water, pure glycerol and viscous mineral oil. The profilometer measures in direct time the profile of the formes film and its thickness for each back and forth motion. In Figure 58 we show the profile of the deposit after 30 back and forth motion for different fluids. Note that because the refractive index of glycerol matches the one of the PMMA substrate, the measure was difficult to carry and the results are noisier than in the case of water-based fluids.

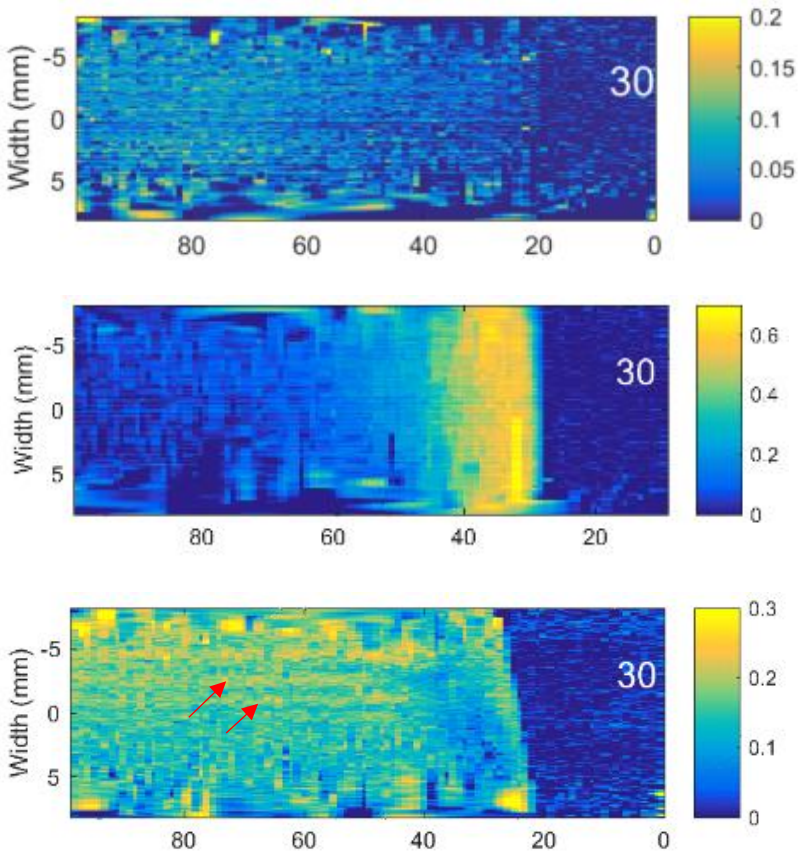

Figure 58: Profile of a deposited film of 30%$_w$ glycerol solution, pure glycerol and 72 Pa.s mineral oil after 30 back and forth movements. The Thickness colormap is given in mm.

When the 30%$_w$ glycerol solution is spread, it is found that the Newtonian mixture forms a smooth film of constant thickness. However, for pure glycerol, the film is also smooth but the thickness is variable with a bump that the diluted glycerol does not form, or does not form for a time long enough to be detected by the profilometer which measures the profile of the film few seconds after it is formed. Since pure glycerol is much more viscous than the 30%$_w$ solution (1.49 Pa.s and 2.1x10^{-3} Pa.s respectively), the bump formed suffers more gravity in the case of pure glycerol. The competition between viscosity and gravity can be estimated by the Galilei number: $Ga = \frac{g\,L^3}{\nu^2}$ with L a characteristic length we choose equal to 500 µm which corresponds to the approximate thickness of the bump and $\nu = \frac{\eta}{\rho}$ the kinematic viscosity of fluids (equal to 1.18x10^{-3} m^2/s and 1.92x10^{-6} m^2/s respectively). Under these conditions the Galilei numbers yield to 8.8x10^{-4} for pure glycerol and 3.2x10^2 for the 30%$_w$ solution highlighting the difference of behaviour between both solutions. Since gravity dominates viscosity for diluted glycerol, the bump relaxes and does not appear on the profilometric surface. Spreading even more viscous fluids, such as a mineral oil with a viscosity of 72 Pa.s, following the same procedure show the formation of small striations in the motion direction that we wasn't able to detect for glycerol. Such streaks seem to create whatever is the liquid but relax too quickly to detect if the fluid is not viscous enough.

In the case of yield-stress fluids such as carbopol gels, theyact as a liquid under a sufficiently stress but remain solid with theoretically an infinite viscosity at rest. Thus, if the streaks are formed, they should not be able to relax at rest. This way, this is not surprising to observe such striation in Figure 59.

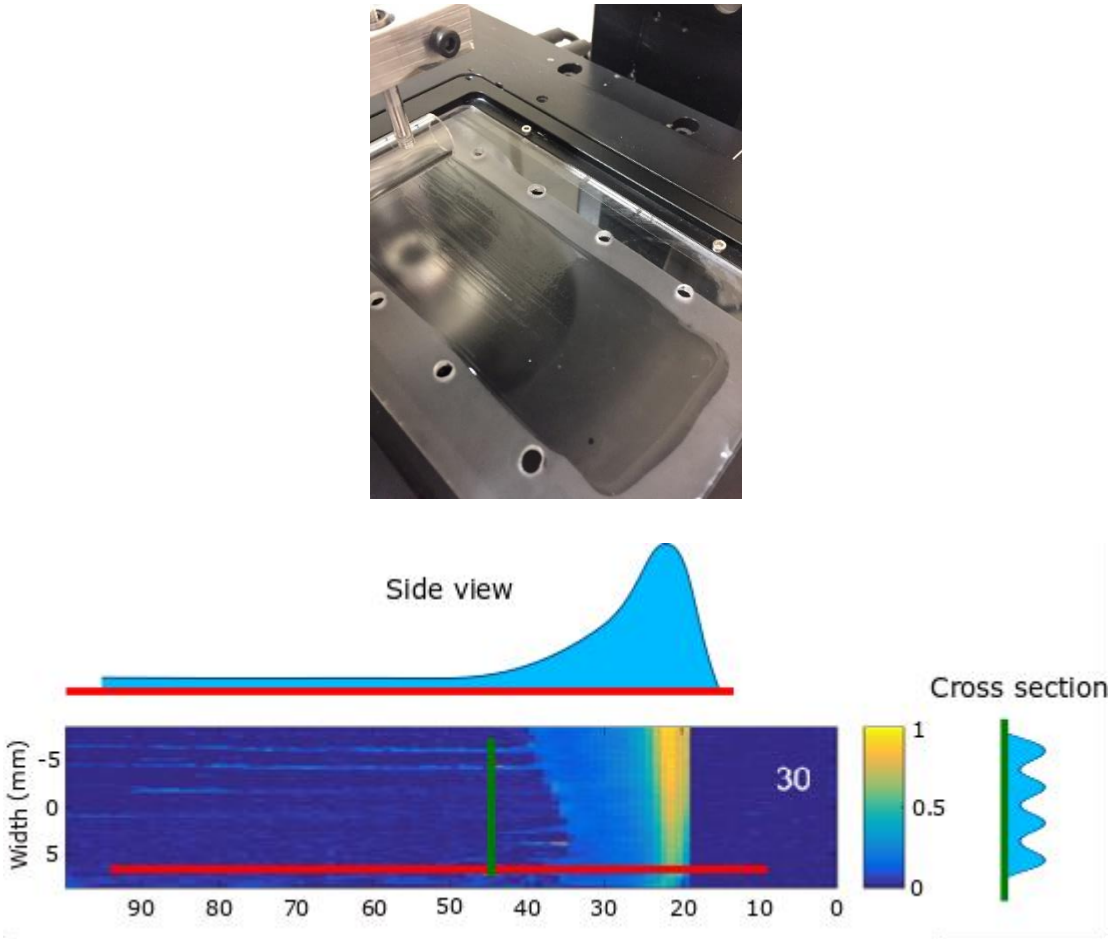

Figure 59: Picture of a coated film of a 0.2%$_w$ carbopol gel (top) and its profile (bottom) and after 30 back and forth movements.

Therefore, fluids with long relaxation time, able to maintain a shape at rest for a sufficiently long time, can form films with streaks. We wonder if fluids, such as shear-thickening fluids with solid character under stress and a liquid character at rest, also show striations.

We have prepared a 40%$_v$ starch shear-thickening suspension in water and spread it following the same procedure. Interestingly, the shear-thickening behaviour of the suspension results in the formation of bumps parallel to the spreading direction. During spreading, matter accumulates behind the rod-coater and the stress imposed by the rod-coater makes the shear-thickening fluid to contract and increase its viscosity temporally. The rod is then pushed up to release an excess of matter onto the substrate. Over a 10 cm spreading, this phenomenon occurs about 4 times, and the general profile is completely different from what we observed with viscous and yield-stress fluids. The

starch suspension also dries throughout the spreading process leading to the structure of the deposit to fix in a solid static shape.

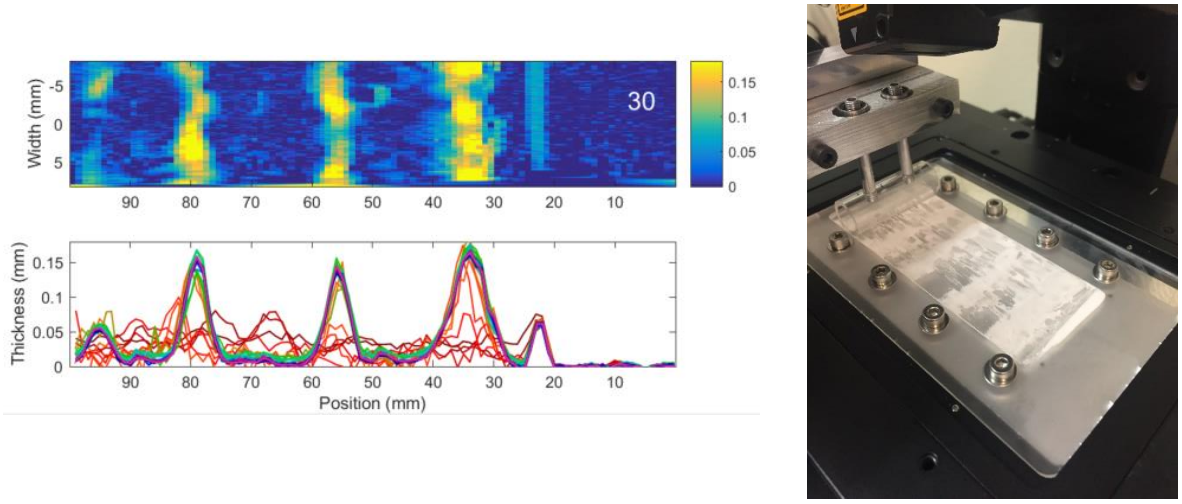

Figure 60: Profile of a deposit film of 40%$_v$ starch suspension in water.

We wonder which of these effects dominates if we mix both starch particles within a carbopol gel. We thus prepared a 20%$_v$ starch suspension in a 0.2%$_w$ carbopol gel. As we showed in Chapter 2.IV, even if the yield stress of carbopol gels is reduced by the presence of an increasing volume fraction of starch particles, the rheology of such preparations are closer to yield-stress fluid behaviour of carbopol gels than the shear-thickening behaviour of starch suspensions, even for higher concentrations of starch. Hence, with this starch-carbopol formula, streaks form very quickly in the direction of spreading after only 4 back and forth movements (instead of 15 for simple carbopol), and remain almost unchanged over the whole spreading process. This might be due to the drying of the formulation that highly modify the rheology of the suspension in carbopol. The initial yield-stress formulation forms streaks, and dry depositing particles on the streak paths. The drying makes the formulation to remain stuck in the streak configuration. In the case of simple carbopol gels, drying only induce the increasing of the concentration of polymer within the gel, hence the yield-stress increases. However, the effect of drying on carbopol gel do not modify its fundamental behaviour since it remains a yield-stress fluid, there is no particles accumulation. The streaks are formed, but remain liquid under stress and are free to unstructured and restructure throughout the spreading process, resulting in shallower streaks.

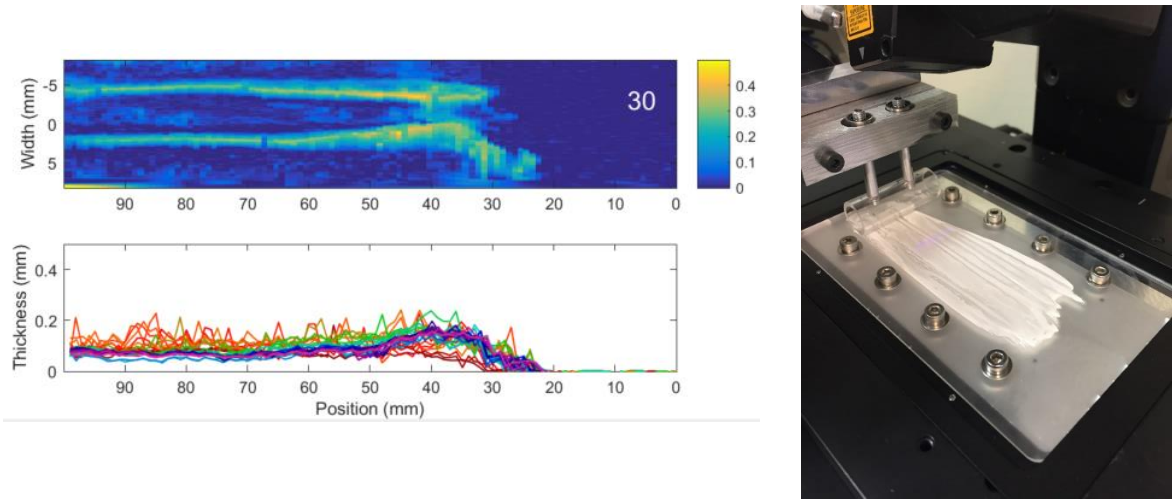

Figure 61: Profile of a deposit film of 20%$_v$ starch suspension in a 0.2%$_w$ carbopol gel.

b. How do streaks form?

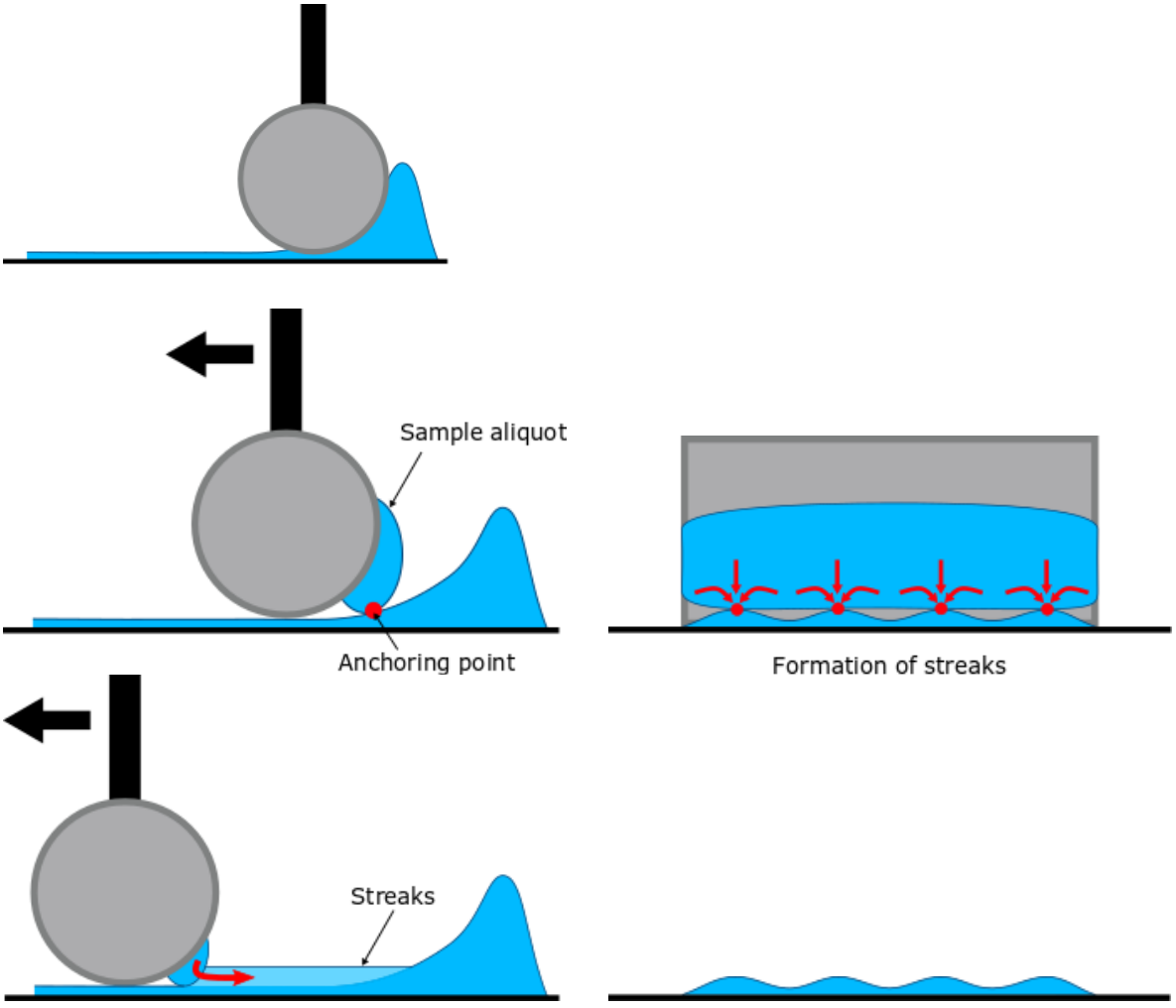

Figure 62: Schematic explanation of the formation of streaks through multiple back and forth spreading.

The streaks seem to form naturally during back and forth spreading movements. Such profiles have already been reported for the simple spreading of viscoelastic solutions of polymer[67], and it was associated to non-Newtonian viscoelastic behaviour of the fluid. Here, we observe that streaks appear for both Newtonian and non-Newtonian fluids, so the non-Newtonian behaviour cannot explain by itself the streaks formation. We also imagined that such pattern may appear to spatial differences of concentration within the deposited film. However, since non-volatile systems, such as viscous oil, also show the striated pattern, the drying effect hypothesis can also be rejected. From what we observe, streaks are more likely to be form from a simple re-deposition from the rod onto the substrate. Doing back and forth spreading leads to matter accumulation at the two edges of the spreading zone, feeding the rod at each pass. When it hits the matter accumulated at the edge, the rod carries an aliquot away. This aliquot is subjected to gravity and fall until reaching the substrate or the deposited film. It then enters into contact by preferential points and most of the volume of the aliquot escape through these anchoring points forming streaks along spreading (Figure 62). This is a first explanation of the formation of streaks obtained by macroscopic observation. Therefore, it should be more investigated in the future.

4. Formulation impact on the deposit quality

a. Preparation of simplex formulations and spreading default risk test

In cosmetic applications, spreading cosmetics on skin consist in making thin films of formulation and let it dry on a rough and soft surface. Hence, the composition of the bulk formulation is completely different from the dried formulation on skin, and their behaviour differs drastically. For example, slippery formulations based on starch and carbopol becomes powdery when dried since the whole liquid phase which played the role of lubricant evaporates and only particles and polymer chains remain in the dried deposit. Two types of deposits are therefore determined, the solid-powder deposit which is white and consists mainly in particles, and the liquid deposit which is transparent and contains a substantial non-volatile liquid phase. As we are trying to understand the impact of different cosmetic formulation ingredients, we have decided in the first place to limit ourselves to simplex systems based on carbopol, starch and glycerol. In order to understand the impact of each of these ingredients, we perform a dose effect test by modifying the proportions of the components as followed.

Formula	$\%_w$ carbopol (in liquid phase)	$\%_v$ starch (global volume)	$\%_w$ glycerol (in liquid phase)	Spreading defect risk	φ_{starch} (In the dry film)	τ_y (Pa)	k ($Pa.s^{1/n}$)	n
1	0.3	6.4	10	3	0.46	50.8	18.4	0.40
2		9.3		5	0.56	48.3	16.9	0.42
3		12.0		5	0.63	44.0	16.0	0.44
4		6.9	50	1	0.14	46.8	29.1	0.44
5		10.0		1	0.20	41.5	27.4	0.45
6		12.9		3	0.25	37.6	25.7	0.47

Table 4: Composition and rheological characterisation of the formulations.

The formulations are prepared using a $1\%_w$ stock carbopol gel diluted in a suitable mixture of water and glycerol to obtain the desired water-glycerol ratios. Then starch particles are dispersed using an anchor agitator at 2000 rpm for few minutes. The mass fractions in the liquid phase are calculated by ignoring all non-liquid ingredients (i.e. starch) since the local concentration of carbopol is not impacted by the presence of a surrounding solid phase, whereas the volume fraction of solid particles is calculated considering the whole volume of sample (liquid and solid) in order to have a view of the steric encumbrance in the sample. Once the formulation is duly prepared, we carry the industrial spreading default risk test on artificial skin to rate them with a mark from 1 to 5 corresponding respectively to low and high risk to form spreading defects during spreading. Formulations 4 and 5 present a slippery feeling and are visually shiny all along the spreading process. We give them a score of 1 out of 5. Formulations 1 and 6 are slippery at the beginning of the spreading process, but end up being sticky and even powdery and leaving a slight white deposit on the spreading finger for the formulation 1. We give them a score of 3 out of 5. Finally, formulations 2 and 3 end up being powdery and leaving frank white deposit on both the spreading finger and the artificial skin on which we spread the formulations. We give them a score of 5 out of 5.

b. Observation of the dry deposit

We show here the aspect of the artificial skin after spreading formulations 3 and 4, which represent the extremes in terms of risk of spreading defect formation (Figure 63). To do so, we use a KH-7700 Hirox videomicroscope allowing us to observe directly both the microstructure of the substrate and the aspect of the deposit at a microscopic scale.

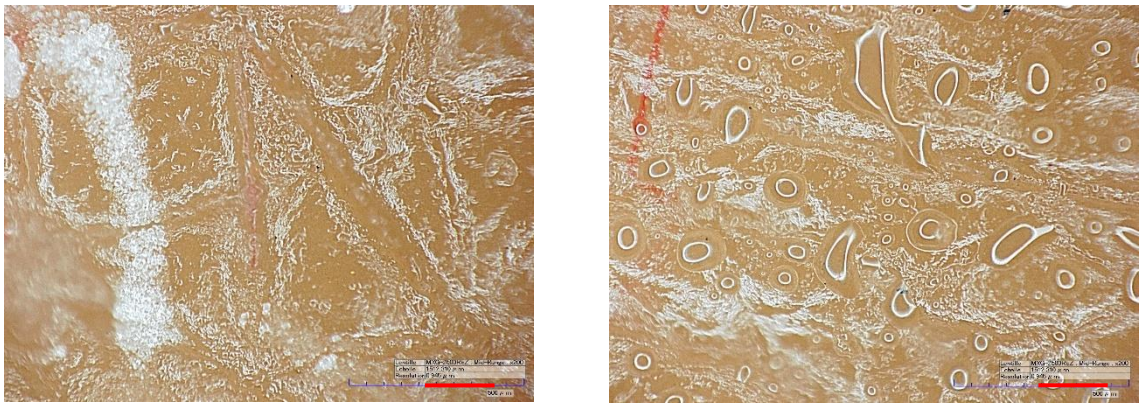

Figure 63: Pictures from Hirox microscope of formulation 3 (left) and formulation 4 (right) after drying. The red scale represents 2 mm.

It is clear that both dry deposits do not have the same aspect, even at microscopic scale. The formula 3 leaves aggregates of starch particles on the surface which are responsible of the powdery deposit. On the other hand, formula 4 leaves droplets of liquid, certainly corresponding to non-volatile glycerol, responsible for the shiny slippery deposit. Doing a 50 µm thin film of these suspensions on a glass slide and observing it with a classical microscope allows us to get an even closer look to the microstructure of the dry deposit.

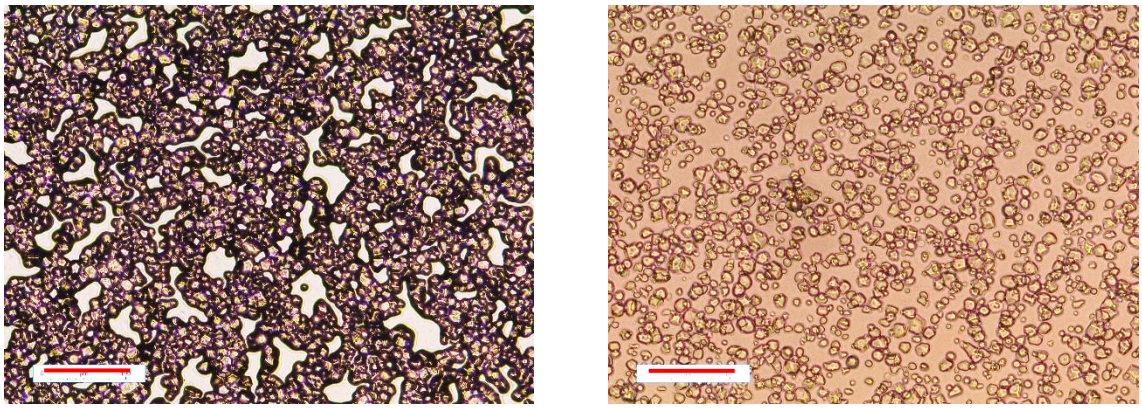

Figure 64: Pictures of 50 µm films of formulation 3 (left) and formulation 4 (right) after drying using an inverse microscope. The red scale represents 100 µm.

On the picture of formulation 3, the particles are packing together forming aggregates of particles. The particles are linked by the remaining non-volatile liquid in the dry deposit, i.e. the glycerol which makes capillary bridges and glues particles within the aggregates. On the other hand, the particles in the pictures of formulation 4 seem to be well dispersed. In this dry film, the remaining volume of glycerol is sufficiently high to embed and disperse particles. These observations are consistent with the calculation of the starch volume fraction in dry films which are 0.63 and 0.14 for formulation 3 and 4 respectively. We showed before that above a critical volume fraction corresponding to the random close packing volume fraction of a system, the media is in a crumble-like

state and globally behaves like a solid (as in formulation 3 dry film). However, a lower volume fraction of particles leads to a liquid mixture. Hence, the random close packing volume fraction of a system seems to be an important parameter to take into account in order to predict if the risk of forming spreading defects is high or not.

c. Rheological approach

We understand that the spreading behaviour of these formulations are differing from one to the other. Hence, studying the rheological properties of the formulations should help us to investigate spreading behaviour differences between formulations. The rheological properties of formulations are determined by flow sweep experiment and Herschel-Bulkley fit ($\tau = \tau_c + k\dot{\gamma}^n$) to get the following rheological parameters. We observe that, as reported by Maillard[58], increasing the glycerol ratio in a carbopol gel does not modify the yield stress of the media but increases the viscosity parameter k and the shear-thinning index n. On the other hand, as we showed before, increasing the volume fraction of starch decrease the stress at low shear rate and the yield stress of the formulation.

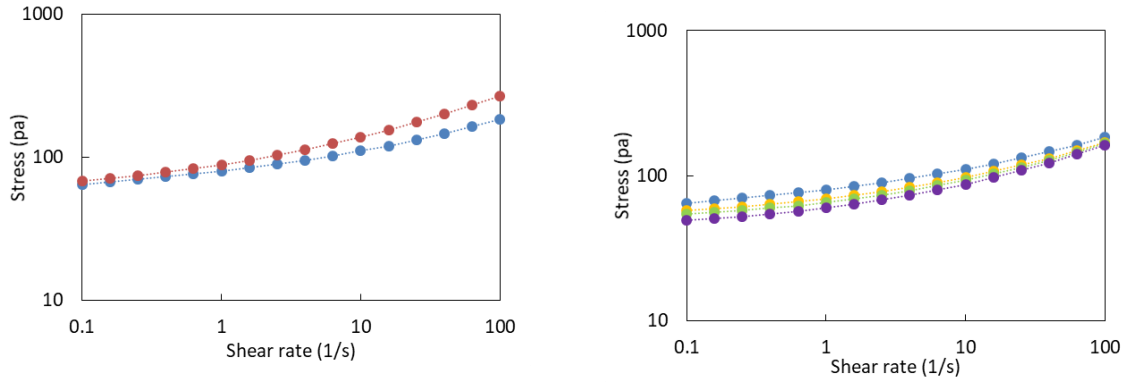

Figure 65: Rheological properties of 0.3%$_w$ carbopol gels at 10%$_w$ (blue) and 50%$_w$ (red) of glycerol (left) and of a 0.3% carbopol gel containing 10 %$_w$ of glycerol at 0 (blue), 6.4%$_v$ (yellow), 9.3%$_v$ (green), 12%$_v$ (purple) volume fraction of starch (right).

As previously showed, bulk rheological parameters only show slight differences between formulations and are not enough to understand why the spreading behaviours are that different. Therefore, we investigate the rheological properties of formulation during spreading. To do so, we let the formulation progressively dry in an oven at 40°C. The oven is kept at 40°C in order to avoid any denaturation of starch particles during drying. Since drying is a surface phenomenon, the mixture has to be homogenized before use in order to avoid crusts. We choose to focus on formulation 3 and 4 because they represent extremum of the previous experiment. However, the formulations we actually used in this drying experiment had a little bit higher volume fraction comparing to the previous formulations 3 and 4 (about 2%$_v$). Nevertheless, the formulations 3' and 4' that we present here still represent systems that have high (5/5) and low risk (1/5) of forming spreading defects. We obtain 4 samples (A, B, C and D) resulting from 3 successive

drying sessions. The composition of each sample is calculated by water weight loss over time.

Formula	$\%_w$ carbopol (in liquid phase)	$\%_v$ starch (global volume)	$\%_w$ glycerol (in liquid phase)	φ_{starch} (In the dry film)	τ_y (Pa)	k ($Pa.s^{1/n}$)	n
3'A	0.30	14.6	10.0	0.68	19.9	10.3	0.46
3'B	0.43	19.8	14.3		31.5	17.1	0.48
3'C	0.75	30.5	25.0		67.5	62.0	0.48
3'D	1.15	40.9	38.2		225	226	0.77
4'A	0.30	8.5	50.0	0.17	28.0	20.8	0.45
4'B	0.38	10.7	62.5		36.7	37.4	0.46
4'C	0.45	13.0	75.6		45.2	104	0.48
4'D	0.60	17.3	99.8		63.4	193	0.51

Table 5: Composition and rehological characterisation of formulations during progressive drying.

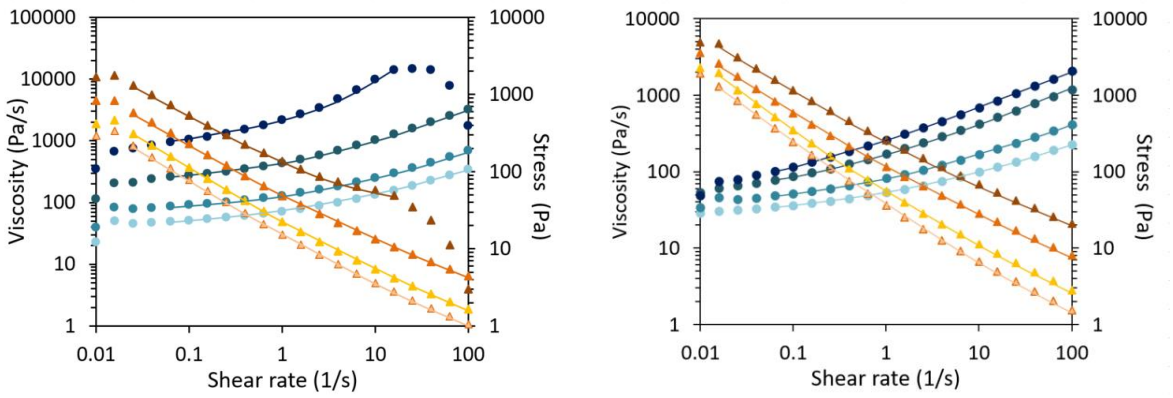

Figure 66: Evolution of formulation 3 and 4 rheological properties during drying.
Stress • 3'A • 3'B • 3'C • 3'D Viscosity ▲ 3'A ▲ 3'B ▲ 3'C ▲ 3'D
Stress • 4'A • 4'B • 4'C • 4'D Viscosity ▲ 4'A ▲ 4'B ▲ 4'C ▲ 4'D

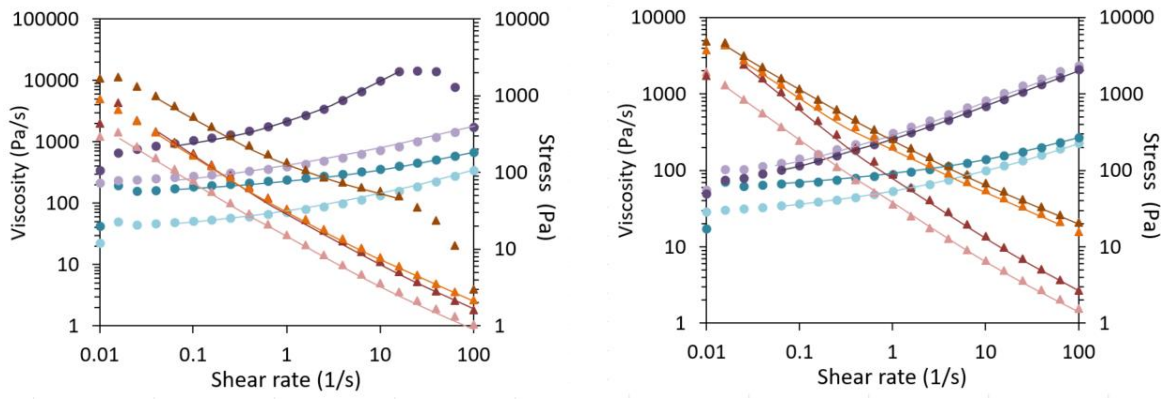

Figure 67: Comparison of the rheological properties between formulations 3 and 4 and their continuous phases without particles.

Stress
3'A *Solvent 3'A* *3'D* *Solvent 3'D*
Viscosity
3'A *Solvent 3'A* *3'D* *Solvent 3'D*

Stress
4'A *Solvent 4'A* *4'D* *Solvent 4'D*
Viscosity
3'A *Solvent 3'A* *3'D* *Solvent 3'D*

We have previously seen that the addition of starch in a carbopol gel tends to lower the yield stress of the gel. On the contrary, the increase in the concentration of carbopol causes the yield stress to increase. By drying the formulations, both the starch and the carbopol concentrations increase. According to the rheological curves, the effect of carbopol dominates, since there is a strong increase in the yield stress when the formulations dry. Since there is a higher quantity of glycerol within the 4' sample, the maximum concentration of carbopol is fixed at a lower concentration than in the case of sample 3' that initially contains 90% of water. Therefore, final drying stage of formulation 4'D contains 0.60%$_w$ of carbopol and 17.3%$_w$ of starch and remains a concentrated suspension of starch in a carbopol-glycerol mixture. On the other hand, the 3' sample dries with a high increase in the concentration of both starch and carbopol resulting in a strong increase of the yield stress. This increase is all the more surprising since the increase in the yield stress for a pure carbopol gel depending on the concentration is logarithmic and at a concentration of 2%$_w$ the yield stress generally obtained is rather in the order of 150 Pa. In our cases the 3'D formulation has a yield stress of more than 200 Pa for a carbopol concentration of 1.15%$_w$. In parallel, we see that the viscosity curve as a function of the shear rate generally decreases linearly. However, for the 3'D formulation, there is a break in the slope before the sample is ejected from the rheometer. It could be the beginning of a shear-thickening effect. Indeed, the volume fraction of starch particles in this sample is around 41%$_v$. Under these conditions, interparticular friction begins to have an effect on the global rheology of the system. However, as Brown et al.[87] showed, shear-thickening effects can be hidden by the presence of a yield stress if it is not strong enough. We did not succeed in making the formulation dry any further in order to have a higher starch concentration. Approaching the random close packing volume fraction makes the sample very difficult to manipulate, and compromises the experiment to

confirm the presence of a shear-thickening effect here. However, the final drying stage of the formulation 3' corresponds to a crumble state mixture, which is really different of what we observe with the formulation 4'. It is possible to screen the impact of particles with the extreme samples (3'A, 3'D, 4'A and 4'D) by checking the difference between their rheological properties those of their liquid phase without particles. Interestingly, the rheology of the 4'D sample and its solvent without particles are very close suggesting that under these conditions, particles do not play a significant role of the global behaviour of the formulation during spreading. On the other hand, the flow curve of the sample 3'D present a much higher stress than its solvent. Here, the impact of particles is not negligible and changes dramatically its rheological profile.

Once again, all these results leads underline the key role of the volume fraction of particles within the dried deposit. We showed that the φ_{RCP} of starch in glycerol was around 55%$_v$ and surprisingly the spreading defect risk swift from a low to a high risk around this value (Formulation 1, φ_{starch} (in the dry film) = 0.46, spreading defect risk = 3/5). Rheological measurements are completely consistent with the behaviour of concentrated suspension. Indeed, a volume fraction closer to φ_{RCP} leads to stronger interparticular interaction.

To conclude, the main parameter to take into account is the volume fraction of solid in the dry deposit. Getting a volume fraction of particles in the dry deposit higher than the φ_{RCP} of the system automatically leads to spreading defects composed of aggregated particles.

5. Impact of the substrate and the applicator on the spreading quality

We showed how fillers like starch particles can affect the global spreading behaviour during drying of formulations. We know that using a high volume fraction of particles, especially when it is higher than the φ_{RCP} of the system leads to white powdery deposit. Industrially, it is also important to understand if the deposit is able to snatch by forming macroscopic aggregates or rolls of matter. In the case of suncare or foundation products, the snatching scrapes sun-active or pigment particles resulting in bad performances of cosmetic products. It has to be avoid in order to optimize their efficiency.

a. Experimental set-up and method

The objective of the following experiments is to test whether a given sample (Formulation 3) that forms a white powdery deposit, can be snatched by the scraping motion of an applicator. As a reminder, the dry deposit of the formulation 3 is composed of starch particles linked by capillary bridges of glycerol. The point of this experiment is to use different type of substrates, applicators, and changing the pressing force during the scraping movement. We thus prepared a smooth PMMA substrate, a sandblasted rough PMMA substrates, and an artificial leather layer stick to a rigid substrate. As for

applicator we prepared a smooth PMMA cylinder and a second one on which we stuck a layer of artificial layer. Therefore, we study the impact of the roughness, but also the impact of the softness on the snatching of the deposit. To do so, we use the in vitro procedure we developed in Chapter 5.I.2 that mimics finger spreading characterization test on artificial skin. The aim is to spread the formulation 3 by doing two sessions of 15 back and forth movements followed by 5 minutes of drying after both spreading sessions. After this step a dry striated deposit is established on the substrate. The pressing force is kept constant and worth 0.063 N over all the experiment to create the dry film. On the other hand, we carry multiple experiments in which we modify the pressing force during snatching process by simply adding weights above the sticks that hold the applicator cylinder.

Two images are taken under a controlled light exposition before and after the 15 back and forth snatching movements. The idea is to quantify the number of white pixels on the pictures corresponding to the dry deposit on both pictures. Comparing the number of pixels before and after snatching leads to an estimation of the surface of matter snatched out of the substrate.

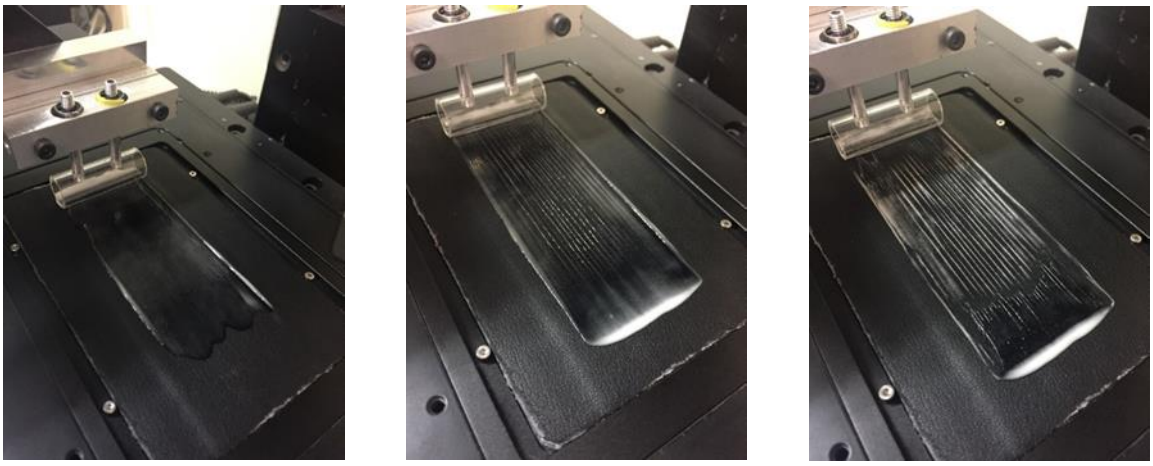

Figure 68: Pictures of the deposit made by a smooth PMMA substrate on an artificial leather substrate after 1, 15 and 30 back and forth movements.

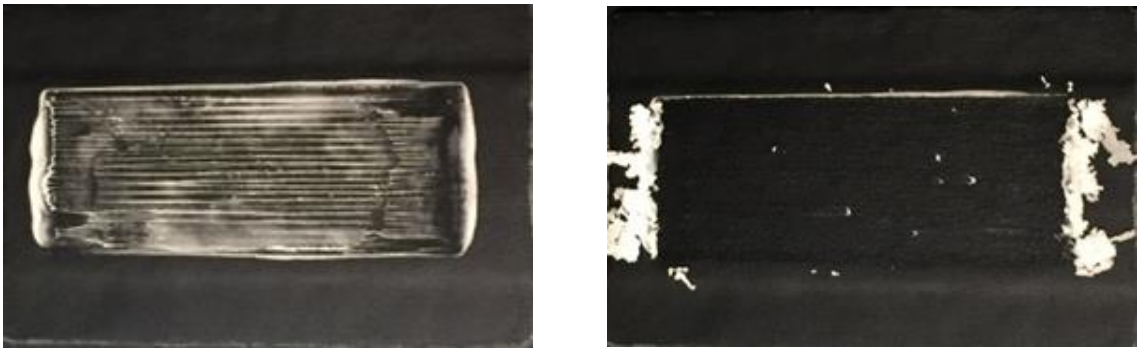

Figure 69: Pictures of the dry deposit before and after 15 strong back and forth scraping using a pressing force of 10.3 N.

b. *Screening the substrate/deposit and applicator/deposit interactions*

Here we present the percentage of surface snatched by the 15 high pressing force back and forth movements depending of the nature of the applicator and the substrate. It is clear that the nature of the applicator and the substrate has an impact on the snatching of the dry deposit. Indeed, we can imagine that a rough substrate will easily trap particles within its rugosities making the dry film harder to snatch. This is what we observed throughout this experiment.

Snatching a dry film from a smooth PMMA substrate using a smooth PMMA rod as applicator

The green points correspond to a dry deposit on a smooth PMMA substrate scraped by a smooth PMMA substrate. In this case, there is no need to apply a strong pressing force to snatch most of the deposit surface. The contact between the substrate and the applicator is solid and continuous since they do not present any roughness, moreover, the dry deposit can slip on the smooth substrate surface leading to an easy snatching. However, snatching is a progressive phenomenon following a snowball effect. First, a defect in the film has to be formed and an aliquot of the dry deposit has to be snatched. Once the first aliquot is snatched, it is dragged all along the spreading displacement, bringing a full line of matter with it. Then, the snatched matter can either settle down at the edge of the deposit, or stick to the applicator dragging more matter during the backward movement, or settle down farther onto the dry deposit, constituting this way a starting point for another snowball effect.

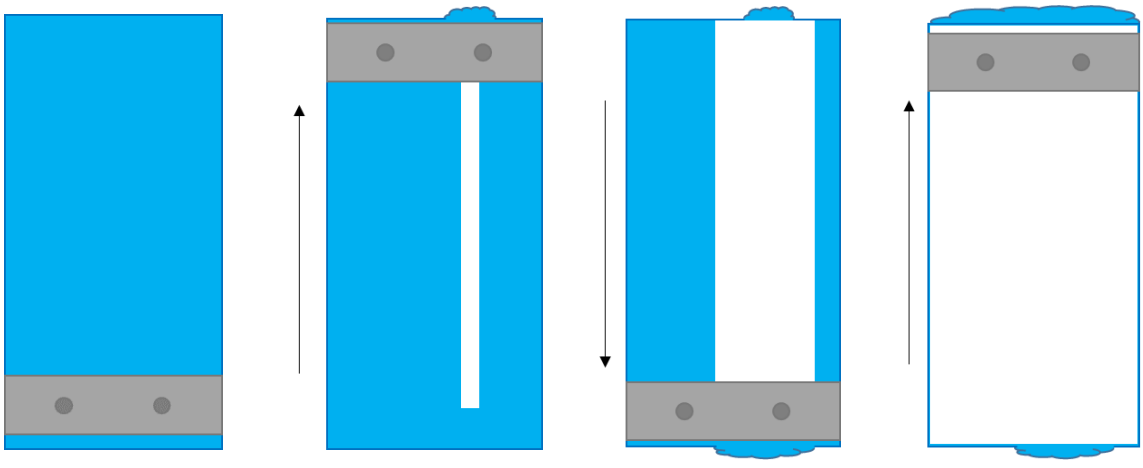

Figure 70: Schematic illustration of the snowball effect leading to the snatching of the deposit on the substrate over 2 back and forth movements.

Even though the pressing force is constant during the whole process, the contact between the applicator and the surface of the deposit is discontinuous and variable,

making the pressing stress difficult to estimate. At the very beginning of the snatching process, the smooth applicator is mainly in contact with the streaks of the dry deposit. Since streaks are thin, the pressure they undergo is quite high, and is generally sufficient to flatten the streaks. During the flattening process, the pressing stress decreases because the contact surface increases. On the other hand, the flattening of the streaks induces the formation of microscopic defects in the dry deposition. These defects are favourable areas that will tend to form snatching aliquots of matter responsible for dragging a complete line of material. Then, since the pressing force is concentrated on a smaller surface area, the more the deposition surface is torn off, the higher the pressing stress on the remaining deposit is. Theoretically, the dry deposit should be torn off under a specific stress and the surface of deposit snatched should either 0% if the scraping stress is lower than the snatching stress, or 100% if it's higher. However, because the pressing stress is inhomogeneous during scraping, we observe the progressive snatching we presented before. Hence, 15 back and forth movements may not be sufficient for a complete snatching process. However, comparing the surface of deposit torn off after 15 back and forth movements still gives us good information about the deposit/applicator and deposit/substrate interactions. Let's further analyse the results obtain by the other experiments.

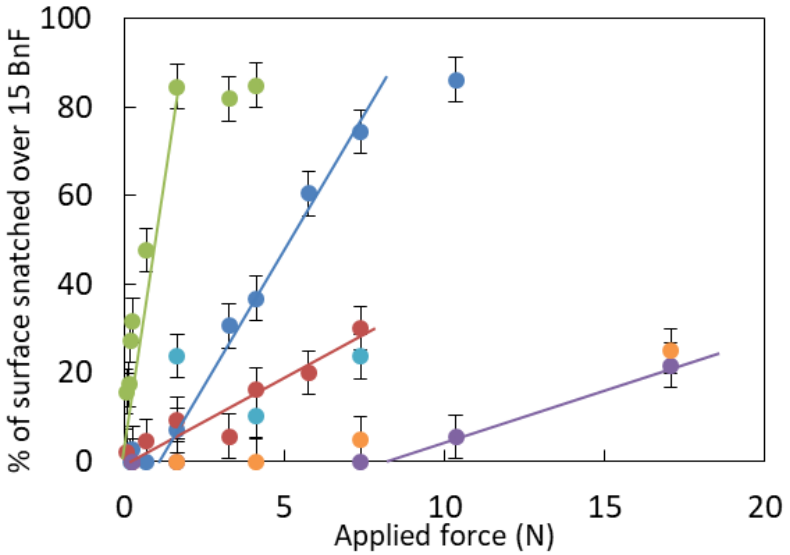

Figure 71: Comparison of the surface of deposit snatched by the scraping motion depending on the nature of the substrate and the applicator. Error bars at 5% are estimated by the typical error of image analysis and pixel quantification.

- *Smooth PMMA/Smooth PMMA*
- *Artificial leather/Artificial leather*
- *Artificial leather/Smooth PMMA*
- *Artificial leather/Sandblasted PMMA*
- *Smooth PMMA/Sandblasted PMMA*
- *Smooth PMMA/Artificial leather*

Impact of the smoothness on the snatching of the dry film

The blue points correspond to an experiment using a substrate and an applicator coated with an artificial leather layer, thus they are rough and softer than the smooth PMMA. Hence, the substrate sticks better the dry deposit since it can trap the particles within its micro relief. On the other hand, the applicator is also stickier and scratch more efficiently the deposit. Moreover, since artificial leather is soft, the applicator and the substrate can deform and create punctual defects that wouldn't be formed with harder materials. Overall, we observe that a stronger pressing force is needed to torn off the deposit from the substrate.

Interestingly, using an applicator coated of an artificial leather layer on a smooth PMMA substrate leads to a lower percentage of surface torn off for a given pressing force. Since the applicator is rough and soft while the applicator is slippery and smooth, we could have imagined that the minimum pressing force to snatch the deposit would be lower than in the case of artificial leather on artificial leather case. However, since the applicator is able to deform, the contact surface with the deposit is high, thus the pressing stress is lower than in the case of smooth PMMA applicator, so it is more difficult to torn the deposit off.

The red points correspond to an experiment using a smooth PMMA substrate and an applicator coated with an artificial leather layer. In this case, the substrate is slippery but is not deformable. On the other side, the applicator is soft and its shape adapt to the surface of the dry deposit, so the pressing stress is low. Hence, the deposit is not easily snatched under this conditions. It thus confirms the impact of the deformability and the pressing force, since the percentage of surface snatched is way lower than the smooth PMMA/smooth PMMA case and the artificial leather/artificial leather for a given force. Surprisingly, the results given by the cyan point (a rough PMMA substrate and an applicator coated with an artificial leather layer) are very close those given by the red point whereas the substrates present very different roughness. Comparing blue, cyan and red point leads to compare the impact of the substrate for an applicator coated with an artificial leather layer. Here, the roughness does not seem to have a strong impact, even though the surface snatched for a given force is a little lower for a rough substrate than for a smooth substrate. The limiting parameter for a soft applicator is the formation of microscopic defects that is particularly difficult since the pressing force is spread over a higher surface of contact. Hence, using a soft substrate helps to create these defects by the elastic deformation of the substrate.

Purple and orange points represent the case where the deposit is the least torn off and correspond to the case of a smooth PMMA applicator over a sandblasted PMMA substrate and an artificial leather coated substrate respectively. Comparing to the green point where a low pressing force was needed to snatch the whole dry deposit, here most of the material remains stuck to the substrate even under a pressing force of 1.7 N.

Interestingly, the softness of the substrate does not play a significant role for a smooth PMMA applicator. Thus, it proves that under these conditions, the limiting parameter remains in the ability to tear off the deposit from the substrate. The smooth applicator is slippery, so even if the substrate can deform, the applicator simply slip over the deposit without using the deformability of the substrate to create defects. Under these conditions, the deposit is torn off if it is able to slip from the substrate by the use of a sufficiently high pushing force.

As a conclusion to this part, we observe that a formulation made with a high dry volume fraction of particles forms spontaneously a white striated powdery deposit on the surface after a simple back and forth spreading motion. It is clear that the nature of the substrate and the applicator has a strong effect on the quality of this dry deposit. Depending on these, the dry deposit can either remain stuck to the surface of be torn off resulting in the formation of macroscopic aggregates on the surface which drastically reduce the efficiency of cosmetic products and may induce unpleasant sensation during spreading. From this study we understand that not only the formulation is important when it comes to spreading, an optimized applicator can help to obtain better performances.

The main parameter here is the hanging force of the deposit comparing to the scratching force of the applicator. For now, we begin to qualitatively feel these forces as we explained why the surface is torn off or not. We started to set up a more quantitative experiment allowing the measurement of both axial and normal forces in direct time. We do not report it in this manuscript since it has to be furtherly developed, but first results sound promising and we put a lot of hope in interesting results coming in the future.

Take home message – Chapter 5

In this chapter we studied more realistic spreading motions, closer to the real application of cosmetic products.

a. We discovered that even simple back and forth spreading movements on carbopol gels can induce the formation of heterogeneous deposits. The presence of particles also plays a role on the homogeneity of the final deposit. If the suspension is highly concentrated, shear-thickening effects can play a role during spreading and form bumps of matter on the deposit.

b. We also investigated the loss of matter by successive scratching of a deposit. We observed that the quantity of matter snatched depends on the nature of the substrate and the applicator, but also on the applied force.

Such phenomena are of major interest for industrial applications, therefore, further studies are planned to get more quantitative results in the future.

Conclusion and perspectives

In this thesis we studied the spreading of complex fluids for cosmetic applications. Although cosmetic formulations can be extremely complex, due to the large number of ingredients they contain, we have succeeded in preparing model systems that are consistent with real systems but perfectly controlled in terms of their composition. Each of the ingredients has been studied and their impacts on the rheological properties of the formula were extracted. In most cases we have used carbopol gels, which are model yield-stress fluids commonly used in cosmetic applications. We first studied the dip-coating problem in which an object is immersed into a fluid reservoir and then pulled out. During the withdrawal, a liquid layer is entrained by viscous drag. For Newtonian fluids, the coating thickness is determined by the shape of the meniscus between the object and the liquid bath. In dip-coating experiments with carbopol gels we find that the thickness of the formed coating film be determined by the flow inside the bath. Until now, this feature had only been understood empirically. We provide a complete description of the flow in the bath and observe that the thickness results exclusively from a liquefied layer in the bath whose thickness depends on the geometry of the bath, the rheology of the fluid, and the withdrawing velocity.

We also studied the spreading of carbopol gels with a flexible blade. The physics in this problem is similar to dip coating with Newtonian fluids, except that the surface tension that played a role in simple dip coating is replaced by the elasticity of the blade. Blade coating of yield-stress fluids are interesting since the volume of spread sample has a strong impact on the thickness of the deposit, although no such effects have been observed for Newtonian fluids. An analysis of the fluid flow under the blade reveals zones in which the gel flows, as well as zones in which the gel behaves like a solid or even flows against the spreading direction. These behaviours induce various phenomena that might generate homogeneous films whose thickness can be predicted, or inhomogeneous films containing holes and whose presence would be dramatic in the case of cosmetic application.

In a last step, we installed an experimental setup allowing to make more realistic spreading in the form of back and forth movements using materials closer to reality, both for the substrate and for the applicator, i.e. rough and soft materials. Complex phenomena intrinsic to the back-and-forth movements induce instabilities and spreading defects instead of forming a smooth and homogeneous film. The presence of a large quantity of suspended solid particles in the formulation also leads to the formation of aggregates of matter that reduces both the effectiveness of the spread product and the sensations during spreading. We notice that the amount of material that comes off when aggregates are formed is highly dependent on the applied normal force but also on the nature of the substrates and applicators.

In practical applications, substrates, applicators and movements are much more diverse than those we have used.

Thus, some parameters have been unexplored because of experimental limitations. For example, the spreading velocity of the films has never exceeded 10 mm/s due to the technology of the employed motorized stage. In collaboration with L'Oréal, the experiments can be adapted with a multifunctional collaborative robot. The latter will make it possible to carry out complex spreading movements, i.e. circular movements, at much higher velocity than those that our motorized stage allowed us to achieve. On the other hand, coupling this robot with image taking and force measurements in the three directions of space would certainly provide an even deeper knowledge of the physical phenomena that occur during spreading. The Young modulus, i.e. the softness of the substrate is also an interesting parameter that will be furtherly investigated in the future. It would also be interesting to study issues that are more related to chemistry and the impact of the different formulation ingredients by increasing the complexity of the systems, through the use of oil phase or suspended particles of different kinds.

As at the end of any thesis, still many questions and perspectives remain to be explored. I had the honour of starting this subject from the very beginning and discovering many exciting physico-chemical phenomena that explain the observed macroscopic behaviours. This research will be continued by another PhD student and I have no doubt that the sequel of this thesis and the science it covers will have many stimulating and enriching surprises in store.

Conclusion et perspectives

Dans cette thèse nous avons étudié l'étalement des fluides complexes pour des applications cosmétiques. Bien que les formulations cosmétiques puissent être extrêmement complexes, de par le nombre important d'ingrédients qu'elles peuvent contenir, nous avons réussi a préparé des systèmes modèles qui sont cohérents avec les systèmes cosmétiques réels mais parfaitement contrôlés vis-à-vis de leur composition. Tous les ingrédients ont été étudiés et leurs impacts sur les propriétés rhéologiques de la formule ont été déduis. Dans la plupart des cas, nous avons utilisé des gels de carbopol qui sont des fluides à seuil modèles couramment utilisés dans les applications cosmétiques. Nous avons d'abord étudié la thématique de l'enduction par trempage dans lequel un objet est immergé puis retiré d'un réservoir fluide. Pendant le retrait, une couche liquide est entrainée par l'entrainement visqueux. Pour des fluides Newtonien, l'épaisseur du revêtement formé est déterminée par la forme du ménisque entre l'objet et le bain liquide. Pour l'enduction par trempage avec un gel de carbopol nous avons trouvé que l'épaisseur du film formé était déterminée par le flux de matière à l'intérieur du bain. Jusqu'à présent, cet effet n'a été compris que de manière empirique. Nous avons fourni une description complète de l'écoulement dans le bain et observons que l'épaisseur résulte exclusivement d'une couche liquéfiée dans le bain dont l'épaisseur dépend de la géométrie du bain, de la rhéologie du fluide et de la vitesse de prélèvement.

Nous avons également étudié l'étalement de gels de carbopol avec une lame flexible. La physique de ce problème est similaire à celle de l'enduction par trempage avec des fluides newtoniens, sauf que la tension superficielle qui a joué un rôle dans l'enduction par trempage simple est remplacée par l'élasticité de la lame. L'étalement à la lame de fluides à seuil est intéressant car le volume de l'échantillon étalé a un fort impact sur l'épaisseur du dépôt, bien qu'aucun effet de ce type n'ait été observé pour les fluides newtoniens. Une analyse de l'écoulement du fluide sous la lame montre qu'il y a des zones dans lesquelles le gel s'écoule, ainsi que des zones dans lesquelles le gel se comporte comme un solide, ou même, s'écoule dans le sens contraire de l'étalement. Ces comportements induisent des phénomènes divers qui peuvent générer des films homogènes dont l'épaisseur est prévisible, ou des films inhomogènes contenant des trous et dont la présence serait dramatique dans le cas d'une application cosmétique.

Dans une dernière étape, nous avons installé un dispositif expérimental permettant d'effectuer un étalement plus réaliste sous forme de mouvements de va-et-vient en utilisant des matériaux plus proches de la réalité, tant pour le support que pour l'applicateur, c'est-à-dire des matériaux rugueux et mous. Les phénomènes complexes inhérents aux mouvements de va-et-vient induisent des instabilités et des défauts d'étalement au lieu de former un film lisse et homogène comme on l'aurait attendu. La présence d'une grande quantité de particules solides en suspension dans la formulation

entraîne également la formation d'agrégats de matière qui réduisent à la fois l'efficacité du produit étalé et les sensations lors de l'étalement. Nous avons remarqué que la quantité de matière qui se détache lors de la formation des agrégats dépend fortement de la force normale appliquée mais aussi de la nature des substrats et des applicateurs.

Dans la pratique, les substrats, les applicateurs et les mouvements sont beaucoup plus variés que ceux que nous avons utilisés. Ainsi, certains paramètres n'ont pas été explorés en raison de limites expérimentales. Par exemple, la vitesse d'étalement des films n'a jamais dépassé 10 mm/s à cause de la technologie de la platine motorisée que nous avons utilisée. En collaboration avec L'Oréal, les expériences peuvent être adaptées avec un robot collaboratif multifonctionnel. Ce dernier permettra d'effectuer des mouvements d'étalement complexes, c'est-à-dire des mouvements circulaires, à des vitesses bien supérieures à celles que notre platine motorisée nous a permis d'atteindre. D'autre part, coupler ce robot à la prise d'images et à la mesure des forces dans les trois directions de l'espace permettrait certainement d'approfondir la connaissance des phénomènes physiques qui se produisent lors de l'étalement. Le module de Young, c'est-à-dire la dureté du substrat, est également un paramètre intéressant qui fera l'objet d'études plus approfondies à l'avenir. Il serait également intéressant d'étudier certaines questions plus liées à la chimie et à l'impact des différents ingrédients de formulation en augmentant la complexité des systèmes, via l'utilisation de phases grasses ou de particules en suspension de différentes sortes.

Comme à la fin de toute thèse, de nombreuses questions et perspectives restent à explorer. J'ai eu l'honneur de commencer ce sujet depuis son commencement et de découvrir de nombreux phénomènes physico-chimiques passionnants qui expliquent les comportements macroscopiques observés. Cette recherche sera poursuivie par une autre doctorante et je ne doute pas que la suite de cette thèse et la science qu'elle couvre aura de nombreuses surprises stimulantes et enrichissantes en réserve.

Appendix section

I. Dimensionless description

In this section, we provide a nondimensional description of the bath-flow model. The following dimensionless quantities are used in terms of dimensional ones:

$$\tilde{r} = \frac{r}{r_1};\ \tilde{h} = \frac{h}{r_1};\ \tilde{z} = \frac{z}{l};\ \tilde{P} = \frac{P}{\rho g l};\ \tilde{\dot{\gamma}} = \frac{V\dot{\gamma}}{r_2 - r_1};\ \tilde{\tau} = \frac{\tau}{\tau_y};\ \tilde{v}_z = \frac{v_z}{V};$$
$$Bm = \frac{\tau_y}{k}\left(\frac{r_2 - r_1}{V}\right)^n ; W = \frac{\tau_y}{\rho g r_1} \tag{A.1}$$

We drop the tildes and write Equations (3.2-3.6) of the main manuscript in the following non dimensional form.

For equation (3.2)

$$-1 - \frac{\partial P}{\partial z} + \frac{W}{r}\frac{\partial r\tau_{rz}}{\partial r} = 0 \tag{A.2}$$

For equation (3.3)

$$\tau_{rz}(r) = \frac{1}{\lambda_i - \lambda_o}\left(r - \frac{\lambda_i \lambda_o}{r}\right) \tag{A.3}$$

For equation (3.4)

$$\int_1^{r_2} \dot{\gamma}\,(r)dr = 1 - r_2 \tag{A.4}$$

For equation (3.5)

$$\int_1^{r_2} r v_z(r)dr = -\frac{1}{2} \tag{A.5}$$

For equation (3.6)

$$\dot{\gamma} = \begin{cases} -Bm^{\frac{1}{n}}\left(\dfrac{\frac{\lambda_i\lambda_o}{r} - r + \lambda_i - \lambda_o}{\lambda_o - \lambda_i}\right)^{\frac{1}{n}} & \text{for } 1 \le r \le \lambda_i \\ 0 & \text{for } \lambda_i \le r \le \lambda_0 \\ Bm^{\frac{1}{n}}\left(\dfrac{r - \frac{\lambda_i\lambda_o}{r} + \lambda_i - \lambda_o}{\lambda_o - \lambda_i}\right)^{\frac{1}{n}} & \text{for } \lambda_0 \le r \le r_2 \end{cases} \tag{A.6}$$

For equation (3.7)

$$h = -1 + \sqrt{\frac{\int_1^{\lambda_i} r^2\dot{\gamma}\,(r)dr}{\int_1^{\lambda_i}\dot{\gamma}\,(r)dr}} \tag{A.7}$$

To obtain the laminar flow inside the bath, equation (A.4) and (A.5) needto be solved for $\{\lambda_i, \lambda_o\} \in [1, r_2]$. The flow inside the bath is determined by two dimensionless parameters, i.e. r_2 and the Bingham number $Bm = \frac{\tau_y}{k}\left(\frac{r_2 - r_1}{V}\right)^n$. As a consequence, no single master curve can be presented on which all data collapses. We note that the thickness of deposit h also depends upon n for given values of r_2 and Bm.

II. Withdrawal of a plate from a liquid bath

Here we derive the two-dimensional flow of a plate withdrawn from a liquid reservoir. In Cartesian coordinates, the Stokes' equation is given by

$$-\rho g - \frac{\partial P}{\partial z} + \frac{\partial \tau_{xz}}{\partial x} = 0 \tag{A.8}$$

with ρ the fluid density, g the gravitational acceleration, x the horizontal axis, z the vertical axis, and $\frac{\partial P}{\partial z}$ the vertical pressure gradient. The general solution for a steady laminar flow of a yield-stress liquid through a slot of width L is given by

$$\frac{\tau_{xz}(x)}{\tau_y} = \frac{2}{{\lambda_o}^{plate} - {\lambda_i}^{plate}}\left(x - \frac{{\lambda_o}^{plate} + {\lambda_i}^{plate}}{2}\right) \tag{A.9}$$

${\lambda_o}^{plate}$ and ${\lambda_i}^{plate}$ are the unknown locations of the inner and outer yield surfaces, i.e. $\tau_{xz}\left({\lambda_i}^{plate}\right) = -\tau_y$ and $\tau_{xz}\left({\lambda_o}^{plate}\right) = \tau_y$. They can be determined by the following conditions:

1. Velocity continuity with the boundary conditions $v_z(0) = V$ and $v_z(L) = 0$ yields

$$-V = \int_0^L \dot{\gamma}\,(x)dx \tag{A.10}$$

2. Mass conservation imposes

$$-\frac{e}{2}V = \int_0^L v_x(x)dx \tag{A.11}$$

with e the width of the plate.

For a Herschel-Bulkley fluid, the shear rate is given by

$$\dot{\gamma}(x) = \begin{cases} -\left(\frac{2\tau_y}{k}\right)^{\frac{1}{n}}\left(\frac{{\lambda_i}^{plate} - x}{{\lambda_o}^{plate} - {\lambda_i}^{plate}}\right)^{\frac{1}{n}} & \text{for } 1 \le x \le {\lambda_i}^{plate} \\ 0 & \text{for } {\lambda_i}^{plate} \le x \le {\lambda_o}^{plate} \\ \left(\frac{2\tau_y}{k}\right)^{\frac{1}{n}}\left(\frac{{\lambda_i}^{plate} - x}{{\lambda_o}^{plate} - {\lambda_i}^{plate}}\right)^{\frac{1}{n}} & \text{for } {\lambda_o}^{plate} \le x \le r_2 \end{cases} \tag{A.12}$$

The velocity profile is obtained by integration and is given by

$$\dot{\gamma}(x) = \begin{cases} V - \frac{n}{1+n}\left(\frac{2\tau_y}{k\left({\lambda_o}^{plate} - {\lambda_i}^{plate}\right)}\right)^{\frac{1}{n}}\left(\left({\lambda_i}^{plate}\right)^{1+\frac{1}{n}} - \left({\lambda_i}^{plate} - x\right)^{1+\frac{1}{n}}\right) & \text{for } 1 \le x \le {\lambda_i}^{plate} \\ V - \frac{n}{1+n}\left(\frac{2\tau_y}{k\left({\lambda_o}^{plate} - {\lambda_i}^{plate}\right)}\right)^{\frac{1}{n}}\left({\lambda_i}^{plate}\right)^{1+\frac{1}{n}} & \text{for } {\lambda_i}^{plate} \le x \le {\lambda_o}^{plate} \\ -\frac{n}{1+n}\left(\frac{2\tau_y}{k\left({\lambda_o}^{plate} - {\lambda_i}^{plate}\right)}\right)^{\frac{1}{n}}\left(\left(L - {\lambda_o}^{plate}\right)^{1+\frac{1}{n}} - \left(x - {\lambda_o}^{plate}\right)^{1+\frac{1}{n}}\right) & \text{for } {\lambda_o}^{plate} \le x \le r_2 \end{cases} \tag{A.13}$$

The integrals in equation (A.10) and (A.11) then yield

$$\frac{1+n}{2^{\frac{1}{n}}n}\left(\frac{{\lambda_o}^{plate}}{L} - \frac{{\lambda_i}^{plate}}{L}\right)^{\frac{1}{n}} = Bm^{\frac{1}{n}}\left(\left(\frac{{\lambda_i}^{plate}}{L}\right)^{1+\frac{1}{n}} - \left(1 - \frac{{\lambda_o}^{plate}}{L}\right)^{1+\frac{1}{n}}\right) \tag{A.14}$$

$$(1+2n)\left(\left(\frac{{\lambda_i}^{plate}}{L}\right)^{1+\frac{1}{n}} - \left(1 - \frac{{\lambda_o}^{plate}}{L}\right)^{1+\frac{1}{n}}\right)\frac{e}{2L} = \left(\left(1 + n + n\frac{{\lambda_o}^{plate}}{L}\right)\left(1 - \frac{{\lambda_o}^{plate}}{L}\right)^{1+\frac{1}{n}} - n\left(\frac{{\lambda_i}^{plate}}{L}\right)^{1+\frac{1}{n}}\right) \tag{A.15}$$

respectively, where the Bingham number is given by

$$Bm = \frac{\tau_y}{k}\left(\frac{L}{V}\right)^n \tag{A.16}$$

The thickness of the liquid region along the plate λ_i^{plate} can be obtained by numerically solving equations (A.14) and (A.15). In figure S1, we compare our model with experimental observations by Maillard et al.[50] Both the thickness if the liquid region λ_i^{plate} as function of Bm and the velocity profiles are in excellent agreement with experiments.

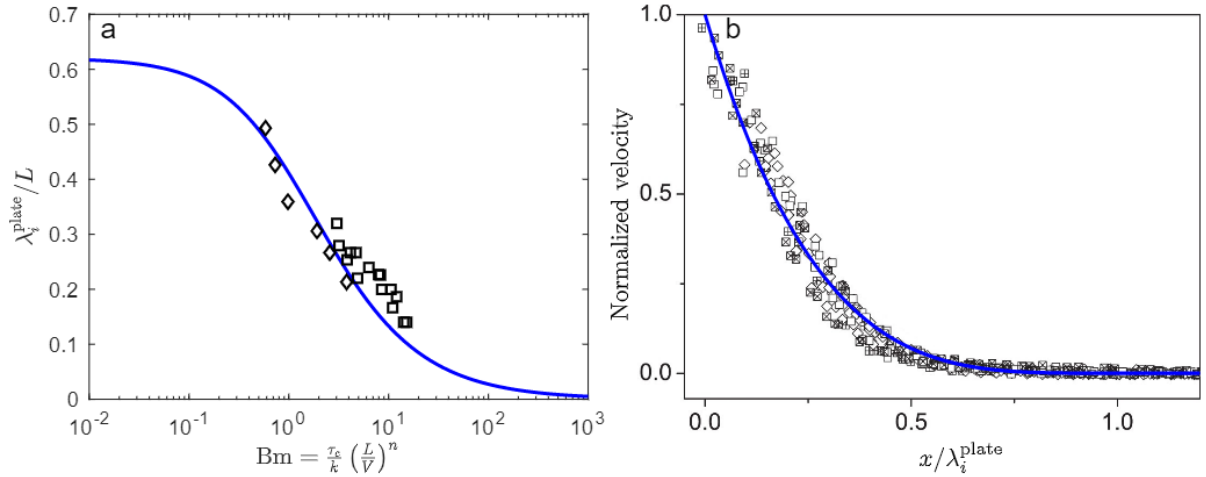

Figure S1: Comparison between our model and experimental observations by Maillard et al.(A.12) for a plate of thickness e = 1.9 mm withdrawn for a bath of size L = 75 mm. (a) Thickness of the liquid region along the plate as function of Bingham number (Bm). Velocity and mass-conservation give the theoretical predictions of our model for n = 0.35 (blue solid line). Experimental data points have been obtained form velocity profiles of aqueous Carbopol gels of various yield stress (circles) and a mixture of Carbopol and glycerol (diamonds), shown in panel b. (b) Normalized velocity rescaled to the liquid-zone width λ_i^{plate}. Experimental profiles have been obtained for various gels and velocities in the range of 0.2-17 mm/s (adapted from Reference[50]).

Large Bingham numbers

When the bath size L is large in comparison with the product of the withdrawal speed V and the characteristic rheological time $\left(\frac{\tau_y}{k}\right)^{\frac{1}{n}}$, the Bingham number $Bm >> 1$ and on finds.

$$\lambda_i^{plate} = \left[\left(\frac{1+n}{n}\right)^n \left(1+\frac{e}{2L}\right)^n \frac{kV^nL}{2\tau_y}\right]^{\frac{1}{1+n}} \tag{A.17}$$

Hence, for finite plate thickness e, the thickness of the liquid region is found to diverge as $\lambda_i^{plate} \propto L^{\frac{1}{1+n}}$.

Bibliographic references

1. Xie, F., Halley, P. J. & Avérous, L. Rheology to understand and optimize processibility, structures and properties of starch polymeric materials. *Prog. Polym. Sci.* **37,** 595–623 (2011).

2. Harini, M. & Deshpande, A. P. Rheology of poly(sodium acrylate) hydrogels during cross-linking with and without cellulose microfibrils. *J. Rheol* **53,** 31–47 (2009).

3. Gu, S.-Y., Zou, C., Zhou, K. & Ren, J. Structure-Rheology Responses of Polyactide/Calcium Carbonate Composites. *J. Appl. Polym. Sci.* **114,** 1648–1655 (2009).

4. Cloitre, M. Dynamique et rhéologie des systèmes polymères. (2015).

5. McKinley, G. H. & Jaishankar, A. Power-law rheology in the bulk and at the interface: quasi-properties and fractional constitutive equations. *Proc. R. Soc. A.* 1–18 (2012). doi:10.1098/rspa.2012.0284

6. Barnes, H. A., Hutton, J. E. & Walters, K. *An introduction to rheology.* (1989).

7. Lenk, R. S. *The Hagen-Poiseuille Equation and the Rabinowitsch Correction. The Pressure Drop in Tapered Channels. Polymer Rheology* (1978).

8. Fall, A., Bertrand, F., Ovarlez, G. & Bonn, D. Yield Stress and Shear Banding in Granular Suspensions. (2009). doi:10.1103/PhysRevLett.103.178301

9. Kansal, A. R., Torquato, S. & Stillinger, F. H. Diversity of order and densities in jammed hard-particle packings. *Phys. Rev. E* **66,** (2002).

10. Kansal, A. R., Torquato, S. & Stillinger, F. H. Computer generation of dense polydisperse sphere packings. *J. Chem. Phys* **117,** 8212 (2002).

11. Gonçalves, A. D. *et al.* The effect of protein concentration on the viscosity of a recombinant albumin solution formulation. *RSC Adv* **6,** 15143–15154 (2016).

12. Mari, R., Seto, R., Morris, J. F. & Denn, M. M. Shear thickening, frictionless and frictional rheologies in non-Brownian suspensions. *Cit. J. Rheol.* **58,** 1693 (2014).

13. Boyer, F., Guazzelli, E. & Pouliquen, O. Unifying Suspension and Granular Rheology. *Phys. Rev. Lett.* 1–5 (2011). doi:10.1103/PhysRevLett.107.188301

14. Wyart, M. & Cates, M. E. Discontinuous Shear Thickening without Inertia in Dense Non-Brownian Suspension. *Phys. Rev. Lett.* 1–5 (2014).

15. Comtet, J. *et al.* Pairwise frictional profile between particles determines discontinuous shear thickening transition in non-colloidal suspensions. *Nat.*

Commun. **8,** (2017).

16. Chatté, G. *et al.* Shear thinning in non-Brownian suspensions. *Soft Matter* **14,** 879 (2018).

17. Brown, E. & Jaeger, H. M. Shear thickening in concentrated suspensions: phenomenology, mechanisms, and relations to jamming. (2013).

18. Barnes, H. A. Shear-Thickening "Dilatancy" in Suspensions of Nonaggregating Solid Particles Dispersed in Newtonian Liquids. *J. Rheol.* **33,** (1989).

19. Dinkgreve, M., Fazilati, M., Denn, M. M. & Bonn, D. Carbopol: From a simple to a thixotropic yield stress fluid. *Cit. J. Rheol.* **62,** 773 (2018).

20. Seth, J. R., Bonnecaze, C. T., Seth, J. R., Cloitre, M. & Bonnecaze, R. T. Influence of short-range forces on wall-slip in microgel pastes. *J. Rheol. J. Rheol. J. Rheol.* **52,** (2008).

21. Bocquet, L., Colin, A. & Ajdari, A. Kinetic Theory of Plastic Flow in Soft Glassy Materials. *Phys. Rev. Lett.* 1–4 (2009).

22. Bocquet, L., Colin, A. & Ajdari, A. A kinetic theory of plastic flow in soft glassy materials. *Phys. Rev. Lett.* (2009).

23. Bergeron, V., Fagan, M. E. & Radke, C. J. Generalized entering coefficients: a criterion for foam stability against oil in porous media. *Langmuir* **9,** 1704–1713 (1993).

24. Zisman, W. A. Relation of the Equilibrium Contact Angle to Liquid and Solid Constitution. *Adv. Chem. Ser.* (1964). doi:10.1021/ba-1964-0043.ch001

25. Harkins, W. D. & Feldman, A. Films. The Spreading Of Liquids And the Spreading COefficient. *Am. Chem. Soc.* **44,** (1922).

26. Young, T. An Essay on the Cohesion of Fluids. *Philos. Trans. R. Soc. London* **95,** 65–87 (1805).

27. Yonger, M. Dynamique du mouillage pseudo-partiel de la silice par des fondus de polymere. (2016).

28. Podgorski, T., Flesselles, J. M. & Limat, L. Corners, cusps, and pearls in running drops. *Phys. Rev. Lett.* **87,** 361021–361024 (2001).

29. Rio, E., Daerr, A., Andreotti, B. & Limat, L. Boundary conditions in the vicinity of a dynamic contact line: Experimental investigation of viscous drops sliding down an inclined plane. *Phys. Rev. Lett.* **94,** 1–4 (2005).

30. Le Grand, N., Daerr, A. & Limat, L. Shape and motion of drops sliding down an

inclined plane. *J. Fluid Mech.* **541,** 293 (2005).

31. Dussan, E. On the spreading of liquids on solid surfaces: static and dynamic contact lines. *Annu. Rev. Fluid Mech.* **11,** 371–400 (1979).

32. Goucher, F. S. & Ward, H. A Problem in Viscosity : The Thickness of Liquid Films Formed on Solid Surfaces Under Dynamic Conditions. *Phil. Mag.* **44,** 1002–1014 (1922).

33. Landau, L. & Levich, B. Dragging of a liquid by a moving plate. *Acta Physicochim. Urss* **17,** 42–54 (1942).

34. Derjaguin, B. V. Trimness of liquid layer adhering to walls of vessels on their emptying and theory of photo and motion picture film coating. *Comptes Rendus L'Académie Des Sci. L'URSS* **39,** 13–16 (1943).

35. Voinov, O. V. Hydrodynamics of wetting. *Fluid Dyn.* **11,** 714–721 (1976).

36. Cox, R. G. The dynamics of the spreading of liquids on a solid surface. Part 1. Viscous flow. *J. Fluid Mech.* **168,** 169–194 (1986).

37. Joanny, J. F. A model for contact angle hysteresis. *J. Chem. Phys.* **81,** 552 (1984).

38. Golestanian, R. & Raphaël, E. Dissipation in dynamics of a moving contact line. *Phys. Rev. E. Stat. Nonlin. Soft Matter Phys.* **64,** (2001).

39. Nikolayev, V. S. & Beysens, D. a. Equation of motion of the triple contact line along an inhomogeneous surface. *Europhys. Lett.* **64,** 763–768 (2003).

40. Hocking, L. M. Meniscus draw-up and draining. *Eur. J. Appl. Math.* **12,** 195–208 (2001).

41. Eggers, J. Hydrodynamic theory of forced dewetting. *Phys. Rev. Lett.* **93,** 1–4 (2004).

42. Eggers, J. Existence of receding and advancing contact lines. *Phys. Fluids* **17,** 1–10 (2005).

43. De Gennes, P. G., Hua, X. & Levinson, D. P. Dynamics of wetting : local contact angles. *J. Fluid Mech* **212,** 55–63 (1990).

44. De Gennes, P. G. Deposition of Langmuir-Blodgett layers. *Colloid Polym. Sci.* **264,** 463–465 (1986).

45. Delon, G. Nature de la transition de Landau-Levich. (2007).

46. Snoeijer, J. H. & Andreotti, B. Moving Contact Lines: Scales, Regimes, and Dynamical Transitions. *Annu. Rev. Fluid Mech.* **45,** 269–292 (2013).

47. Derjaguin, B. V. *Film Coating Theory.* (1964).

48. Blake, T. D. & Ruschak, K. J. A maximum speed of wetting. *Nature* **282,** 489–491 (1979).

49. Ramé, E., Garoff, S. & Willson, K. R. Characterizing the microscopic physics near moving contact lines using dynamic contact angle data. *Phys. Rev. E. Stat. Nonlin. Soft Matter Phys.* **70,** 1–9 (2004).

50. Maillard, M., Bleyer, J., Andrieux, A. L., Boujlel, J. & Coussot, P. Dip-coating of yield stress fluids. *Phys. Fluids* **28,** 1–25 (2016).

51. Maillard, M., Boujlel, J. & Coussot, P. Solid-solid transition in landau-levich flow with soft-jammed systems. *Phys. Rev. Lett.* **112,** 2–5 (2014).

52. Sullivan, T. M. & Middleman, S. Film thickness in blade coating of viscous and viscoelastic liquids. *J. Nonnewton. Fluid Mech.* **21,** 13–38 (1986).

53. Sullivan, T., Middleman, S. & Keunings, R. Use of a finite-element method to interpret rheological effects in blade coating. *AIChE J.* **33,** 2047–2056 (1987).

54. Hsu, T. C., Malone, M., Laurence, R. L. & Middleman, S. Separating forces in blade coating of viscous and viscoelastic liquids. *J. Non-Newtonian Fluid Mech. F. Full J. TitleJournal Non-Newtonian Fluid Mech.* **18,** 273–294 (1985).

55. Mitsoulis, E. & Athanasopoulos, G. Numerical Simulation of Blade-over-Roll Coating Forming Flows. *Comput. Methods Geosci.* 214–224 (2010).

56. Kistler, S. F. & Scriven, L. E. Coating flow theory by finite element and asymptotic analysis of the navier-stokes system. *Int. J. Numer. Methods Fluids* **4,** 207–229 (1984).

57. Romero, O. J., Scriven, L. E. & Carvalho, M. S. Slot coating of midly viscoelastic liquids. *J. Non-Newtonian Fluid Mech.* 63–75 (2006).

58. Maillard, M. Étalements de fluides à seuil. (2016).

59. Middleman, S., Greener, J. & Malone, M. *Fundamentals of polymer processing.* (1977).

60. Greener, Y. & Middleman, S. A theory of roll coating of viscous and viscoelastic fluids. *Polym. Eng. Sci.* **15,** 1–10 (1975).

61. Sofou, S. & Mitsoulis, E. Roll-over-web coating of pseudoplastic and viscoplastic sheets using the lubrication approximation. *J. Plast. Film Sheeting* **21,** 307–333 (2005).

62. Davard, F. & Dupuis, D. Flow visualisation experiments in a blade coating process. *J. Nonnewton. Fluid Mech.* **93,** 17–28 (2000).

63. Schmidt, M., Schlosser, U. & Schollmeyer, E. Computational Fluid Dynamics

Investigation of the Static Pressure at the Blade in a Blade Coating Process. *Text. Res. J.* **79,** 579–584 (2009).

64. Seiwert, J. Entraînements visqueux. (2010).

65. Deblais, A., Harich, R., Bonn, D., Colin, A. & Kellay, H. Spreading of an Oil-in-Water Emulsion on a Glass Plate: Phase Inversion and Pattern Formation. *Langmuir* **31,** 5971–5981 (2015).

66. Greener, Y. & Middleman, S. Blade-coating of a viscoelastic fluid. *Polym. Eng. Sci.* **14,** 791–796 (1974).

67. Deblais, A., Harich, R., Colin, A. & Kellay, H. Taming contact line instability for pattern formation. *Nat. Commun.* **7,** 12458 (2016).

68. Pelot, D. D., Klep, N. & Yarin, A. L. Spreading of Carbopol gels. *Rheol. Acta* **55,** 279–291 (2016).

69. Seiwert, J., Quéré, D. & Clanet, C. Flexible scraping of viscous fluids. *J. Fluid Mech.* **715,** 424–435 (2013).

70. Boujlel, J. & Coussot, P. Measuring the surface tension of yield stress fluids. *Soft Matter* **9,** 5898 (2013).

71. Jørgensen, L., Le Merrer, M., Delanoë -Ayari, H. & Barentin, C. Yield stress and elasticity influence on surface tension measurements. *Soft Matter* **11,** 5111 (2015).

72. Mason, T. G., Bibette, J. & Weitz, D. A. *Yielding and Flow of Monodisperse Emulsions. JOURNAL OF COLLOID AND INTERFACE SCIENCE* **179,** (1996).

73. Geraud, B., Bocquet, L. & Barentin, C. Confined flows of a polymer microgel. *Eur. Phys. J. E* **36,** (2013).

74. Princen, H. M. & Kiss, A. D. Rheology of Foams and Highly Concentrated Emulsions III. Static Shear Modulus. *J. Colloid Interface Sci.* **112,** 427–437 (1986).

75. Dubois, M., Gilles, K. A., Hamilton, J. K., Rebers, P. A. & Smith, F. Colorimetric Method for Determination of Sugars and Related Substances. *Anal. Chem.* **28,** 350–356 (1956).

76. Grosso, D. How to exploit the full potential of the dip-coating process to better control film formation. doi:10.1039/c1jm12837j

77. Coussot, P. *Rheometry of Pastes, Suspensions, and Granular Materials: Applications in Industry and Environment.* (2005).

78. Bonn, D., Denn, M. M. & Berthier, L. Yield stress materials in soft condensed matter Sébastien Manneville. (2017).

79. Tsougeni, K., Vourdas, N., Tserepi, A., Gogolides, E. & Cardinaud, C. Mechanisms of Oxygen Plasma Nanotexturing of Organic Polymer Surfaces: From Stable Super Hydrophilic to Super Hydrophobic Surfaces. *Langmuir* **25,** 11748–11759 (2009).

80. Kim, O. & Nam, J. Confinement effects in dip coating. *J. Fluid Mech* **827,** 1–30 (2017).

81. Maillard, M., Boujlel, J. & Coussot, P. Flow characteristics around a plate withdrawn from a bath of yield stress fluid. *J. Nonnewton. Fluid Mech.* **220,** 33–43 (2015).

82. Cheddadi, I., Saramito, P. & Graner, F. Steady Couette flows of elastoviscoplastic fluids are nonunique. *J. Rheol. (N. Y. N. Y).* **56,** 213 (2012).

83. Fordham, E. J., Bittleston, S. H. & Ahmadi Tehrani, M. *Viscoplastic Flow in Centered Annuli, Pipes, and Slots. Ind. Eng. Chem. Res* **30,** (1991).

84. Rio, E., Daerr, A., Lequeux, F. & Limat, L. Moving Contact Lines of a Colloidal Suspension in the Presence of Drying. *Langmuir* 3186–3191 (2006). doi:10.1021/la052989e

85. Timoshenko & Gere. *Theory Of Elastic Stability, 2nd Edition.* (1985).

86. Paiola, J. Ecoulement d'un fluide à seuil dans un milieu poreux. (2017).

87. Brown, E. *et al.* Generality of shear thickening in dense suspensions. *Nat. Mater.* **9,** 220–224 (2010).

RÉSUMÉ

L'étalement des produits cosmétiques, bien qu'il semble trivial à l'échelle du consommateur, met en action de nombreux phénomènes physico-chimiques complexes importants à comprendre et à maitriser. Dans cette thèse, nous étudions en détail les phénomènes qui interviennent lors de l'étalement de fluides complexes. A travers nos études, nous fournissons des leviers scientifiques qui permettront *in fine* d'améliorer les performances des produits cosmétiques. Pour ce faire, nous étudions divers domaines scientifiques comme la rhéologie des fluides complexes (c.-à-d. gels et dispersion de particules solides), le mouillage, la mécanique des fluides et les systèmes d'étalement.

MOTS CLÉS

Fluides complexes, rhéologie, mouillage, étalement.

ABSTRACT

The spreading of cosmetic products, although it seems trivial at the consumer level, involves many complex physico-chemical phenomena that are important to understand and control. In this thesis, we study in detail the phenomena that occur during the spreading of complex fluids. Through our studies, we provide scientific levers that will ultimately improve the performance of cosmetic products. To do this, we study various scientific fields such as complex fluid rheology (i. e. gels and solid particle dispersion), wetting, fluid mechanics and spreading systems.

KEYWORDS

Complex fluids, rheology, wetting, spreading.